UNIVERSITÄT GRAZ
UNIVERSITY OF GRAZ

Higgs-PDF study in proton-proton collisions

Thesis submitted in partial fulfillment of the requirements
for the degree of Master of Science

in the Department of Physics
of the Faculty of Science
at the Karl-Franzens-Universität Graz

Author:
Simon Fernbach

Advisor:
Prof. Axel Maas

May 28, 2019

Abstract

The goal of this thesis is to study the effects of the higgs content in the proton, which is demanded by strict non-perturbative gauge invariance and group theoretical arguments. This is done in proton-proton collisions, in the framework of parton distribution functions. The most higgs sensitive final states and observables are discussed and the effects of different phenomenologically motivated higgs PDF parametrizations on the cross section are tested. For the final states $t\bar{t}$, $t\bar{t}Z$ and the observable $\Phi_{l,\bar{l}}$, in the di-leptonic decay channel of $t\bar{t}$, the deviations from standard model results are studied and the influence of the different shapes is analyzed. Finally exclusion plots are created, that put limits on the maximally allowed higgs component in the proton.

Kurzbeschreibung

Das Ziel dieser Arbeit ist es, die Auswirkungen eines im Proton gebundenen Higgs zu untersuchen, welches aufgrund von strikter, nicht-perturbativer Eichinvarianz und gruppentheoretischer Argumente gefordert ist. Dies geschieht im Rahmen von Proton-Proton Kollisionen mit Hilfe von sogenannten "Parton distribution functions" (PDF). Es wird untersucht, welche Endzustände und Observable am empfindlichsten auf das Higgs reagieren und verschiedene phenomenologisch motivierte Ansätze für die Higgs PDF werden getestet. Für die Endzustände $t\bar{t}$, $t\bar{t}Z$ und die Observable $\Phi_{l,\bar{l}}$, des di-leptonischen Zerfallskanals von $t\bar{t}$, wird die Abweichung zu Ergebnissen des Standardmodels und der Einfluss der verschiedenen funktionalen Formen der Higgs PDF analysiert. Zuletzt werden "Exclusion plots" erstellt, welche den maximal erlaubten Higgsanteil des Protons begrenzen.

Acknowledgements

I would like to express my gratitude to all the different people who contributed to this thesis or even made it possible. First i want to thank my supervisor Axel Maas for the countless hours of discussion and the constant engagement in the project that kept it moving along. Furthermore i want to thank Simon Plätzer, from the Particle Physics group of the University of Vienna, for his invaluable assistance with Herwig that made this project possible, together with frequent technical support he gave. Lastly i want to thank Robert Schöfbeck, from HEPHY and a member of the CMS collaboration and Lukas Lechner, his PHD student, who provided an improved form of the exclusion plots as well as the idea for the spin-correlation in the di-leptonic top-antitop decay channel as another potentially sensitive final state to investigate.

Contents

Introduction

The thesis consists of two major parts. The first and smaller one is the theoretical motivation for why there is a higgs component expected to be bound to all elementary fields found in the standard model. The second and main part investigates this higgs component, in the concrete example of proton-proton collisions, with the help of a Monte-Carlo event generator called Herwig. [1][2][3]

Theoretical Part:

The standard model is a collection of three different gauge theories and even though classically the gauge theories are nothing more than mathmatical simplifications, in quantum mechanics they seem to be fundamental in nature, as can be seen by the difficulty to formulate a gauge independent quantum theory. This is discussed together with a short review of classical gauge theories in Ch. 1 and their quantization in Ch. 2. Nevertheless physical quantities cannot depend on the choice of gauge made by the observer. In the standard model the elementary fields however are gauge dependent, so why is it that the correlation functions are not? For perturbation theory it is the BRST symmetry, that guarantees asymptotically the elementary matter fields and transverse polarization degrees of freedom of the gauge fields, which correspond to the physical particles of perturbation theory, are invariant under BRST transformations and that the longitudinal and time-like gauge field degrees of freedom cancel together with the ghosts in any expectations values. This explains why physical quantities like S-matrix elements are gauge invariant in perturbation theory even though they are calculated from correlation functions containing elementary fields, which are gauge dependent. The topic of BRST quantization and how it leads to gauge invariant, physical states is briefly reviewed in Sec. 3.1. Beyond perturbation theory however BRST symmetry cannot be guaranteed due to a variety of technical difficulties which are elaborated in Sec. 3.2. Instead one has to consider manifestly gauge invariant states, which are composite fields. This is detailed in Ch. 4.

In case a theory posseses an active Brout-Englert-Higgs effect, this leads to an approach called *gauge invariant perturbation theory* developed by Fröhlich, Morchio and Strocchi which will be explained in Ch. 5. In this approach the higgs field is used to form composite states with the elementary fields, thereby creating gauge invariant states even beyond perturbation theory. Such a procedure should lead to observable effects for cross sections since the colliding particles now include the higgs and are thus in all cases, even when elementary fields are considered, bound state collisions, which is treated in Sec. 5.3.

Technical Part:

The treatment of bound state collisions is already well established in regular QCD collider physics and requires the use of the so called parton model and parton distribution functions (PDFs), which leads to the main part of the thesis, the investigation of the aforementioned higgs component in all elementary fields, in proton-proton collisions which is the topic of Ch. 6. For this, standard perturbation theory is used in the form of a Monte-Carlo event generator, called Herwig [1][2][3], together with different higgs PDF Ansätze, which were input into Herwig with the help of a plugin written by a colleague from the University of Vienna and one of the authors of Herwig, Simon Plätzer. The scattering processes, which should display the biggest signal of a higgs in the initial state, are discussed in Sec. 6.1, together with a listing of the different contributing Feynman-diagrams for these processes. In Sec. 6.4, the momentum-sum rule is used to derive a normalized form of the $P'P' \to f$ cross section, where P' stands for the proton with additional higgs contribution and f for a given final state. The different higgs PDFs are listed in Sec. 6.6 together with a theoretical motivation of their particular mathmatical form. From the calculated total cross sections for the different parton-parton processes contributing to the $P'P' \to f$ cross section, together with the experimental errors for said cross section, it is possible to determine so called exclusion plots, that limit the allowed higgs content of the proton for different values of the higgs parameters, which is the topic of Sec. 6.7. A more sophisticated version of these is produced by using the partial cross sections, since they provide more restraining information, and inserting the raw collision data, that was calculated with Herwig, into a detector simulation of CMS, which was done with Delphes [4]. This results in confidence intervals, that show the probability of the higgs fraction being in a certain range. The confidence intervals were created by Robert Schöfbeck and Lukas Lechner and the setup used is the same as in [5] and [6]. Sadly due to time constraints the ones included are preliminary results and can be found in Sec. 6.7. The final version will be published in [7]. In Sec. 6.8 the different observables and partial cross sections, together with Rivet [8], are discussed. Finally in Ch. 7 the effects of the shape of the higgs PDF models on the calculated cross sections are compared and the relation of the cross section's behaviour to a change of shape is inferred. A brief summary of the results is given in Ch. 8. The code for the automated parameter runs and for the generation of the different plots is found in App. B.

1. Classical gauge theories

Modern fundamental physics is built out of gauge theories. For example the standard model is given by the direct product of three different gauge groups $SU(2)_L \times SU(3) \times U(1)_Y$ and classical electrodynamics has the underlying gauge group $U(1)$. Even the general theory of relativity can be formulated as a gauge theory. In gauge theories the gauge symmetry is unphysical, a redundant degree of freedom because the choice of gauge is made by the observer and therefore can not in any way influence the results of physical measurements . While in classical gauge theories this is the case, since the Lagrangian is gauge invariant and there are no other quantities that are not derived from it, for quantized gauge theories it is not as obvious. For one, formulating the theory gauge independent e.g: in terms of electric and magnetic fields, is only possible for abelian gauge theories in a straightforward way, since the fields strength tensor of non-abelian theories is not gauge invariant anymore and therefore the electric and magnetic fields are not aswell. The result of such a formulation for the abelian case gives complicated to solve and impractical expressions and is not suited for practical application. Another option for abelian gauge theories would be to not consider the gauge field fundamental, but the field strength tensor or the electric and magnetic fields, but this yields a theory with different predictions to the one observed experimentally, which suggests that the gauge field is indeed fundamental to the quantum realm. Nevertheless the physical results still need to be gauge independent, even if it is impossible to formulate the theories describing the microscopic in a gauge independant way. This demand however, is on shaky ground for non-perturbative quantum Yang-Mills theories, as will be shown later. In order to guarantee gauge invariance under all circumstances one is led towards formulating correlation functions in terms of composite operators.

1.1. Abelian gauge theory

Classical Electrodynamics is an abelian U(1) gauge theory given by the Lagrangian

$$\begin{aligned} \mathcal{L} &= -\frac{1}{4}F_{\mu\nu}F^{\mu\nu} - J^\mu A_\mu \\ F_{\mu\nu} &= \partial_\mu A_\nu - \partial_\nu A_\mu \end{aligned} \tag{1.1}$$

and the gauge field A_μ transforms as

$$\begin{aligned} A_\mu \to A'_\mu &= A_\mu - \partial_\mu \omega \\ F_{\mu\nu} \to F'_{\mu\nu} &= \partial_\mu A'_\nu - \partial_\nu A'_\mu = F_{\mu\nu} \end{aligned} \tag{1.2}$$

with the gauge function $\omega(x)$. The field strength tensor $F_{\mu\nu}$ is gauge invariant and as a consequence the electric and magnetic fields are aswell and are given by

$$
\begin{aligned}
E_i &= cF_{0i} \\
B_i &= -\frac{1}{2}\epsilon_{ijk}F^{jk}
\end{aligned}
\tag{1.3}
$$

which leads to physical, measurable electric and magnetic fields as well as charge. Since the theory can be formulated in terms of electric and magnetic fields or the field strength tensor, which are themselves gauge invariant, it automatically means that the whole theory is gauge invariant. This is in contrast to the non-abelian case and creates another possibility for quantizing the theory which will be discussed in Sec. 4.1.

For gauge theories the Noether charge can be determined with the help of the second Noether theorem which reads [9]

$$
\sum_i [\Phi]_i a_{\alpha,i} = \sum_i \partial_\mu([\Phi]_i b^\mu_{\alpha,i})
\tag{1.4}
$$

where Φ_i labels the different fields, α labels the continouus symmetries and $[\Phi]_i$ means the Euler-Lagrange equations for Φ_i.

together with

$$
\delta\Phi_i = \sum_\alpha a_{\alpha,i}\Delta\omega(x) + b^\mu_{\alpha,i}\partial_\mu(\Delta\omega(x))
\tag{1.5}
$$

in which $\Delta\omega$ stands for infinitesimal gauge functions.

For classical electrodynamics, which is given by (1.2), this leads to

$$
\begin{aligned}
a_{A_\mu} &= 0 \\
b^\nu_{A_\mu} &= \delta^\nu_\mu
\end{aligned}
\tag{1.6}
$$

which when inserted in (1.4)

$$
\partial_\mu J^\mu = \partial_\mu([A_\mu]) = \partial_\mu(\frac{\partial\mathcal{L}}{\partial A_\mu} - \partial_\nu\frac{\partial\mathcal{L}}{\partial\partial_\nu A_\mu}) = 0
\tag{1.7}
$$

and using

$$\begin{aligned}\frac{\partial\mathcal{L}}{\partial A_\mu} &= 0\\ \frac{\partial\mathcal{L}}{\partial_\nu A_\mu} &= \frac{1}{2}F^{\mu\nu}\\ \mathcal{L} = -\frac{1}{4}F_{\mu\nu}F^{\mu\nu} &= -\frac{1}{2}\partial_\mu A_\nu F^{\mu\nu}\end{aligned} \tag{1.8}$$

finally leads to

$$\partial_\mu J^\mu = \partial_\mu\partial_\nu F^{\mu\nu} = 0 \tag{1.9}$$

Thus a consequence of Noether's second theorem is that the field strength tensor needs to be anti-symmetric.

The Noether charge is given by

$$\begin{aligned}\frac{dQ_\mathcal{N}}{dt} &= \partial_0\int J^0 dV = \partial_0\int\partial_\nu F^{0\nu}dV = -\partial_t\int\boldsymbol{\nabla}\cdot\vec{E}dV\\ Q_\mathcal{N} &= -\int\boldsymbol{\nabla}\cdot\vec{E}dV\end{aligned} \tag{1.10}$$

which is just Gauss's law but for the Noether charge. If additionally the Euler-Lagrange equations, with a non-vanishing external source term, are satisfied, then the Noether charge can be equated to the electric charge

$$Q_\mathcal{N} = -\int\boldsymbol{\nabla}\cdot\vec{E}dV = -\int\frac{\rho}{\epsilon_0}dV = -Q_{el} \tag{1.11}$$

1.2. Non-abelian gauge theory

In a classical non-abelian gauge theory the field strength tensor is given by [10],[11],[12]

$$\begin{aligned}F_{\mu\nu} = \frac{i}{g}[D_\mu, D_\nu] &= \partial_\mu A_\nu - \partial_\nu A_\mu - ig[A_\mu, A_\nu] =\\ &= (\partial_\mu A^a_\nu - \partial_\nu A^a_\mu + gf_{abc}A^b_\mu A^c_\nu)\tau_a = F^a_{\mu\nu}\tau_a\end{aligned} \tag{1.12}$$

and unlike in the abelian case it is not gauge invariant anymore

Proof:

$$
\begin{gathered}
F^{a}_{\mu\nu}{}' = \partial_\mu A^{a\prime}_\nu - \partial_\nu A^{a\prime}_\mu + g f_{abc} A^{b\prime}_\mu A^{c\prime}_\nu = \\
= \partial_\mu (A^a_\nu + D^{ab}_\nu \omega_b) - \partial_\nu (A^a_\mu + D^{ab}_\mu \omega_b) + g f_{abc} (A^b_\mu + D^{bd}_\mu \omega_d)(A^c_\nu + D^{ce}_\nu \omega_e) = \\
= \partial_\mu A^a_\nu - \partial_\nu A^a_\mu + g f_{abc} A^b_\mu A^c_\nu + \partial_\mu (D^{ab}_\nu \omega_b) - \partial_\nu (D^{ab}_\mu \omega_b) + \dots \\
\dots + g f_{abc} \Big(A^b_\mu D^{ce}_\nu \omega_e + A^c_\nu D^{bd}_\mu \omega_d + \mathcal{O}(\omega^2) \Big) = F^a_{\mu\nu} + \delta F^a_{\mu\nu}
\end{gathered}
$$

neglecting terms of order $\mathcal{O}(\omega^2)$ this can be written as

$$
\begin{gathered}
\delta F^a_{\mu\nu} = (\partial_\mu D^{ab}_\nu)\omega_b + D^{ab}_\nu \partial_\mu \omega_b - (\partial_\nu D^{ab}_\mu)\omega_b - D^{ab}_\mu \partial_\nu \omega_b + g f_{abc} (A^b_\mu \partial_\nu \omega_c + A^c_\nu \partial_\mu \omega_b) - \dots \\
\dots - g^2 f_{abc} \Big(f_{cel} A^b_\mu A^l_\nu \omega_e + f_{bdl} A^c_\nu A^l_\mu \omega_d \Big) = \\
= \partial_\mu \partial_\nu \omega_a - g f_{abc} \partial_\mu A^c_\nu \omega_b + \partial_\nu \partial_\nu \omega_a - g f_{abc} A^c_\nu \partial_\mu \omega_b - (\partial_\nu \partial_\mu \omega_a - g f_{abc} \partial_\nu A^c_\mu \omega_b) - \dots \\
\dots - (\partial_\mu \partial_\nu \omega_a - g f_{abc} A^c_\mu \partial_\nu \omega_b) + g f_{abc} (A^b_\mu \partial_\nu \omega_c + A^c_\nu \partial_\mu \omega_b) - g^2 f_{abc} \Big(f_{cel} A^b_\mu A^l_\nu \omega_e + f_{bdl} A^c_\nu A^l_\mu \omega_d \Big) = \\
= g f_{abc} (\partial_\nu A^c_\mu \omega_b + A^c_\mu \partial_\nu \omega_b - \partial_\mu A^c_\nu \omega_b - A^c_\nu \partial_\mu \omega_b + A^b_\mu \partial_\nu \omega_c + A^c_\nu \partial_\mu \omega_b) - \dots \\
\dots - g^2 f_{abc} \Big(f_{cel} A^b_\mu A^l_\nu \omega_e + f_{bdl} A^c_\nu A^l_\mu \omega_d \Big)
\end{gathered}
$$

the $\mathcal{O}(g)$ term simplifies by using anti-symmetry of the structure constants

$$
-g f_{abc} (\partial_\mu A^c_\nu - \partial_\nu A^c_\mu) \omega_b
$$

and the $\mathcal{O}(g^2)$ term can be simplified by renaming dummy indices and using the jacobi identity

$$
\begin{gathered}
-g^2 f_{abc} \Big(f_{cel} A^b_\mu A^l_\nu \omega_e + f_{bdl} A^c_\nu A^l_\mu \omega_d \Big) = -g^2 f_{abc} \Big(f_{cde} A^b_\mu A^e_\nu \omega_d + f_{bde} A^e_\mu A^c_\nu \omega_d \Big) = \\
= -g^2 \Big(f_{abc} f_{cde} A^b_\mu A^e_\nu \omega_d + f_{ace} f_{cdb} A^b_\mu A^e_\nu \omega_d \Big) = -g^2 \Big(f_{abc} f_{cde} + f_{ace} f_{cdb} \Big) A^b_\mu A^e_\nu \omega_d = \\
= g^2 f_{ebc} f_{adc} A^b_\mu A^e_\nu \omega_d = -g^2 f_{abc} f_{cde} A^d_\mu A^e_\nu \omega_b
\end{gathered}
$$

all together this yields

$$
\delta F^a_{\mu\nu} = -g f_{abc} \Big(\partial_\mu A^c_\nu - \partial_\nu A^c_\mu + g f_{cde} A^d_\mu A^e_\nu \Big) \omega_b = -g f_{abc} F^c_{\mu\nu} \omega_b
$$

The absence of gauge invariance for the non-abelian field strength tensor means that the equivalentens of electric/magnetic fields and the charge are not physically observable. This also eliminates the possibility to formulate the theory in terms of these objects rather than the gauge fields as is possible in the abelian case and briefly touched upon in Sec. 4.1.

2. Quantization of gauge theories

In order to quantize gauge theories, the easiest way is to use the path integral formalism. The partition function and the correlation functions, which are the fundamental quantities of the theory are given in this formulation by [10]

$$\begin{aligned} Z &= \int \mathcal{D}\Phi\mathcal{D}A \exp^{iS[A^a_\mu,\Phi_i]} \\ \langle\mathcal{O}\rangle &= \int \mathcal{D}\Phi\mathcal{D}A\, \mathcal{O}(A_\mu,\Phi_i) \exp^{iS[A^a_\mu,\Phi_i]} \end{aligned} \tag{2.1}$$

where $\mathcal{O}$ is a gauge invariant combination of fields and Φ_i are any other fields besides the gauge field. The problem with this however is twofold. For one, before the path integral can be used, it has to be either gauge fixed in the continuum or regulated on the lattice. In the continuum this already leads to problems beyond perturbation theory where the usual Faddeev-Popov gauge fixing procedure breaks down which will be discussed in Sec. 3.2. Another issue that appears non-perturbatively, that is remedied in perturbation theory by the use of BRST symmetry for the asymptotic states, is the gauge variance of the elementary fields and correlation functions thereof. The fields present in the Lagrangian that defines the theory are all gauge dependent and the only reason this is not a problem in perturbation theory is the residual symmetry between the gauge field, ghosts and the Nakanishi-Lautrup field, called BRST symmetry. It is this symmetry that makes it possible to differentiate between physical and unphysical states. Non-perturbatively this symmetry can not be easily guaranteed anymore, which will be elaborated in more detail in Sec. 3.2. A possible solution is using composite fields and comes in different forms for abelian and non-abelian gauge theories. This will be explained in Ch. 4 after briefly outlining the usual Faddeev-Popov gauge fixing procedure Ch. 2 and the problems that arise beyond perturbation theory Sec. 3.2.

2.1. Abelian quantization

The partition function/path integral for the gauge field is given by (2.1) where the integration measure is gauge invariant by construction and so is the action. The weighting is the same for all configurations related by a gauge transformation, which are called a gauge orbit. This leads to a divergence because all the different configurations are added constructively. Even though the path integral seems to be formally ill defined it is possible to solve it exactly in two dimensions for some theories [13],[14] which suggests that we are only incapable of dealing with it properly and the continious infinity of equivalent gauge field configurations are not actually a problem. The standard way this problem is dealt with is a procedure developed by Faddeev and Popov [15] in which a gauge fixing condition $C_a[A_\mu] = 0$ is used together with a functional delta function to pick out only the gauge copy satisfying the gauge fixing condition. For this one uses the following relation

$$\Delta[A^a_\mu]^{-1} = \int \mathcal{D}g\delta(C_a[A^{a;g}_\mu]) \to 1 = \Delta[A^a_\mu] \int \mathcal{D}g\delta(C_a[A^{a;g}_\mu]) \tag{2.2}$$

where g labels the elements of the gauge group and $A_\mu^{a,g}$ stands for the gauge transformed field and the integral is over the gauge group and defined as [16]

$$\mathcal{D}g = I(\vec{\omega}) \prod_i \mathcal{D}\omega_i \tag{2.3}$$

with $I(\vec{\omega})$ being the Haar measure defined as

$$\begin{aligned} I(\vec{\omega}) &= \frac{1}{V_G} det\Big(M\Big) \\ M_{ab} &= -\frac{1}{k} tr\left(\tau_a g^{-1} \frac{\delta g}{\delta \omega_b}\right) \quad \text{with} \quad k = tr\Big(\tau_a \tau_a\Big) \\ V_G &= \int det\Big(M\Big) \prod_i \mathcal{D}\omega_i \\ \int \mathcal{D}g &= 1 \end{aligned} \tag{2.4}$$

Demanding that the gauge fixing conditions $C_a[A_\mu^{a,g}] = 0$ are bijective with respect to ω_b in (2.2), a transformation of integration variables from g to C leads to

$$\begin{aligned} \Delta[A_\mu^a]^{-1} &= \int \mathcal{D}C \left(det \frac{\delta C_a[A_\mu^{a,g}(x)]}{\delta \omega_b(y)} \right)^{-1} \delta(C_a) \\ &= \left(det \frac{\delta C_a[A_\mu^{a,g}(x)]}{\delta \omega_b(y)} \right)^{-1}_{C_a=0} = det M_{ab}(x,y) \end{aligned} \tag{2.5}$$

which after inserting in (2.1) gives the gauge fixed path integral [10]

$$Z = \int \mathcal{D}g \int \mathcal{D}A \, det\Big(M_{ab}\Big) \delta(C_a[A_\mu^{a,g}]) \exp^{iS[A_\mu^a]} \tag{2.6}$$

The determinant in (2.5) is called Faddeev-Popov determinant and the operator in it Faddeev-Popov operator. At this point it is important to note, that the inversion of (2.2) is only possible if the Faddeev-Popov operator does not have zero eigenvalues, which as it turns out is only valid in the perturbative regime. To proceed further a choice of gauge is necessary, which in this case will be a general covariant gauge given by

$$\begin{aligned} D_a[A_\mu^{a,g}] &= C_a[A_\mu^{a,g}] + \Lambda_a(x) \\ C_a[A_\mu^{a,g}] &= \partial_\mu A_a^{\mu,g} \end{aligned} \tag{2.7}$$

with arbitrary functions $\Lambda_a(x)$ which leads to

$$Z = \int \mathcal{D}g \int \mathcal{D}A \left(det \frac{\delta D_a[A_\mu^a]}{\delta g} \right) \delta(C_a[A_\mu^{a,g}] + \Lambda_a) \exp^{iS[A_\mu^a]} \tag{2.8}$$

in order to not leave the gauge fixing condition implicit in all further calculations, it can be added as an extra term to the Lagrangian by replacing on the right hand side of (2.8) the gauge fixing delta function with a properly normalized linear combination of it, leading to [10]

$$Z = N(\xi) \int \mathcal{D}\Lambda \int \mathcal{D}g \int \mathcal{D}A \, det\left(\frac{\delta C[A^a_\mu]}{\delta g}\right) \exp\left(-\frac{i}{2\xi} \int d^d x \Lambda^2\right) \delta(C[A^{a,g}_\mu] + \Lambda_a) \exp^{iS[A^a_\mu]} \tag{2.9}$$

In the abelian case the Faddeev-Popov determinant is independant of the gauge fields in this choice of gauge and can be absorbed into the normalization together with the integral over the gauge group, since the action $S[A^a_\mu]$ and the integration measure $\mathcal{D}A$ are gauge invariant so that the gauge field A^a_μ can be replaced with the transformed gauge field $A^{a,g}_\mu$ everywhere and $A^{a,g}_\mu$ becomes just a dummy variable and can be changed back to A^a_μ. Using the delta function and absorbing constant factors into the measure, this leads to

$$Z = \int \mathcal{D}A \, \exp\left(iS[A^a_\mu] - \frac{i}{2\xi} \int d^d x (\partial_\mu A^\mu_a)^2\right) \tag{2.10}$$

which is the final gauge fixed path integral with an extra term in the Lagrangian corresponding to the gauge fixing condition.

2.2. Non-abelian gauge theory

The only difference to the abelian procedure is that the Faddeev-Popov determinant is not independent of the gauge field anymore and as such can't be absorbed into the normalization. In the generalized covariant gauge the Faddeev-Popov determinant is given by

$$det\left(M_{ab}\right) = det\left(\frac{\delta C_a[A^{a,g}_\mu]}{\delta \omega_b}\right) = det\left(\partial_\mu D^\mu_{ab}\right) = det\left(\delta_{ab}\partial^2 - g f_{abc} \partial_\mu A^\mu_c\right)$$

Starting from 2.9 everything goes through the same way as in the abelian case except that the Faddeev-Popov determinant remains inside the path integral over gauge fields. It is again independent of the gauge functions $\omega_a(x)$ for linear gauge fixing conditions like the covariant gauge, such that the integral over the gauge group can be factored out by replacing A^a_μ with $A^{a,g}_\mu$ everywhere because the measure and the action are gauge invariant and then changing back again. This leaves

$$Z = \int \mathcal{D}A \, det\left(\frac{\delta C_a[A^{a,g}_\mu]}{\delta \omega_b}\right) \exp\left(iS[A^a_\mu] - \frac{i}{2\xi} \int d^d x (\partial_\mu A^\mu_a)^2\right)$$

where the Faddeev-Popov determinant can be rewritten with the help of auxiliary scalar Grassmann fields called Faddeev-Popov ghosts as [15]

$$det\left(\frac{\delta C_a[A^{a,g}_\mu]}{\delta \omega_b}\right) = det\left(\partial_\mu D^\mu_{ab}\right) = \int \mathcal{D}c \mathcal{D}\bar{c} \exp\left(-i \int dx \bar{c}_a \partial_\mu D^\mu_{ab} c_b\right)$$

which finally leads to

$$\begin{aligned} Z &= \int \mathcal{D}A\mathcal{D}c\mathcal{D}\bar{c}\, \exp\Bigg(i\int dx\Bigg(-\frac{1}{4}F^{a}_{\mu\nu}F^{\mu\nu}_{a} - \frac{1}{2\xi}(\partial_\mu A^\mu_a)^2 - \bar{c}_a\partial_\mu D^\mu_{ab}c_b\Bigg)\Bigg) \\ &= \int \mathcal{D}A\mathcal{D}c\mathcal{D}\bar{c}\, \exp\Bigg(iS_0 + iS_{GF} + iS_{Ghost}\Bigg) \end{aligned} \tag{2.11}$$

the gauge fixed path integral. However the form most suitable for studying the physical state space is arrived at after introducing another field called the Nakanishi-Lautrup field, which is an auxiliary field since it has no kinetic term in the Lagrangian, and is essentially just a constraint similar to a Lagrangian multiplier [17]. Using

$$\exp\Bigg(-\frac{i}{2\xi}\int dx C_a[A^a_\mu]^2\Bigg) = \int \mathcal{D}b\exp\Bigg(i\int dx\Big(\frac{\xi}{2}b_a b^a + b^a C_a\Big)\Bigg) \tag{2.12}$$

it is possible to rewrite (2.11) as [10]

$$Z = \int \mathcal{D}A\mathcal{D}b\mathcal{D}c\mathcal{D}\bar{c}\exp\Bigg(i\int dx\Bigg[-\frac{1}{4}F^a_{\mu\nu}F^{\mu\nu}_a + \frac{\xi}{2}b_a b^a + b^a C_a - \bar{c}_a\partial_\mu D^\mu_{ab}c_b\Bigg]\Bigg) \tag{2.13}$$

the final form of the gauge fixed path integral and the starting point for investigating the physical state space, which means states with positive norm, such that a probability interpretation is possible and they are gauge invariant.

3. BRST symmetry and gauge invariance

3.1. Perturbative BRST symmetry

The gauge fixed partition function (2.13) exhibits a global symmetry first found by Becchi, Rouet, Stora and Tyutin [18] simply called BRST symmetry that connects the different fields atleast in linear gauges, which includes the covariant gauge. The BRST transformations are given in their infinitesimal form by

$$\begin{aligned}
&\delta_B A_\mu^a = \lambda s A_\mu = \lambda D_\mu^{ab} c_b \\
&\delta_B c_a = \lambda s c_a = -\lambda \frac{g}{2} f_{abc} c_b c_c \\
&\delta_B \bar{c}_a = \lambda s \bar{c}_a = \lambda b_a \\
&\delta_B b_a = \lambda s b_a = 0 \\
&\delta_B \Psi_m^\pm = ig\lambda c_a \tau_{mn}^a \Psi_n^\pm \qquad \pm \text{ bosonic/fermionic matter}
\end{aligned} \tag{3.1}$$

where λ is a grassmann parameter. It can be shown that these transformations leave the gauge fixed Lagrangian invariant. For the classical part it is trivial since the BRST-transformations for the gauge field/matter are merely normal gauge transformations with the real parameters λc_a and for the rest it can be shown aswell [10].
Another feature of BRST transformations is that they are nilpotent [10]

$$s^2 = 0 \tag{3.2}$$

and that the gauge fixing part of the Lagrangian can be written as

$$\mathcal{L}_{GF} = \frac{\xi}{2} b^a b_a + b^a D_a + \bar{c}_a \partial^\mu D_\mu^{ab} c_b = s\left(\bar{c}_a (\frac{\xi}{2} b^a + D^a)\right) \tag{3.3}$$

thereby making it trivially invariant under BRST transformations. To study the effects of BRST transformations on the state space it is useful to consider the theory in canonical quantization, in which case the generator of BRST transformations is the Noether charge Q_B which acts like s and is given by [19]

$$Q_B = \int d^3x \Big(b_a D_0^{ab} c_b - c_a \partial_0 b^a + \frac{1}{2} g f_{abc} c_b c_c \partial_0 \bar{c}_a \Big) \tag{3.4}$$

For a state to be BRST invariant translates in this formalism to it being destroyed by Q_B. It turns out that the criterion [10]

$$\begin{gathered}
Q_B |\Psi\rangle = 0 \\
[Q_B, \Psi]_\pm = s|\Psi\rangle
\end{gathered} \tag{3.5}$$

is sufficient to determine the physical states. A consequence of the nilpotency is that the state space is separated into three subspaces [10]

- states $|\Psi_0\rangle$ that are obtained by Q_B from other states
  $\rightarrow V_0 = \Big\{|\Psi_0\rangle = Q_B|\Psi_2\rangle, \text{ with } |\Psi_2\rangle \in V_2\Big\}$
- states $|\Psi_1\rangle$ annihilated by Q_B that are not in V_0
  $\rightarrow V_1 = \{Q_B|\Psi_1\rangle = 0, \text{ with } |\Psi_1\rangle \notin V_0\}$
- states $|\Psi_2\rangle$ that are not annihilated by Q_B
  $\rightarrow V_2 = \Big\{Q_B|\Psi_2\rangle \neq 0, \text{ with } |\Psi_2\rangle \in V_2\Big\}$

and since Q_B commutes with the Hamiltonian, states in one subspace remain there under time evolution. It can be shown, that all negative norm states are contained in V_2 which by criterion (3.5) is not physical [19]. The remaining subspaces satisfy 3.5 and can be considered the physical state space

$$V_p = V_0 \cup V_1$$

but since V_0 has zero norm and the inner product with states in V_1 vanishes, states in V_0 do not contribute. Thus the real physical state space would be the quotient space V_p/V_0.

Since perturbation theory is formulated in terms of asymptotic states, called in and out states, it is necessary to also know the asymptotic BRST transformations, but to arrive at these one merely has to turn off the coupling parameter adiabatically to get

$$\begin{aligned}
&\delta_B A^a_{\mu,as} = \lambda s A_{\mu,as} = \lambda \partial_\mu c_a \\
&\delta_B c_{a,as} = \lambda s c_{a,as} = 0 \\
&\delta_B \bar{c}_{a,as} = \lambda s \bar{c}_{a,as} = \lambda b_{a,as} \\
&\delta_B b_{a,as} = \lambda s b_{a,as} = 0 \\
&\delta_B \Psi^\pm_a = \lambda s \Psi^\pm_a = 0
\end{aligned} \tag{3.6}$$

This tells us that the transverse component of the gauge field as well as the matter fields are destroyed and thus belong to V_1, while the longitudinal part, which is the derivative acting on the ghost field since it gives a direction parallel to the momentum, remains together with the anti ghost $\bar{c}_{a,as}$ and so they belong to V_2. The ghost $c_{a,as}$ is produced by a BRST transformation from the longitudinal component of the gauge field and the Nakanishi-Lautrup field $b_{a,as}$ from the anti ghost $\bar{c}_{a,as}$ and as such they belong to V_0. It is by this construction that the physical states can be separated from the unphysical ones and this is also the reason why correlation functions of physical states are gauge invariant in perturbation theory even though the elementary fields themselves are not.

3.2. Non-perturbative BRST symmetry

The following is a short overview of some of the topics in non-perturbative BRST quantization, which is a topic of ongoing research and not at all settled and as such subject to change. Most of what is discussed in this section can be found in [20] for a more thorough treatment of this topic.

In the same way as in perturbation theory before sense can be made of the path integral, there needs to be some way to deal with the degeneracy of physically equivalent gauge field configurations. Thus some kind of gauge fixing needs to be applied and the first choice would be the Faddeev-Popov procedure, which leads to (2.13). In the manipulations that lead there the Faddeev-Popov determinant (2.2) had to be inverted which is only possible if it is non-zero, which is the case if there are no zero modes for the Faddeev-Popov operator. This is where the problems beyond perturbation theory begin. The Faddeev-Popov operator in Landau gauge can be written as

$$M_{ab} = \frac{\delta C_a[A_\mu^{a,g}]}{\delta \omega_b} = \partial_\mu \Big(A_a^\mu + D_{ab}^\mu \omega_b \Big) = \partial_\mu D_{ab}^\mu \tag{3.7}$$

where for the perturbative quantization due to the fact that only gauge transformations are considered that can be built up from infinitesimal ones, the Faddev-Popov operator reduces to

$$M_{ab} = \delta_{ab} \partial^2 - g f_{abc} \partial_\mu A_c^\mu = \delta_{ab} \partial^2 \tag{3.8}$$

because of $g \rightarrow 0$ or in the abelian case since $f_{abc} = 0$. But this is just the Laplace operator which is known to be positiv definite and thus have only positive eigenvalues. This together with the gauge fixing condition being analytic is necessary for it to have a unique solution and does not hold beyond perturbation theory [21]. Non-perturbatively there exist gauge transformations, which cannot be built up from infinitesimal ones, so called large gauge transformations [22], for which $g \rightarrow 0$ does not hold and the Faddeev-Popov operator no longer reduces to the Laplacian [20][21]. These so called large gauge transformations lead to field configurations which also fulfill the gauge condition, called Gribov copies [20][21]. This fact is also called Gribov-Singer ambiguity and can be expressed as

$$\begin{gathered} A_a^{\mu\prime} = A_a^\mu + D_{ab}^\mu \omega_b \\ \partial_\mu A_a^{\mu\prime} = \partial_\mu A_a^\mu = 0 \longrightarrow \partial_\mu A_a^{\mu\prime} = \partial_\mu \Big(A_a^\mu + D_{ab}^\mu \omega_b \Big) = \partial_\mu A_a^\mu + \partial_\mu D_{ab}^\mu \omega_b \\ \longrightarrow \partial_\mu D_{ab}^\mu \omega_b = 0 \end{gathered} \tag{3.9}$$

and as one can see it is the zero modes of the Faddeev-Popov operator

$$\partial_\mu D_{ab}^\mu \omega_b = \lambda \omega_b \quad \text{with} \quad \lambda = 0 \tag{3.10}$$

that determine Gribov copies [20]. Additionally, it is also possible for Gribov copies to have negative eigenvalues in their spectrum, leading to cancellations in the path integral that modify the physical states found beyond perturbation theory [20][23]. Thus the problem is to find a gauge fixing condition that uniquely selects a field configuration, which as can be shown must necessarily be non-local. [20][24]

To get a better understanding of the problem, one can picture the gauge fixing condition as a hypersurface in the gauge field configuration space. Now the set of all field configurations that result from gauge transformations of a physical configuration can be visualized as a curve in this space, called the gauge orbit [11]. The different gauge orbits do not intersect and fill the space densely. Gribov copies are now the intersection points of the gauge orbit with the hypersurface, which always intersects orthogonally in order to fulfill the perturbative gauge fixing condition and the set of all Gribov copies is called the residual orbit [20]. This hypersurface can be organized into different regions depending on the eigenvalue spectrum λ (3.10) of the Gribov copies [21]. The first Gribov region is defined as the section where the Faddeev-Popov operator is positive semi-definite i.e., has no negative eigenvalues [20][21]. It can be shown that the zero eigenvalues all lie on the boundary called the Gribov horizon and that field amplitudes are bounded within [20]. The first Gribov region also contains the origin of field space and therefore perturbation theory [20][21]. Crossing the boundary increases the number of negative eigenvalues by one, such that inside the Nth Gribov region the Faddeev-popov operator has $N-1$ negative eigenvalues [20][21]. The residual orbit is expected to have Gribov copies in every Gribov region though this has not been proven yet.

The starting point for all further attempts to resolve the Gribov-Singer ambiguity is to limit field configurations to the first Gribov region by including a functional Θ-function in the gauge fixed path integral [20][21][25]

$$\begin{aligned} Z &= \lim_{\xi\to 0}\int \mathcal{D}A_\mu \mathcal{D}c\mathcal{D}\bar{c}\,\Theta(-\partial_\mu D^\mu_{ab})\exp^{-\int d^4x\left(\mathcal{L}_A+\mathcal{L}_{GF}+\mathcal{L}_{ghost}\right)} \\ \Theta(-\partial_\mu D^\mu_{ab}) &= \prod_i \Theta(\lambda_i) \end{aligned} \tag{3.11}$$

thereby eliminating the cancellations associated with the negative eigenvalues and also some regularization needs to be employed to take care of the zero modes on the Gribov horizon. However there are still multiple Gribov copies in the first Gribov region left especially on the horizon [26] and no general, method independent prescription on how to effectively implement the restriction to the first Gribov region has been found [20].
One approach is to approximate the Θ-function with a delta function since most of the volume in high dimensional spaces is found around the boundary, which in the end leads to additional ghost fields and the so called Zwanziger Lagrangian [20][25].
Another approach is to randomly select a Gribov copy in the first Gribov region from every residual orbit. If the choice is ergodic, unbiased and well behaved this amounts to averaging over the residual orbit and therefore averaging gauge dependent quantities. The implementation outside lattice calculations is however not yet understood and there are only algorithms for lattice gauge theory [20][27][28].
Further prescriptions exist however none of them are practical for the continuum case [23][29][30][31] and the only known gauge that retains BRST invariance is the Fujikawa-Hirschfeld-Landau gauge [32][33], which essentially averages over all Gribov copies and the restriction to the first Gribov region is not possible. The problem lies in the fact that BRST transformations switch between the different Gribov copies which can be easily seen in the case of perturbative Landau gauge.

$$\partial^\mu\left(A^a_\mu+\delta_B A^a_\mu\right)=\partial^\mu\delta_B A^a_\mu=\partial^\mu D^{ab}_\mu(\lambda c_b) \tag{3.12}$$

So the only valid BRST transformations that do not violate the Landau gauge are those with zero modes of the Faddeev-Popov operator, i.e., Gribov copies. Unless the BRST transformations only convert among a subset of Gribov copies it is therefore necessary to include all of them to retain BRST symmetry [32][33].
The previous discussion shows that while it is possible, the construction of a BRST symmetry is exceedingly difficult in the non-perturbative case which makes it unsuitable to identify physical states beyond perturbation theory. Additionally the asymptotic states beyond perturbation theory are not the same ones anymore as can be seen in the case of QED with for example positronium or in QCD the hadrons. So even though BRST symmetry might yield gauge invariant results it still neglects the non-perturbative states.

4. Composite states and gauge invariance

Since the spectrum beyond perturbation theory also includes bound states which are composite fields it is natural to try to achieve gauge invariance through those. Also the argument that there is no valid target for the BRST transformation of the ghost breaks down together with the argument that the transverse part of the gauge field vanishes under BRST transformation since now the coupling is not turned of adiabatically to get the free separated wavepacket in and out states that are used in perturbation theory.
Thus a certain way to guarantee gauge invariance is to make all the fields used in correlators gauge invariant themselves which works diffferently for abelian/non-abelian theories.

4.1. Abelian gauge theories

To see that the transverse part of the gauge field does not transform under gauge transformations consider it in momentum space [34]

$$\left(g_{\mu\nu} - \frac{p_\mu p_\nu}{p^2}\right) A^{\mu\prime} = \left(g_{\mu\nu} - \frac{p_\mu p_\nu}{p^2}\right)(A^\mu + p^\mu g(p)) = \left(g_{\mu\nu} - \frac{p_\mu p_\nu}{p^2}\right) A^\mu \tag{4.1}$$

Using this to define the physical gauge field as

$$A^\mu_P = \left(g_{\mu\nu} - \frac{p_\mu p_\nu}{p^2}\right) A^\mu \tag{4.2}$$

and Fourier transforming it back to position space leads to [34]

$$A^P_\mu(x) = \int d^4p \left(g_{\mu\nu} - \frac{p_\mu p_\nu}{p^2}\right) A_\mu(p) \exp^{ipx} = \left(g_{\mu\nu} \int d^4y \delta(x-y) - \frac{1}{4\pi} \int d^4y \frac{\partial_\mu \partial_\nu}{|x-y|}\right) A^\nu(y) \tag{4.3}$$

which is non-local and transverse. So it seems that one needs to give up on locality in order to get a gauge invariant theory beyond perturbation theory as seen by the necessity of non-local gauge fixing conditions for the BRST construction. It is also possible to create such a gauge invariant construction for the fermions by using the Dirac phase [34][35]

$$D(x) = \exp\left(-ie \int_x^\infty dy_\mu A^\mu(y)\right) \tag{4.4}$$

which transforms as

$$D(x)' = \exp\left(-ie \int_x^\infty dy_\mu \left(A^\mu(y) + \partial^\mu g(y)\right)\right) = D(x) \exp\left(-ieg(x)\right) \tag{4.5}$$

where it has been assumed that the gauge functions vanish at infinity. This means the extra factor cancels the transformation of the fermion such that

$$\Psi_P(x) = D(x)\Psi(x) \tag{4.6}$$

is gauge invariant and thus a physical fermion. This is an almost-local object called Dirac string and even though it can be shown that physical processes do not depend on the form of the Dirac string it creates paths that can not be contracted and thus the non-locality can not be ignored [36]. The Dirac string transports information of coordinate systems from one point to another, thereby making them comparable. For small fields with line integrals of order one the Dirac phase can be expanded yielding corrections to the normal perturbative fermion one order higher $1+\mathcal{O}(e)$ in the coupling. The same goes for the physical gauge field (4.3) if the field is well localized and has a small amplitude the second term can be neglected yielding again the elementary gauge field.
Another way to ensure gauge invariance in an abelian gauge theory is to formulate the path integral in a gauge independant manner. One way of doing this is by changing variables from A_μ to either the electric/magnetic fields $\vec{E}, \vec{B}$ or the field strength tensor $F_{\mu\nu}$, which are both gauge invariant in an abelian gauge theory. Thus the path integral would read symbolically

$$Z = \begin{cases} \int \mathcal{D}\vec{E}\mathcal{D}\vec{B} det \left(\frac{\delta A_\mu(\vec{E},\vec{B})}{\delta(\vec{E},\vec{B})}\right) \exp\left(iS[\vec{E},\vec{B}]\right) & A_\mu \to (\vec{E},\vec{B}) \\ \int \mathcal{D}F_{\mu\nu} det \left(\frac{\delta A_\mu(\vec{E},\vec{B})}{\delta F_{\mu\nu}}\right) \exp\left(iS[F_{\mu\nu}]\right) & A_\mu \to F_{\mu\nu} \end{cases}$$

The determinant in this case is not just a Jacobian since the mapping from $A_\mu \to \vec{E}, \vec{B}$ is not unique. The result is a complicated expression that makes this approach unsuitable for any practical applications.

4.2. Non-abelian gauge theories

The same approach used in the abelian case does not work here since the gauge transformation $\partial_\mu g$ is replaced with $D_\mu^{ab}\omega_b$, which does not cancel anymore in the Dirac string because of the gauge field in the covariant derivate. A different approach is found in the use of products of fields like

$$\mathcal{O} = \begin{cases} \Psi^\dagger(x)\Psi(x) & \text{for the matter content} \\ F_{\mu\nu}F^{\mu\nu} & \text{for the gauge field} \end{cases} \tag{4.7}$$

which are gauge invariant by themselves and do not correspond to single particles but bound states. Another way to create gauge invariant objects is by using the Wilson line [37]

$$\begin{gathered} W(x,y) = \mathcal{P}\exp\left(-ig\int_{C_{x\to y}} dx_\mu A^\mu\right) \\ W(x,y)' = G(x)W(x,y)G^{-1}(y) \quad \text{for} \quad A_\mu \to A'_\mu \end{gathered} \tag{4.8}$$

here P denotes the path ordering symbol, which states that in an expansion of 4.8 the gauge fields have to be ordered in declining curve parameter from left to right, since they do not commute anymore. In the case of non-abelian gauge theories the Wilson line is algebra valued like the field and, even though it is not gauge invariant itself, it is possible to create a gauge invariant quantity by simply taking the trace of a closed Wilson line called Wilson loop and using the cyclic permutability of the trace

$$tr\left(W(x,x)\right) \quad \rightarrow \quad tr\left(G(x)W(x,x)G^{-1}(x)\right) = tr\left(W(x,x)\right) \tag{4.9}$$

It is possible to connect fields at different points with a Wilson line

$$\Psi^\dagger(x)W(x,y)\Psi(y) \rightarrow \Psi^\dagger(x)G^{-1}(x)G(x)W(x,y)G^{-1}(y)G(y)\Psi(y) = \Psi^\dagger(x)W(x,y)\Psi(y)$$

to create gauge invariant non-local objects which when expanding for small gauge fields again reduce to the regular propagator of perturbation theory.

$$\Psi^\dagger(x)W(x,y)\Psi(y) = \Psi^\dagger(x)\Big(1+\mathcal{O}(g)\Big)\Psi(y) = \Psi^\dagger(x)\Psi(y) \tag{4.10}$$

All of these objects require non-perturbative methods to investigate them, which makes them unsuitable for use in perturbation theory. Nevertheless it is possible to use composite fields similar to those encountered here in perturbation theory, which will be covered in the next chapter.

5. Gauge invariant perturbation theory

Provided a gauge theory posses an active Brout-Englert-Higgs effect, it is possible to formulate correlation functions entirely in terms of gauge invariant composite fields and expand them around the vacuum expectation value of the higgs field, to get a series of terms that are all computable with standard perturbation theory. This method was developed by Fröhlich, Morchio and Strocchi and is called gauge invariant perturbation theory [38][39]. The idea is that while in perturbation theory use is made of asymptotic states, which are single particle wave packets that are found to be gauge invariant by use of BRST symmetry, they are only a part of the non-perturbative spectrum since they do not include bound states which clearly also are a part of the theory, even for theories which are weakly coupled like QED. Bound states are described by composite fields and therefore non-perturbatively one is allowed to use composite fields to describe a state Ch. 4. With composite states it is possible to use combinations that result in gauge invariant states and the obvious candidate to build such composite states with is the higgs, which has spin zero, is uncharged and a weak isospin doublet. Thus the first step in the gauge invariant perturbation theory procedure is to formulate all quantities in a gauge invariant manner. For this to work however, there has to be an active BEH effect. The underlying mechanism by which non-perturbative correlation functions reduce to a sum of terms accessible with perturbation theory is called FMS mechanism and is the second step in gauge invariant perturbation theory.

The whole gauge invariant perturbation theory scheme will be layed out for the case of the standard model weak sector, without matter, given by the Lagrangian

$$\begin{aligned} \mathcal{L} &= -\frac{1}{4}F^a_{\mu\nu}F_a^{\mu\nu} + (D_\mu\Phi)^\dagger D^\mu\Phi - \gamma\left(\Phi^\dagger\Phi - \nu^2\right)^2 \\ F^a_{\mu\nu} &= \partial_\mu A^a_\nu - \partial_\nu A^a_\mu - g f_{abc} A^b_\mu A^c_\nu \\ D^{ab}_\mu &= \delta^{ab} - igA^c_\mu \tau^{ab}_c \end{aligned} \tag{5.1}$$

with Φ the higgs doublet, A^a_μ the SU(2) gauge field, g the gauge coupling, γ and ν parameters of the higgs potential, τ^{ab}_c the generators in the fundamental representation and f_{abc} the structure constants.

5.1. Gauge invariant formulation of elementary states

Any physical state must be such that only global quantum numbers like spin, parity and custodial index characterize it. This is achieved by adding a new global symmetry to the gauge symmetry, called custodial symmetry, which takes the place of flavor, since flavor itself is in a fixed generation nothing but weak isospin. In the end this symmetry will be broken by the Yukawa interaction, thereby creating the different masses for components of custodial multiplets. As a consequence the new flavor is no longer the same as the weak charge, which is gauge dependent and should not be observable but corresponds to the custodial charge. To differentiate between the indices for weak isospin and custodial symmetry, a bar will be added on top of the custodial index in the following.

The simplest object in this FMS picture would be a scalar field that is also a custodial singlet given by

[40],[41],[42]

$$\mathcal{O}(x) = \Phi^\dagger(x)\Phi(x) \tag{5.2}$$

the next more complicated object would be something that replaces fields in the fundamental representation of the gauge group, which in this case would be a custodial doublet [43][44]

$$F = X^\dagger f \Rightarrow F_{\tilde{a}}(x) = X^\dagger_{\tilde{a}a}(x) f_a(x) \quad \text{with} \quad X = \begin{pmatrix} \Phi_2^* & \Phi_1 \\ -\Phi_1^* & \Phi_2 \end{pmatrix} \tag{5.3}$$

with f a field in the fundamental representation, a and $\tilde{a}$ denoting flavor/custodial indices, Φ_i the components of the higgs doublet and $X^\dagger$ a matrix representation of the higgs field which transforms under gauge and custodial transformations like

$$X \rightarrow \begin{cases} XC & \text{for custodial transformations } C \\ GX & \text{for gauge transformations } G \end{cases} \tag{5.4}$$

this leads to fields in the fundamental custodial representation transforming like

$$F \rightarrow \begin{cases} \left(XC\right)^\dagger f = C^\dagger X f = C^\dagger F & \text{for custodial transformations C} \\ \left(GX\right)^\dagger G f = X^\dagger G^\dagger G f = F & \text{for gauge transformations G} \end{cases} \tag{5.5}$$

For the adjoint representation the custodial version reads [41][44]

$$\mathcal{A}^{\bar{a}}_\mu = \tau^{\bar{a}}_{cb} \Phi^\dagger_b (D_\mu \Phi)_c \tag{5.6}$$

which is gauge invariant by virtue of the gauge covariant derivative

$$\mathcal{A}^{\bar{a}\,\prime}_\mu = \tau^{\bar{a}}_{bc} \Phi^\dagger_b G^\dagger (D'_\mu G \Phi)_c = \tau^{\bar{a}}_{bc} \Phi^\dagger_b G^\dagger G (D_\mu \Phi)_c = \mathcal{A}^{\bar{a}}_\mu$$

Finally the contraction of two field strength tensors $tr(F_{\mu\nu}F^{\mu\nu})$, called W-ball, the SU(2) equivalent of the glueball found in quantum chromodynamics.

5.2. FMS mechanism

Now that some of the custodial replacements for the relevant fields have been discussed, the next step is to apply the FMS mechanism, which consist of writing the correlation functions in terms of the composite fields, expanding the higgs fields around the vacuum expectation value and finally expanding the resulting terms in the couplings [40][43][45]. This will be demonstrated for the propagator of the custodial singlet as well as the custodial doublet.

Starting with the higgs field, a gauge has to be chosen such that the vacuum excpectation value (v.e.v) does not vanish, which in this case will be the Feynman t'Hooft gauge [40],[42]

$$\vec{\Phi}(x) = \nu\vec{n} + \vec{\eta}(x)$$
$$\mathcal{O}(x) = \vec{\Phi}^\dagger\vec{\Phi} = \left(\nu\vec{n} + \vec{\eta}\right)^\dagger\left(\nu\vec{n} + \vec{\eta}\right) = \nu^2 + \nu(\vec{n}^\dagger\vec{\eta} + \vec{n}\vec{\eta}^\dagger) + \vec{\eta}^\dagger\vec{\eta} = \nu^2 + \nu Re(\vec{n}^\dagger\vec{\eta}) + \vec{\eta}^\dagger\vec{\eta}$$

with ν the norm of the higgs doublet, $\vec{n}$ the gauge group direction and $\vec{\eta}$ the higgs fields fluctuations around the vacuum value.
Then the propagator of the singlet state $\langle\mathcal{O}^\dagger(x)\mathcal{O}(y)\rangle$ is written down and expanded [40],[42]

$$\begin{aligned}
\left\langle\mathcal{O}^\dagger(x)\mathcal{O}(y)\right\rangle &= \left\langle\left(\nu^2 + 2\nu Re(\vec{n}^\dagger\vec{\eta}_x) + \vec{\eta}_x^\dagger\vec{\eta}_x\right)\left(\nu^2 + 2\nu Re(\vec{n}^\dagger\vec{\eta}_y) + \vec{\eta}_y^\dagger\vec{\eta}_y\right)\right\rangle \\
&= \nu^4 + \nu^2\left\langle\vec{\eta}_y^\dagger\vec{\eta}_y\right\rangle + 4\nu^2\left\langle Re(\vec{n}^\dagger\vec{\eta}_x\vec{n}^\dagger\vec{\eta}_y)\right\rangle + 2\nu\left\langle Re(\vec{n}^\dagger\vec{\eta}_x)\vec{\eta}_y^\dagger\vec{\eta}_y\right\rangle + ... \\
&\quad + \nu^2\left\langle\vec{\eta}_x^\dagger\vec{\eta}_x\right\rangle + 2\nu\left\langle Re(\vec{n}^\dagger\vec{\eta}_y)\vec{\eta}_x^\dagger\vec{\eta}_x\right\rangle + \left\langle\vec{\eta}_x^\dagger\vec{\eta}_x\vec{\eta}_y^\dagger\vec{\eta}_y\right\rangle \\
&= d + 2\nu\left(\left\langle Re(\vec{n}^\dagger\vec{\eta}_y)\vec{\eta}_x^\dagger\vec{\eta}_x\right\rangle + x \leftrightarrow y\right) + 4\nu^2\left\langle Re(\vec{n}^\dagger\vec{\eta}_x\vec{n}^\dagger\vec{\eta}_y)\right\rangle + \left\langle\vec{\eta}_x^\dagger\vec{\eta}_x\vec{\eta}_y^\dagger\vec{\eta}_y\right\rangle
\end{aligned} \tag{5.7}$$

where d are the constant terms and $\langle\vec{\eta}^\dagger(x)\vec{\eta}(x)\rangle = c.$ together with $\langle\vec{\eta}(x)\rangle = 0$ has been used. The left hand side of (5.7) is gauge invariant by construction while the right hand side is only gauge invariant if all terms are included. Finally the terms on the right of (5.7) are expanded in a perturbative series which at leading order yields [40],[42]

$$\left\langle\mathcal{O}^\dagger(x)\mathcal{O}(y)\right\rangle = d' + 4\nu^2\left\langle Re(\vec{n}^\dagger\vec{\eta}_x)Re(\vec{n}^\dagger\vec{\eta}_y)\right\rangle_{tl} + \left\langle Re(\vec{n}^\dagger\vec{\eta}_x)Re(\vec{n}^\dagger\vec{\eta}_y)\right\rangle_{tl}^2 + \mathcal{O}(g^2, \gamma) \tag{5.8}$$

where the second term in (5.7) has been dropped since there is no possible contraction at leading order, the fourth term reduces to a product of two higgs propagators at leading order and tl denotes the tree level quantity. Thus the result given by gauge invariant perturbation theory for the propagator of the custodial scalar $\mathcal{O}$ at leading order is a term corresponding to the higgs propagator with a pole at the higgs mass and another term, which is strongly suppressed by the largeness of ν^2, with two higgs propagators starting and terminating at the same space-time points, which has a mass cut at twice the higgs mass [40][42]. This procedure can be applied to any correlation function and yields the standard model results at the appropriate order of expansion, a surprising result called bound-state-elementary-state duality (BSES-duality), which has been checked for different scattering processes. [41]

5.3. Bound-state-elementary-state duality

The equality of poles on both sides in leading order is called bound-state-elementary-state duality since it relates the masses of composite fields and therefore bound states to those of the elementary fields found in regular perturbation theory. The equivalence of both sides of (5.7) has been established for the pure standard model weak sector in lattice simulations [41][46][47]. Since the right hand side of (5.7) was expanded in a perturbative series it could be possible that there are additional non-perturbative poles arising spoiling this correspondence, however in the standard model this does not seem to be the case [48]. There are also contributions of the three and four-point Green's functions beyond leading order that could have a significant effect on the BSES-duality, however this is a topic of ongoing investigation and will be studied by someone else, as it is of no direct interest to this thesis.

One of the core features of gauge invariant perturbation theory is that it drastically changes the way one views scattering processes, as now the scattering states are not the usual asymptotic states, i.e: single particle wavepacket states but bound states with potentially complicated intermediate states. What is seen in scattering experiments are resonances in the cross section, which for leading order would coincide with the elementary particle resonances [41]. Beyond leading order it is not clear if the BSES-duality holds since not only are there additional terms, but also the calculation becomes renormalization scheme dependent and so do the mass poles [11]. Resonances in cross sections however are neither renormalization scheme/scale dependent nor gauge dependent, which leads one to believe that they correspond to the bound states and not the elementary states [41].

5.4. Application to QCD bound states and the proton in particular

Lastly one has to consider how to incorporate this into QCD bound states as they also need to be gauge invariant under SU(3) transformations. For a meson, which is a bound state made of a quark and an anti quark, it is possible to form a weak isospin scalar by using (5.3) as [40]

$$\bar{F}F = \bar{f}XX^\dagger f = \left(\Phi_2^*\bar{f}_1 - \Phi_1^*\bar{f}_2\,,\,\Phi_1\bar{f}_1 + \Phi_2\bar{f}_2\right)\begin{pmatrix}\Phi_2 f_1 - \Phi_1 f_2\\ \Phi_1^* f_1 + \Phi_2^* f_2\end{pmatrix}$$

which yields for the different custodial combinations

$$\begin{aligned}
\bar{F}_1F_1 &= (\Phi_2^*\bar{f}_1 - \Phi_1^*\bar{f}_2)(\Phi_2 f_1 - \Phi_1 f_2) = |\Phi_2|^2\bar{f}_1f_1 + |\Phi_1|^2\bar{f}_2f_2 - 2Re(\Phi_1\Phi_2^*\bar{f}_1f_2)\\
&= \nu^2\bar{f}_1f_1 + \mathcal{O}(\vec{\eta})\\
\bar{F}_2F_2 &= (\Phi_1\bar{f}_1 + \Phi_2\bar{f}_2)(\Phi_1^* f_1 + \Phi_2^* f_2) = |\Phi_1|^2\bar{f}_1f_1 + |\Phi_2|^2\bar{f}_2f_2 + 2Re(\Phi_1\Phi_2^*\bar{f}_1f_2)\\
&= \nu^2\bar{f}_2f_2 + \mathcal{O}(\vec{\eta})\\
\bar{F}_1F_2 &= (\Phi_2^*\bar{f}_1 - \Phi_1^*\bar{f}_2)(\Phi_1^* f_1 + \Phi_2^* f_2) = \Phi_1^*\Phi_2^*(\bar{f}_1f_1 - \bar{f}_2f_2) + \Phi_2^{*2}\bar{f}_1f_2 - \Phi_1^{*2}\bar{f}_2f_1\\
&= \nu^2\bar{f}_1f_2 + \mathcal{O}(\vec{\eta})\\
\bar{F}_2F_1 &= (\Phi_1\bar{f}_1 + \Phi_2\bar{f}_2)(\Phi_2 f_1 - \Phi_1 f_2) = \Phi_1\Phi_2(\bar{f}_1f_1 - \bar{f}_2f_2) - \Phi_1^2\bar{f}_1f_2 + \Phi_2^2\bar{f}_2f_1\\
&= \nu^2\bar{f}_2f_1 + \mathcal{O}(\vec{\eta})
\end{aligned}$$

where the higgs field was expanded around the vacuum with $\Phi_i = \nu\delta_{ij} + \eta_i$.
These are the equations for the propagators of the different custodial components and it is found that the propagators for fields of different custodial charge vanish to all orders. This is necessary in order for physical particles not to suddenly transform to different particles without any interaction mediating this transformation. As one can see, the products of bound state fields expands to the elementary field propagators, with the custodial index becoming the flavor index in leading order, which demonstrates the BSES-duality again. In a similar manner baryons are formed by [40][44]

$$\begin{aligned} \epsilon_{abc} F^a_{\tilde{i}} F^b_{\tilde{j}} F^c_{\tilde{k}} = \epsilon_{abc} X^\dagger_{\tilde{i}i} X^\dagger_{\tilde{j}j} X^\dagger_{\tilde{k}k} q^a_i q^b_j q^c_k \quad \text{three open custodial indices} \\ \epsilon_{abc} c_{ijkl} X^\dagger_{\tilde{i}l} q^a_i q^b_j q^c_k \quad \text{one open custodial index} \end{aligned} \tag{5.9}$$

with a, b, c color, i, j, k flavor and $\tilde{i}, \tilde{j}, \tilde{k}$ custodial indices and q^a_i quark fields. The coefficients c_{ijkl} have to be chosen such that the resulting state is a weak isospin scalar and totally anti-symmetric. Because baryons are also parity eigenstates the actual form of the bound state is slightly more complicated, as the right-handed components are SU(2) singlets. It is given by [49]

$$N^{\bar{a}\bar{b}\bar{c}} = \epsilon_{IJK} F^{\bar{a}\bar{b}\bar{c}}_{def} \Psi_{Id} \left(\Psi^T_{Je} C \gamma_5 \Psi_{Kf} \right) \tag{5.10}$$

where $F^{\bar{a}\bar{b}\bar{c}}_{def}$ are coefficients in custodial and right-handed flavor space, $C = i\gamma_2\gamma_0$ is the charge conjugation matrix, ϵ_{IJK} contracts to a color singlet and Ψ is an eight component spinor given by

$$\Psi = \begin{pmatrix} X^\dagger \Psi_L \\ U_R \\ D_R \end{pmatrix}$$

where Ψ_L is a left-handed doublet of two component Weyl spinors and U_R, D_R are also two component Weyl spinors, which are all singlets with respect to weak isospin. A more in-depth discussion of QCD bound states in gauge invariant perturbation theory can be found in [44].

A consequence of gauge invariant perturbation theory is that there must be additional higgs content in regular QCD bound states. While it is possible to study such bound states with the help of non-perturbative methods, like lattice QCD or by treating all terms resulting from the FMS mechanism perturbatively, another method, which one is naturally lead to, since this theory deals with bound state scattering, is the framework of parton distribution functions (PDFs). An area already well established in the perturbative treatment of QCD bound state scattering and most accessible to experimental verification, which is why this is the approach chosen for studying collisions of the proton-higgs bound states P' in the next chapter.

6. Perturbative treatment of $P'P'$ scattering

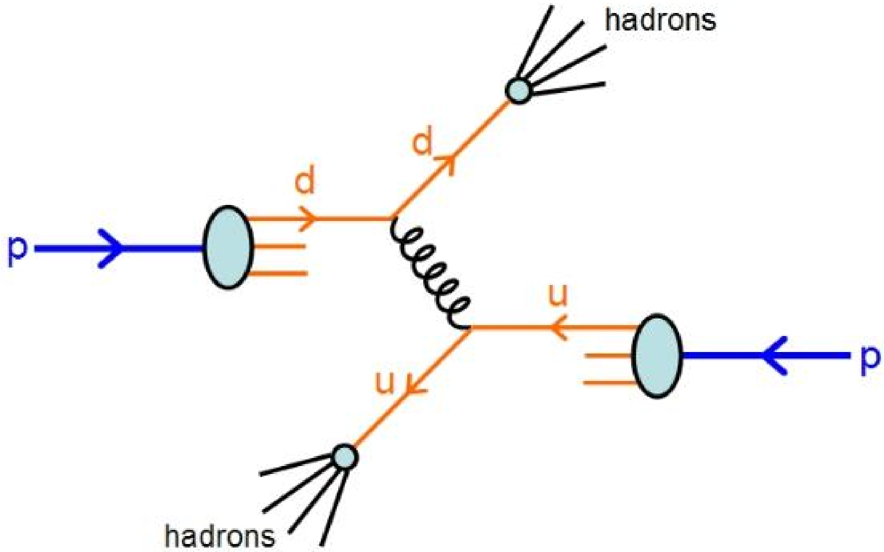

Fig. 6.1.: Proton-Proton scattering

Since the form of the proton operator is rather complicated by itself Sec. 5.4, when used in gauge invariant perturbation theory the different terms on the right hand side of (5.7) proliferate, especially when each term itself is expanded in a perturbative series. If one is only interested in showing there is a higgs component in the proton as well as investigating the magnitude of such a contribution and if it is compatible with experimental data, a much easier solution is to use parton distribution functions to describe it. Thus in the practical part of this thesis, the change in structure of the proton due to the higgs or simply the structure of the modified proton P', will be studied numerically in $P'P'$ collisions at $E_{cm} = 13$ TeV, with the help of a Monte-Carlo event generator framework, named Herwig [1][2][3]. The scattering will only be treated at leading order and the Q^2-evolution of the higgs PDF will be neglected, due to the limited scope of this thesis. For $P'P'$ collisions there are many possible final states with non-vanishing cross section and the choice of those most sensitive to an initial state higgs contribution is discussed in the next section.

6.1. Higgs sensitive final state selection

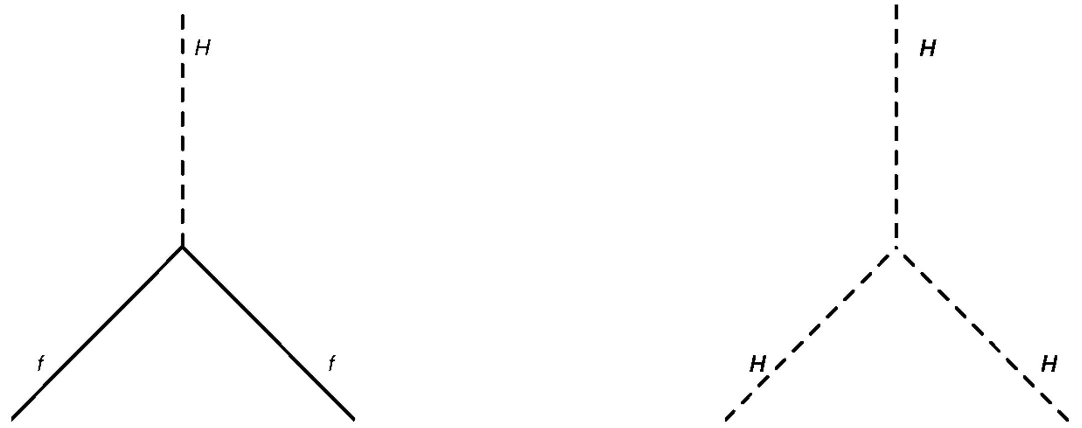

(a) $= -i\frac{m_f}{v} \overset{f=t}{\rightarrow} \approx -0.7i$ (b) $= -i3\frac{m_H^2}{v} \approx -190iGeV$

Fig. 6.2.: Feynman rules regarding higgs

It is useful to go over the Feynman rules for the higgs, which are given in 6.2, to get an understanding of the scattering processes most affected by an initial state higgs component. As one can see there, the fermion-higgs coupling is proportional to the mass of the particle with the proportionality constant being the inverse of the higgs VEV $\frac{1}{\nu} \approx 4 \cdot 10^{-3} GeV^{-1}$. Therefore only processes involving top quarks coupled to the higgs contribute an appreciable amount but since top quarks have a negligible PDF and are not implemented for the proton in Herwig, they are not considered in the initial state. Thus any process with tops in the final state should show an increased effect due to the inital state higgs contributions. Generally the total cross sections decrease rapidly with the number of particles in the parton level final state and therefore scattering processes will be limited to those with three particles in the final state or less, as those are also the most commonly measured at particle colliders for top quarks. For scattering processes with atleast one higgs in the initial state and a pair of top quarks in the final state, the only possibilities are gH and HH, since color conservation prohibits all amplitudes with only one quark in the initial state. So far the amount of processes has decreased considerably to just $gH \rightarrow t\bar{t}$ and $HH \rightarrow t\bar{t}$ but adding a Z boson to the final state gives a number of extra diagrams with ZH and HHH couplings making it more sensitive to the higgs. Also an observable that was found to be especially sensitive to the spin of the initial state particles and thus should also be to the additional spin-0 higgs component, is the angular distribution of the leptons produced in di-leptonic decay of a pair of top quarks given by $I \rightarrow t\bar{t}$ with $t \rightarrow W^+b$ and $W^+ \rightarrow \bar{l}\nu_l$. It turned out however, that this particular observable is less sensitive than expected and will therefore be mostly ignored and instead the biggest focus is put on the process $t\bar{t}Z$. All in all this leaves two scattering amplitudes $t\bar{t}$, $t\bar{t}Z$ and a specific observable for the di-leptonic decay channel in the amplitude for $t\bar{t}$, that should see a strong signal:

- $P'P' \rightarrow t\bar{t}$
- $P'P' \rightarrow t\bar{t}$ with $t \rightarrow b\bar{l}\nu_l$ and measurment of the angular differences $\Phi_{l,\bar{l}}$ of lepton pairs
- $P'P' \rightarrow t\bar{t}Z$

All Feynman diagrams contributing in leading order to the relevant cross sections are listed in the next section.

6.2. Feynman diagrams for $P'P' \to t\bar{t}$, $P'P' \to t\bar{t}Z$

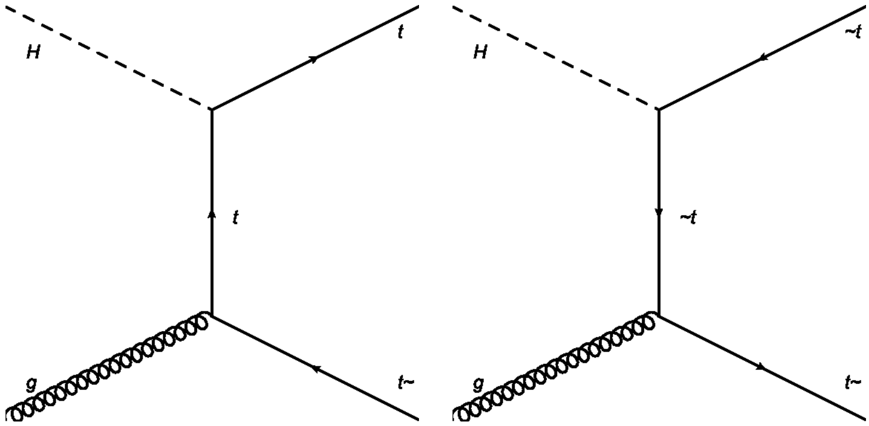

Fig. 6.3.: Feynman diagrams for $gH \to t\bar{t}$

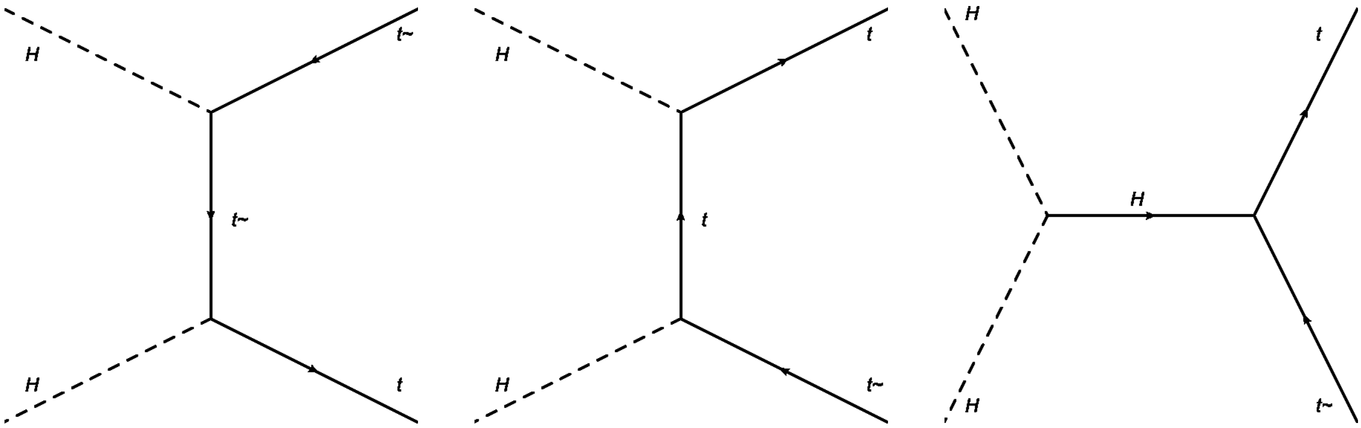

Fig. 6.4.: Feynman diagrams for $HH \to t\bar{t}$

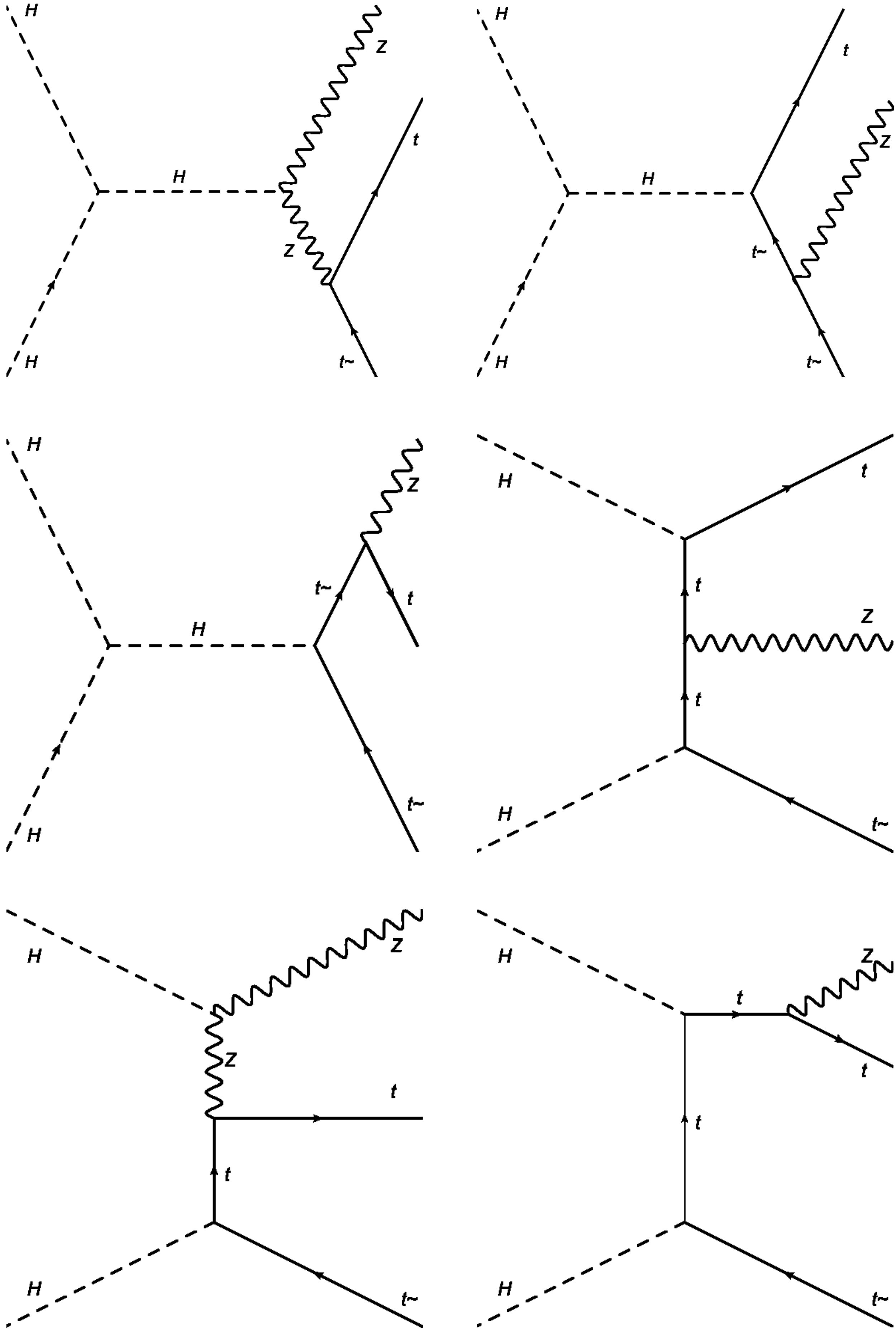

Fig. 6.5.: Feynman diagrams for $HH \to t\bar{t}Z$

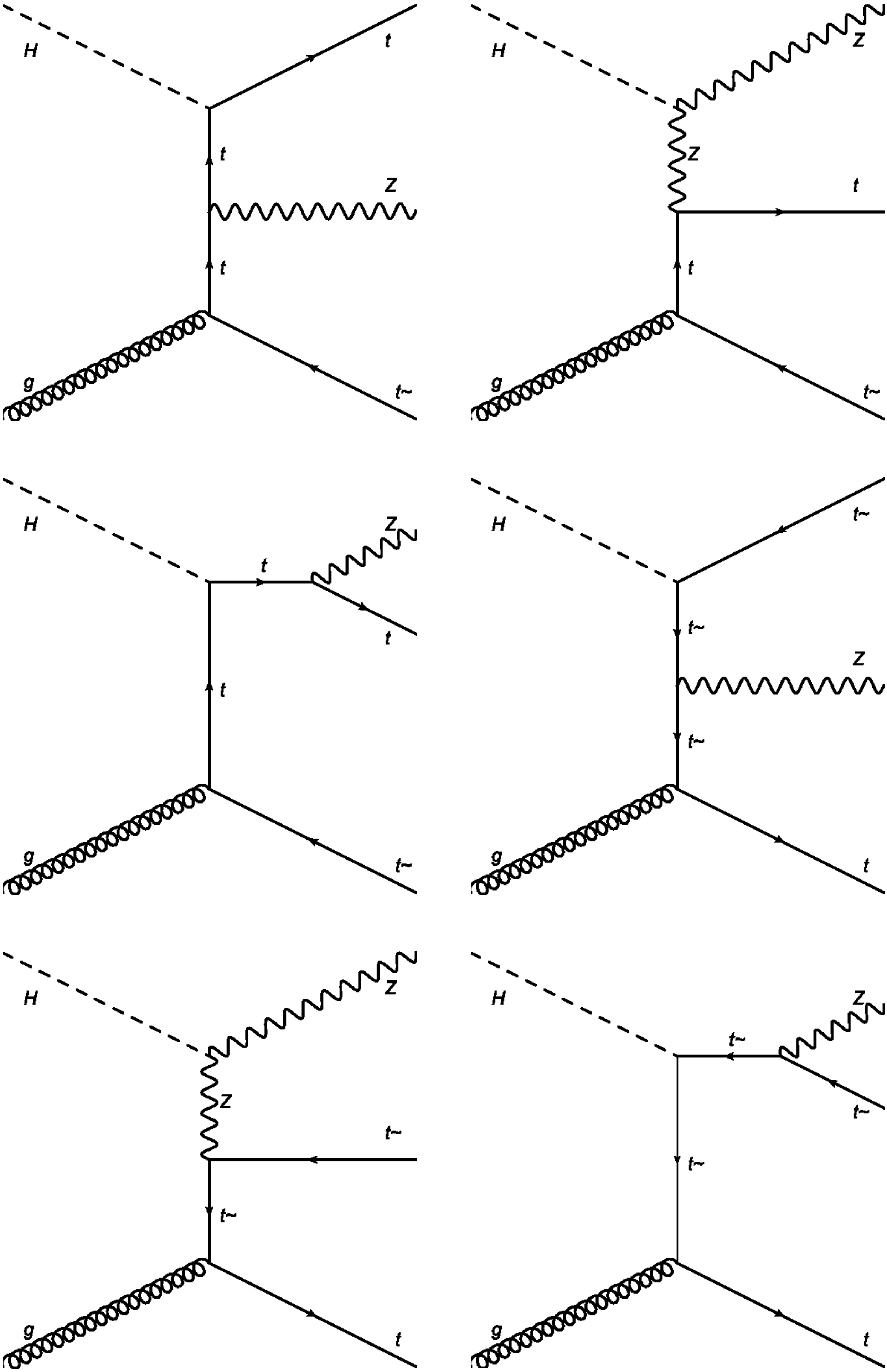

Fig. 6.6.: Feynman diagrams for $GH \rightarrow t\bar{t}Z$

6.3. Hadron-Hadron cross sections

Since the hadron-hadron cross section is used in Sec. 6.5, to derive a properly normalized formula for adding up the different contributions to $P'P' \to f$ scattering, that also takes into account the influence on the other PDFs due to the momentum sum rule, as well as to draw from the final state kinematic phase space in Herwig, it is briefly stated here.

$$\frac{d\sigma}{d\Omega} = \sum_{i,j} \int_0^1 \int_0^1 dx_1 dx_2 f_{i,H_1}(x_1, Q^2) f_{j,H_2}(x_2, Q^2) \frac{d\hat{\sigma}_{i,j\to f}}{d\Omega_f}(x_1 K_1, x_2 K_2, Q^2) \tag{6.1}$$

where H_1, H_2 stand for the hadrons, i, j label the quark/anti quark flavors as well as the gluon, Ω_f stands for all of the final state kinematic variables, x_1, x_2 are the momentum fractions of the partons, K_1, K_2 the momenta of the hadrons and the hat signifies the corresponding parton level quantity.

6.4. Sum rules

Since the parton distribution functions are supposed to describe number densities of partons in hadrons, they have to fulfill charge and momentum and flavor sum rules given by

Charge sum rule:

$$\sum_i \int_0^1 dx q_i f_{i,P}(x) = +e \tag{6.2}$$

Momentum sum rule:

$$\sum_i \int_0^1 dx x f_{i,P}(x) = 1 \tag{6.3}$$

Valence quark sum rules:

$$\begin{aligned} &\int_0^1 dx(f_{u,P}(x) - f_{\bar{u},P}(x)) = 2 \\ &\int_0^1 dx(f_{d,P}(x) - f_{\bar{d},P}(x)) = 1 \\ &\int_0^1 dx(f_{i,P}(x) - f_{\bar{i},P}(x)) = 0 \quad \text{for } i \neq \{u, d\} \end{aligned} \tag{6.4}$$

with P being the proton, i labeling the different parton species that contribute to the proton and $\bar{i}$ the anti particle to that parton.

Additionally to the direct impact of the higgs PDF on the structure of the proton, it also impacts it through the momentum sum rule by taking away from the other PDFs through their common normalization. This needs to be accounted for by a reweighting of the different contributing PDFs and is the topic of the next section.

6.5. Cross section normalization and PDF reweighting

Adding the higgs PDF to the proton means, that through the momentum sum rule, all the other PDFs are influenced as well and ideally one would refit the whole set including the higgs PDF. Since this is a big undertaking that needs sufficient motivation, it is hoped that this thesis might help in providing some of said motivation. In the absence of a global refit, the influence of the higgs PDF will be accounted for by an adequately normalized weighting of the different contributions to the complete $P'P'$ cross section. Starting out with (6.1) the effects of a modified proton would be to add terms with one or two higgs in the initial state, as well as change the remaining PDFs in the proton. The change of PDFs is assumed to be in the form of a rescaling, meaning shape independent $f_i(x)' = (1 - f_i)f_i(x)$ and the overall normalization will be factored out of the higgs PDF $f_H(x) = f_H f_H(x)$. Here the parameter f_H can be thought of as the fraction of higgs in the proton and will simply be called higgs fraction from here on out. Using the momentum sum rule, this leads to

$$\begin{aligned}1 = \int dxx\left(\sum_i f_i(x)' + f_H f_H(x)\right) &= \int dxx\left(\sum_i (1-f_i)f_i(x) + f_H f_H(x)\right)\\ &= \sum_i (1-f_i)F_i + f_H F_H\end{aligned} \tag{6.5}$$

where $F_i = \int_0^1 dxx f_i(x)$. At this point the only assumption made is, that the additional higgs PDF has not changed the shape of the other PDFs but merely rescaled them by a constant factor $f_i(x)' = (1 - f_i)f_i(x)$. Since the higgs content comes from the interaction with the higgs condensate, which is centered at zero momentum where the gluon PDF dominates all other parton contributions, one would set $f_i = 0$ for $i \neq g$ which yields

$$\begin{aligned}1 = \sum_i (1-f_i)F_i + f_H F_H &= 1 - f_g F_g + f_H F_H\\ \longrightarrow f_g &= \frac{F_H}{F_g} f_H\end{aligned} \tag{6.6}$$

The problem is, that for this to work, it is necessary to rescale the gluon PDFs used for the proton in Herwig or alternatively the contributing cross sections with gluons in the initial state σ_{gf}, σ_{gg} and σ_{gH}, which means splitting up the standard model proton in Herwig because it is treated as a whole. Therefore what is done instead is making the approximation $f_i = f_H = f$, which amounts to symmetrically subtracting from all contributing PDFs in the proton. This leads to

$$\begin{aligned}1 = (1-f)\sum_i F_i + fF_H &= 1 - f + fF_H\\ \longrightarrow f &= F_H f\end{aligned} \tag{6.7}$$

which for unnormalized higgs PDFs $F_H \neq 1$ violates the sum rule. Since the normalization was already split out and the different PDFs are in general not normalized to unity as well as some PDF models not being normalizable, this can not be avoided. For small higgs fractions $f \leq 0.1$ this leads for the considered parameter ranges to a maximum violation of $0 = f(F_H - 1) \approx 0.1(0.08 - 1) \approx -0.1$. In general for the model PDFs chosen, the narrower peaked, the bigger the violation because for a gaussian shape the integral $F_H(a, b) = \int_0^1 dxx \exp\left(-a(x-b)^2\right)$ is always between 0 for $a = \infty$ and 0.5 for $a = 0$ and therefore the violation of the sum rule between -0.1 and -0.5. Using this approximation the cross section for

$P'P'$ collision can be written as

$$\begin{aligned} \frac{1}{\sigma_{P'P'}(f)}\frac{d\sigma_{P'P'}}{d\Omega_f}(f) &= \int_0^1\int_0^1 dx_1 dx_2 \Bigg(\sum_{i,j} \frac{f_i(x_1)' f_j(x_2)'}{\sigma_{P'P'}(f)}\frac{d\hat{\sigma}_{ij\to f}}{d\Omega_f}(x_1,x_2) \\ &+ \frac{f_g(x_1)' f_H(x_2)}{\sigma_{P'P'}(f)}\frac{d\hat{\sigma}_{gH\to f}}{d\Omega_f}(x_1,x_2) + \frac{f_H(x_1) f_H(x_2)}{\sigma_{P'P'}(f)}\frac{d\hat{\sigma}_{HH\to f}}{d\Omega_f}(x_1,x_2)\Bigg) \\ &= \frac{(1-f)^2}{\sigma_{P'P'}(f)}\frac{d\sigma_{PP}}{d\Omega_f} + \frac{(1-f)f}{\sigma_{P'P'}(f)}\frac{d\sigma_{gH}}{d\Omega_f} + \frac{f^2}{\sigma_{P'P'}(f)}\frac{d\sigma_{HH}}{d\Omega_f} \end{aligned} \tag{6.8}$$

with

$$\sigma_{P'P'}(f) = (1-c)^2\sigma_{PP} + f(1-f)\sigma_{gH} + f^2\sigma_{HH} \tag{6.9}$$

C1	$\frac{1}{x}\exp\Big(-c_1 x^2\Big)$
C2	$\exp\Big(-c_2 x^2\Big)$
C34	$\exp\Big(-c_3(x-c_4)^2\Big)$
C5	$\frac{1-x}{x}\exp\Big(-c_5 x^2\Big)$
C6	$(1-x)\exp\Big(-c_6 x^2\Big)$

Tab. 6.1.: higgs PDF models

6.6. Higgs PDF Ansätze

The different higgs PDFs that were studied are found in Tab. 6.1 and are part of a more general Ansatz given by [43]

$$f_H(x) = (1-x)\Theta((xp)^2 - m_H^2)\left(c_1 \exp\Big(-c_2 x^2\Big) + c_3 \exp\Big(-c_4(x-c_5)\Big) + \frac{c_6}{x}\exp\Big(-c_7 x^2\Big)\right) \tag{6.10}$$

The first term describes that the higgs comes from an interaction with a condensate and is therefore strongly centered around $x = 0$ with the third term being a modification that adds a singular behaviour at $x = 0$ like it is found for the gluon PDF in the proton. The second term emulates the effect of a Q^2-evolution of the higgs PDF, which due to the limited scope of this thesis can not be treated properly. Additionally the PDF Ansatz has an overall $1 - x$ factor, such that it is impossible for the higgs to carry all the momentum of the proton and an on-shell factor $\Theta((xp)^2 - m_H^2)$ that takes care that the incoming higgs is on-shell. Because the simulation is computationally expensive, the investigation of the full Ansatz is cumbersome and it is therefore split up into the different terms seen in Tab. 6.1. The amplitude is, as mentioned in Sec. 6.5 split out of the higgs PDF and determines the higgs fraction c in the proton. In a more thorough treatment, the higgs PDF would be a generalized PDF with on and off-shell PDFs, but since the CM energy is $\sqrt{s} = 13\,TeV$, the higgs should have enough energy to be on-shell most of the time. If there is not enough energy, the parton level cross section vanishes, which means the on-shell theta function $\Theta((xp)^2 - m_H^2)$ can be neglected. The higgs PDF labeled C6 from Tab. 6.1 will be the one focused on in the remainder of this thesis, since it produces the smallest deviation from the standard model predictions and thus makes it possible to hide a bigger higgs fraction in the proton.

$t\bar{t}$		$t\bar{t}Z$	
σ (pb)	Δ_{rel}	σ (pb)	Δ_{rel}
888	3%	0.95	13%

Tab. 6.2.: Experimental cross sections and relative errors for $PP \to t\bar{t}$ and $PP \to t\bar{t}Z$ [50][51]

$t\bar{t}$		$t\bar{t}Z$	
σ (pb)	Δ_{rel}	σ (pb)	Δ_{rel}
354	0.28%	0.394	0.25%

Tab. 6.3.: LO cross sections and relative errors for $PP \to t\bar{t}$ and $PP \to t\bar{t}Z$ calculated with Herwig 7 [1][2][3]

6.7. Exclusion plot

From the total cross sections that Herwig [1][2][3] calculates it is possible to create a plot which depicts the maximally allowed higgs fractions f for a given higgs parameter c. They are found by dividing the total cross section as a function of f given in (6.9) by the experimentally measured cross section and setting the result to $1 \pm \Delta_{rel}$, where Δ_{rel} is the total relative error for the given process found in Tab. 6.2.

$$\frac{\sigma(f)}{\sigma_{exp}} = 1 \pm \Delta_{rel} = \frac{1}{\sigma_{exp}}\Big((1-f)^2\sigma_{PP} + f(1-f)\sigma_{gH} + f^2\sigma_{HH}\Big) \tag{6.11}$$

This yields predictions for the maximum higgs fraction that is still allowed by the experimental error, provided σ_{PP} does not deviate from σ_{exp} too much, which unfortunately it does for leading order calculations as can be seen in Tab. 6.3. To solve this problem it is assumed that the difference between LO and experiment is about the same for all the different contributions to $\sigma(f)$, in this case: σ_{PP}, σ_{gH} and σ_{HH} and to rescale them all by the ratio $\frac{\sigma_{exp}}{\sigma_{PP}}$ of observed total cross section σ_{exp} to the LO standard model prediction σ_{PP}. The result is a quadratic equation and the smallest, positive, real root is the desired higgs fraction.

$$\begin{aligned}\frac{\sigma(f)'}{\sigma_{exp}} &= 1 \pm \Delta_{rel} = \frac{\sigma_{exp}}{\sigma_{exp}\sigma_{PP}}\Big((1-f)^2\sigma_{PP} + f(1-f)\sigma_{gH} + f^2\sigma_{HH}\Big)\\ &= (1-f)^2 + f(1-f)\frac{\sigma_{gH}}{\sigma_{PP}} + f^2\frac{\sigma_{HH}}{\sigma_{PP}} = \left(1 + \frac{\sigma_{HH}-\sigma_{gH}}{\sigma_{PP}}\right)f^2 + \left(\frac{\sigma_{gH}}{\sigma_{PP}} - 2\right)f + 1\end{aligned}$$

$$\to 0 = \left(1 - \frac{\sigma_{HH}-\sigma_{gH}}{\sigma_{PP}}\right)f^2 + \left(\frac{\sigma_{gH}}{\sigma_{PP}} - 2\right)f \mp \Delta_{rel} \tag{6.12}$$

As can be seen in Fig. 6.11b the maximum allowed higgs fraction for C6 is $f \approx 2.5\%$ at $c \approx 1$, while the smallest allowed higgs fraction throughout the entire parameter range is $f \approx 1.5\%$.

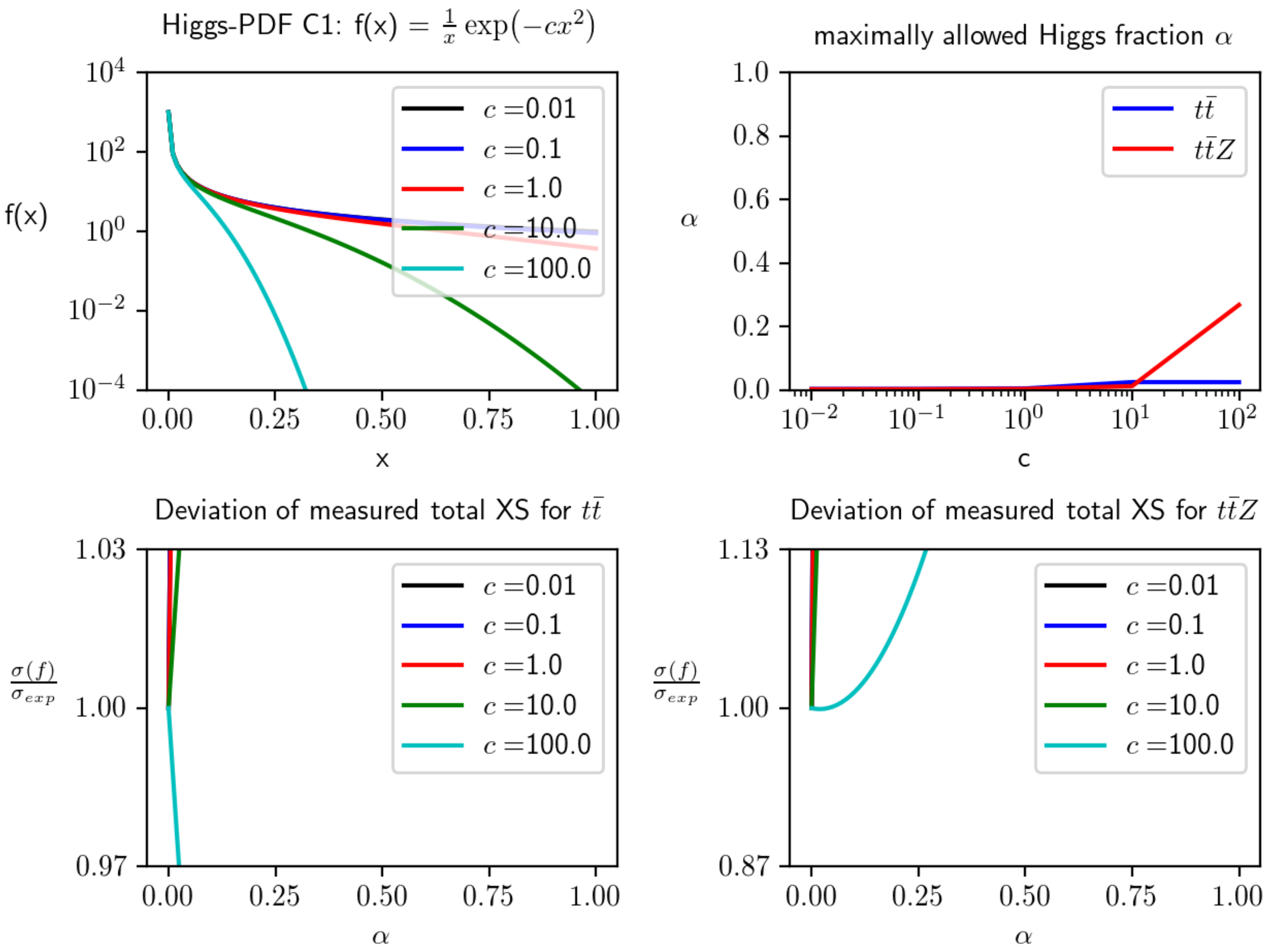

(a) Exclusion plot together with higgs PDF and deviation from standard cross section

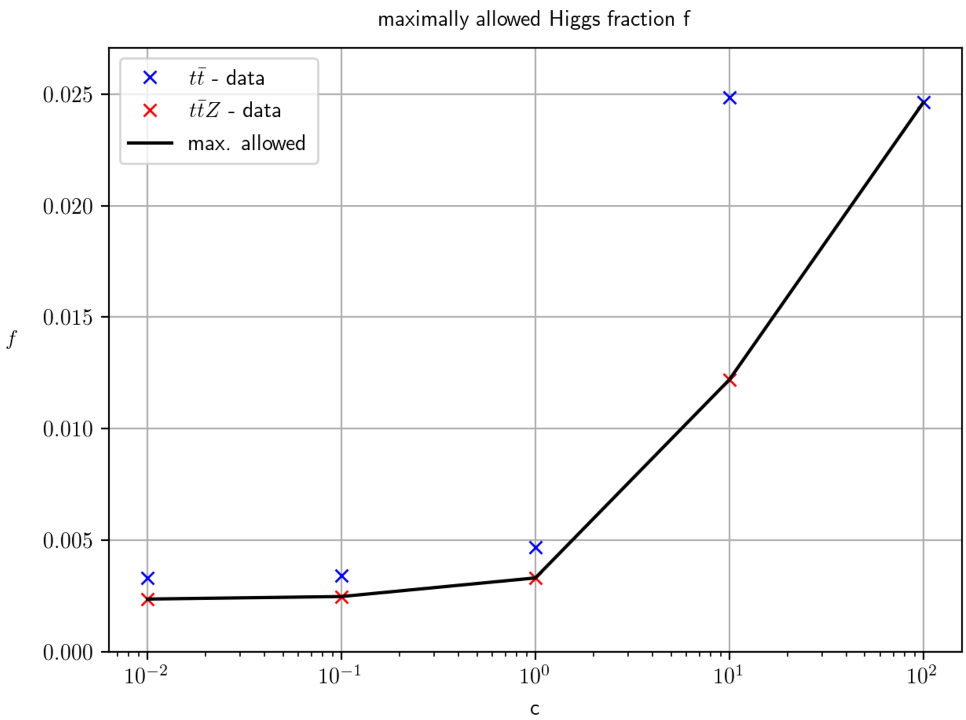

(b) Zoom at the region with the highest allowed higgs fraction f

Fig. 6.7.: Exclusion Plot for higgs PDF C1: $\frac{1}{x}\exp\left(-cx^2\right)$

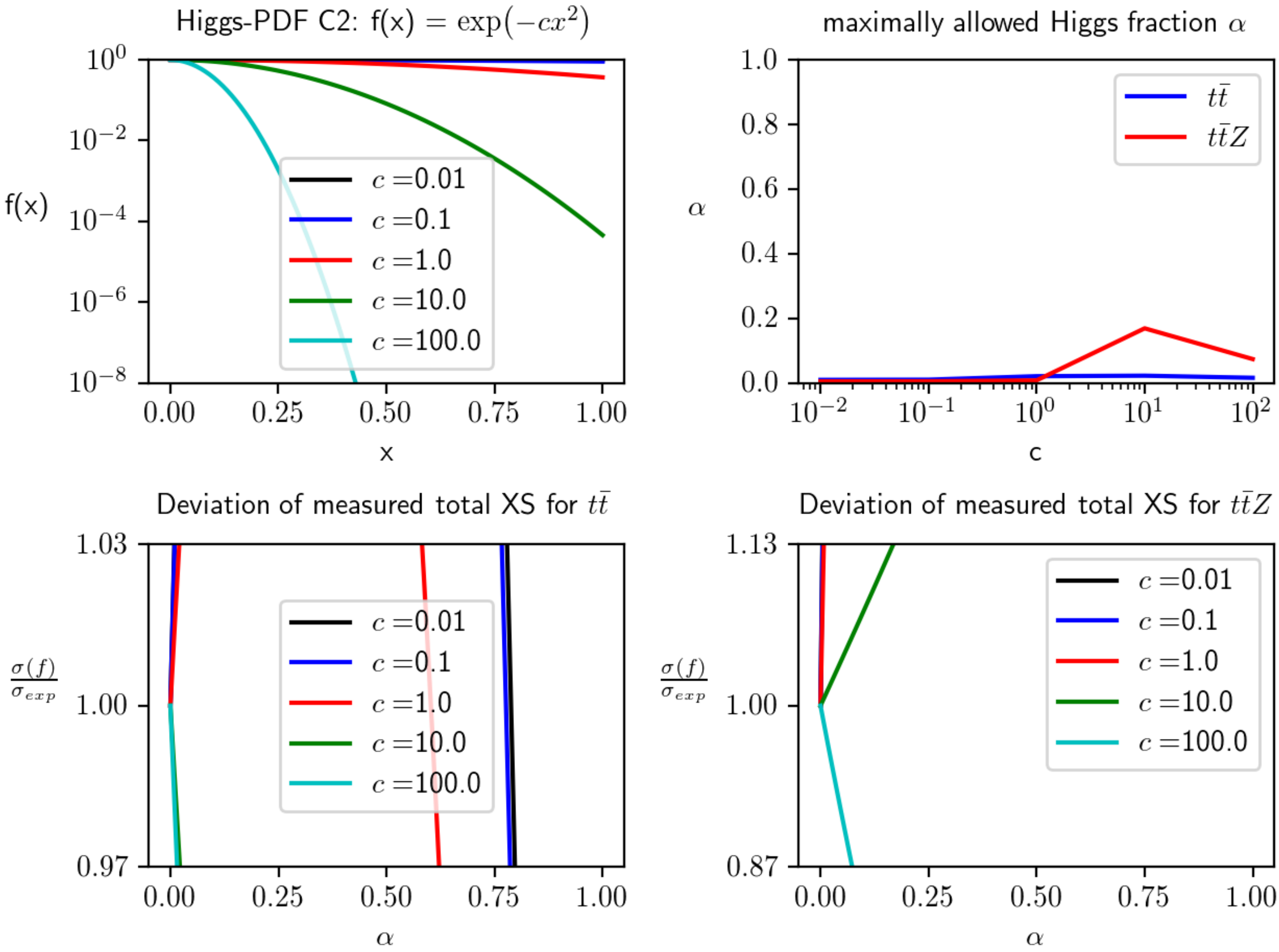

(a) Exclusion plot together with higgs PDF and deviation from standard cross section

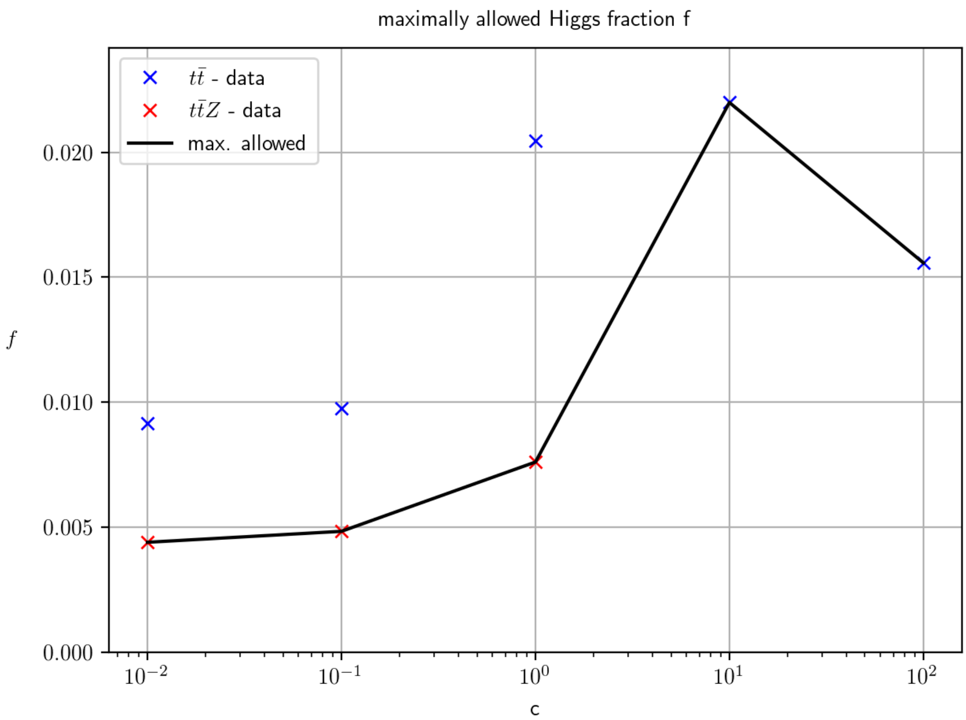

(b) Zoom at the region with the highest allowed higgs fraction f

Fig. 6.8.: Exclusion Plot for higgs PDF C2: $\exp\left(-cx^2\right)$

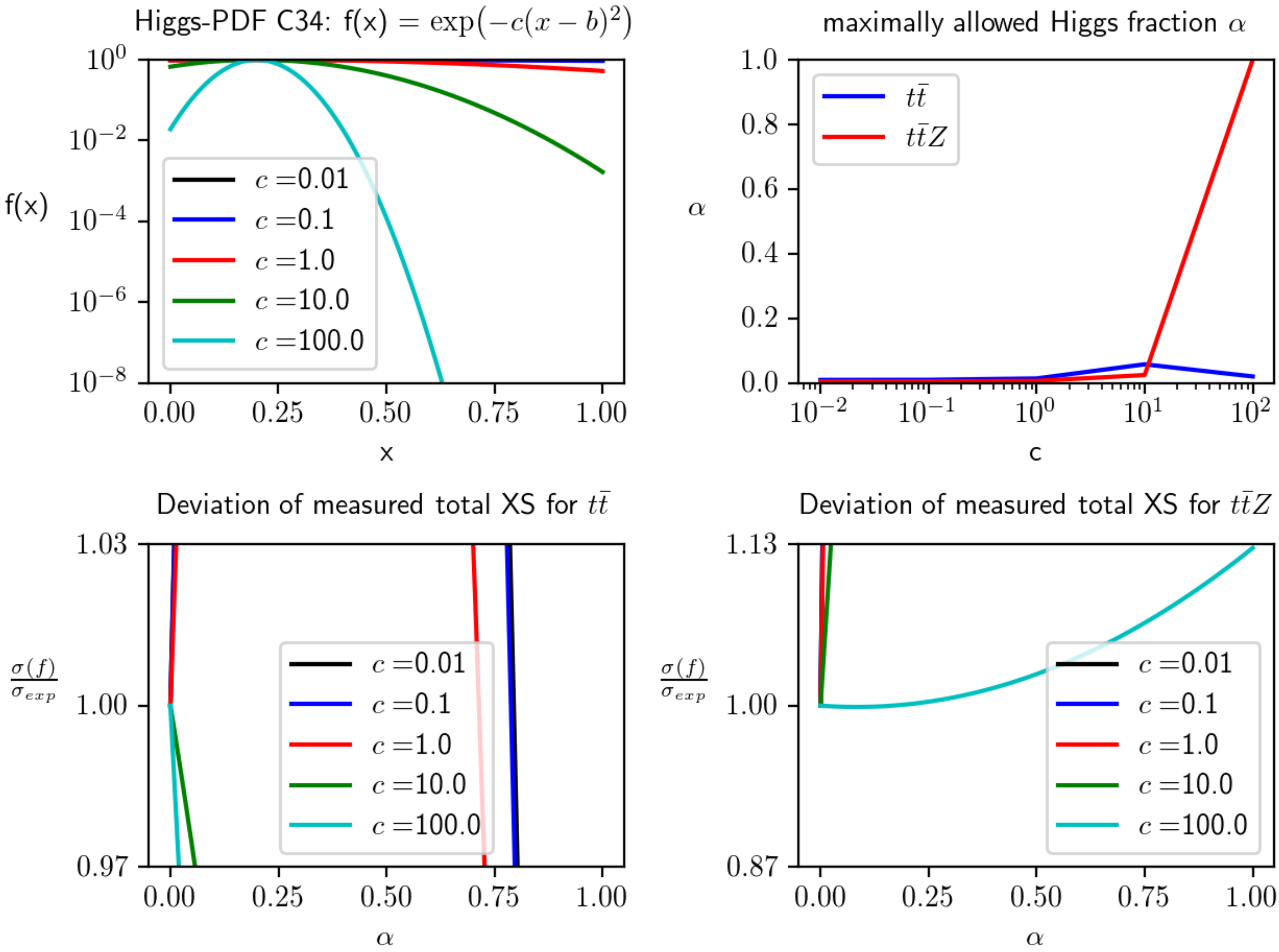

(a) Exclusion plot together with higgs PDF and deviation from standard cross section

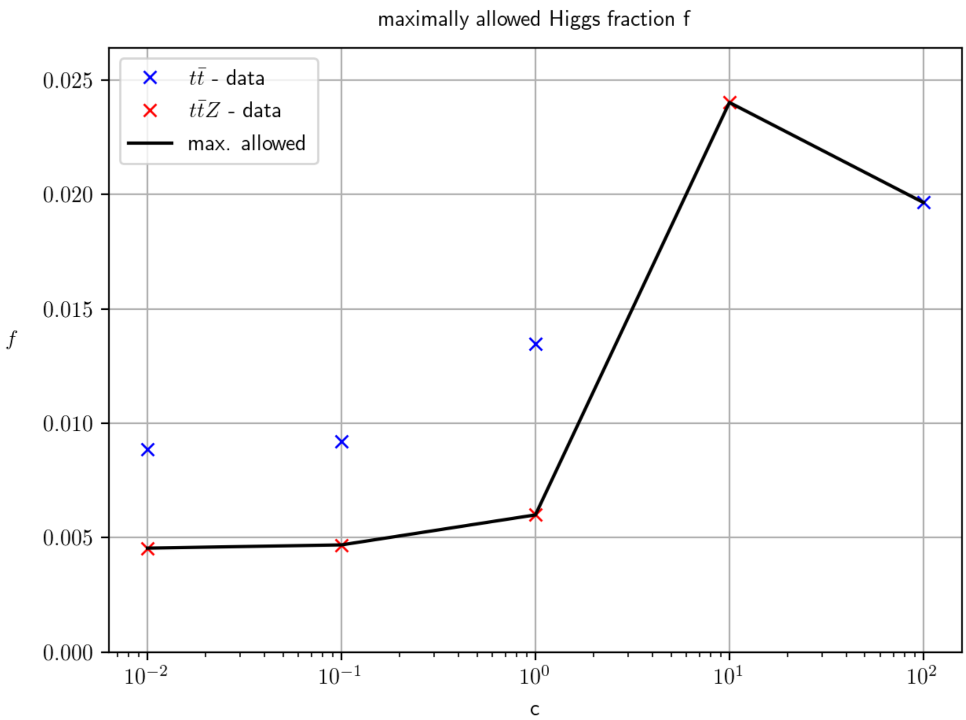

(b) Zoom at the region with the highest allowed higgs fraction f

Fig. 6.9.: Exclusion Plot for higgs PDF C34: $\exp\left(-c(x-0.2)^2\right)$

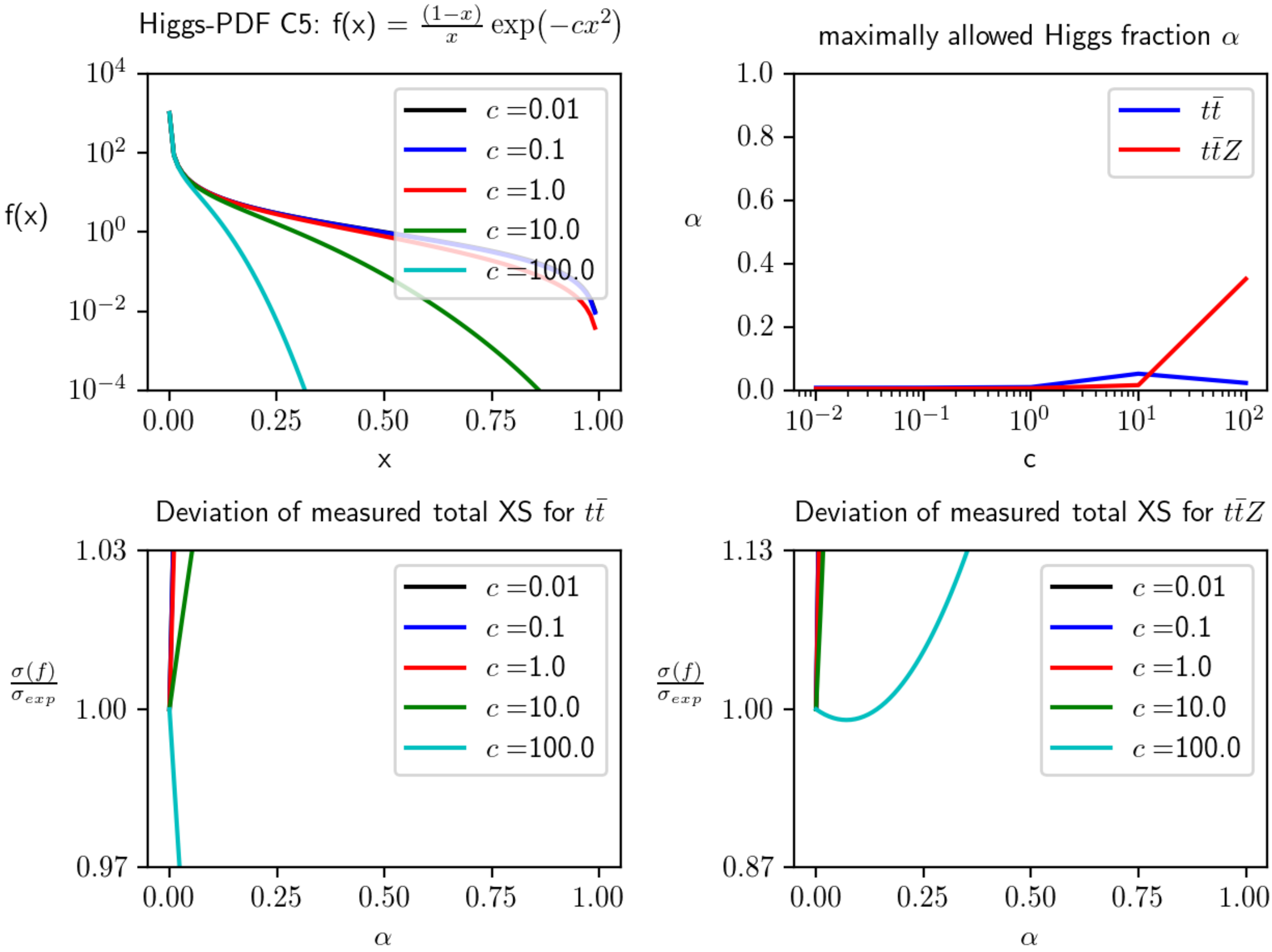

(a) Exclusion plot together with higgs PDF and deviation from standard cross section

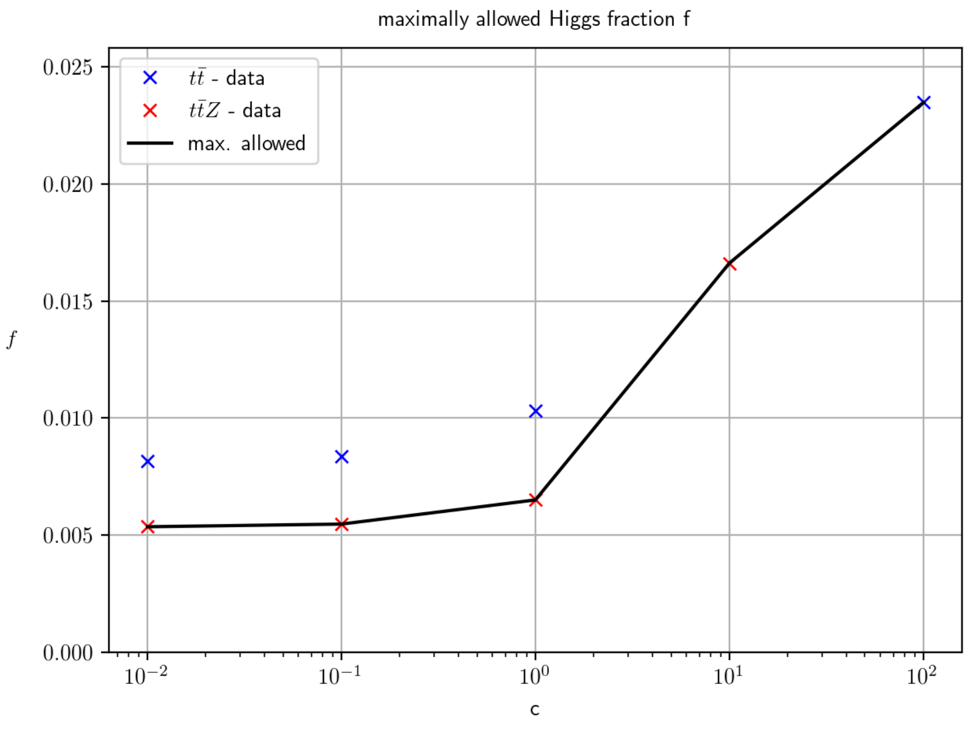

(b) Zoom at the region with the highest allowed higgs fraction f

Fig. 6.10.: Exclusion Plot for higgs PDF C5: $\frac{(1-x)}{x}\exp\left(-cx^2\right)$

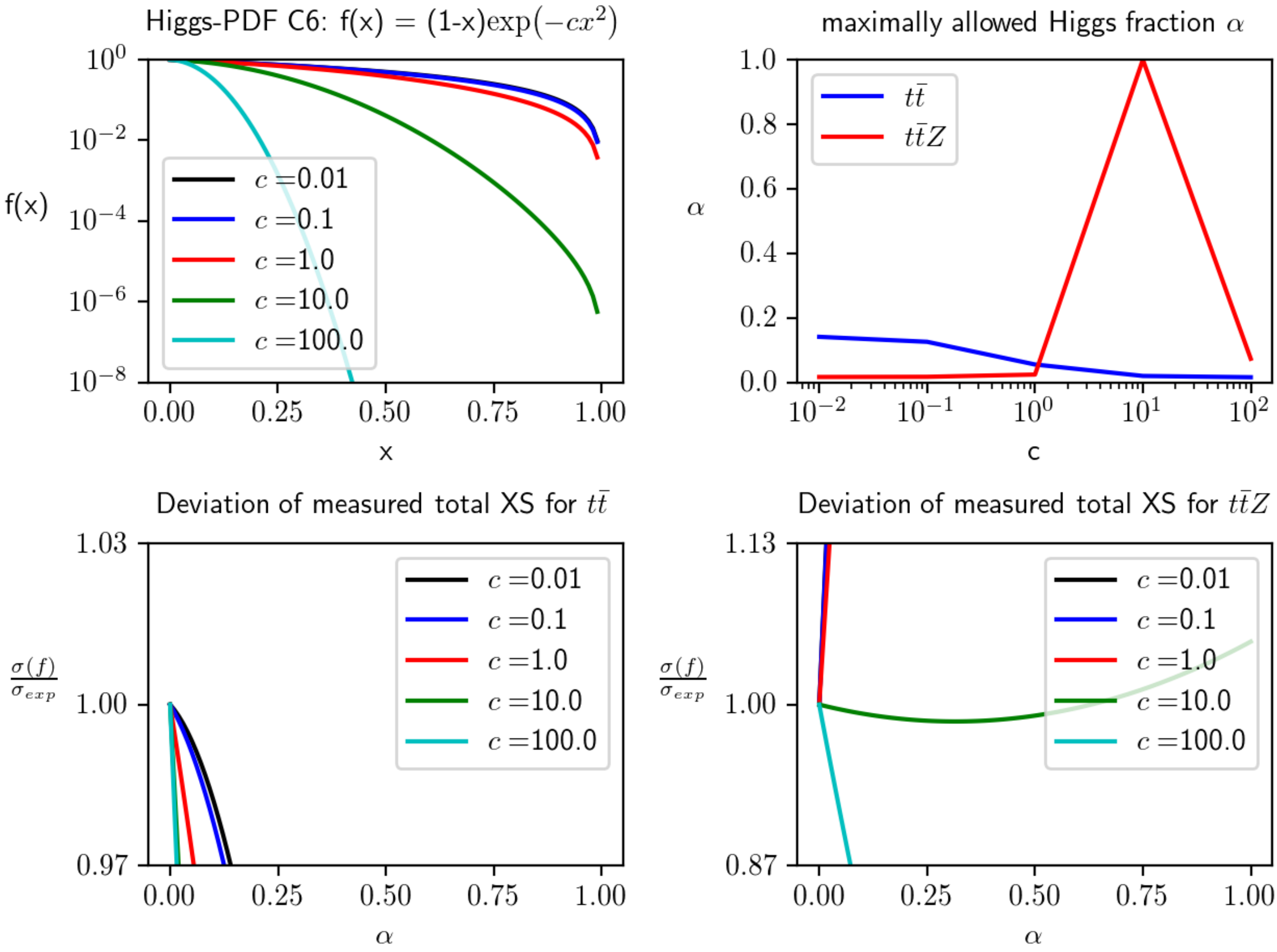

(a) Exclusion plot together with higgs PDF and deviation from standard cross section

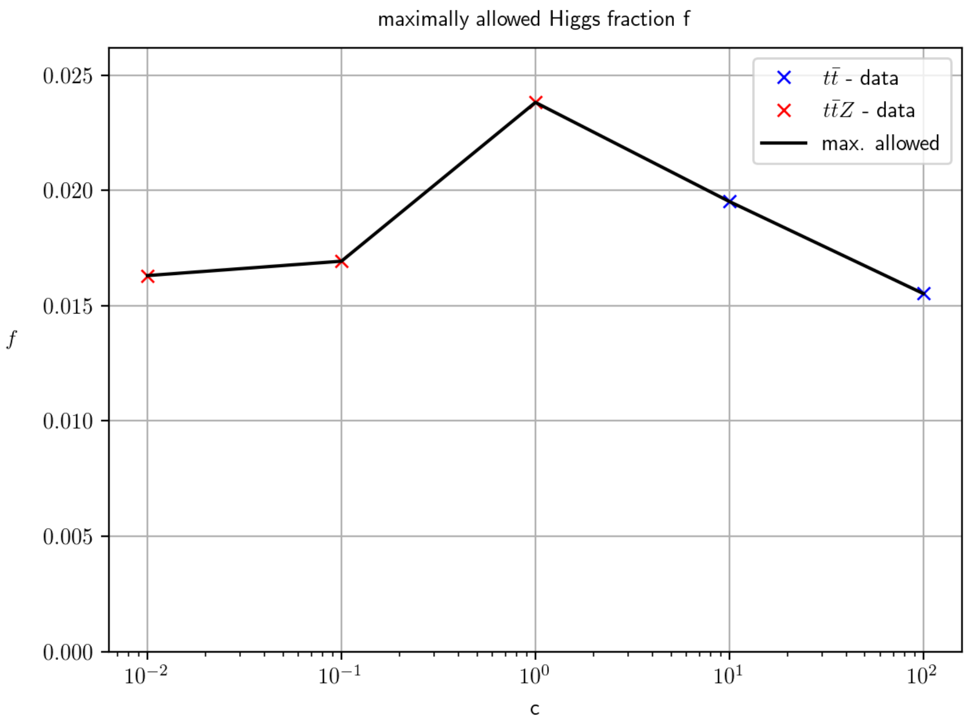

(b) Zoom at the region with the highest allowed higgs fraction f

Fig. 6.11.: Exclusion Plot for higgs PDF C6: $(1-x)\exp\left(-cx^2\right)$

While these exclusion plots are a good start for trying to narrow down the parameter space, it is possible to place stronger restrictions on it by using the partial cross sections for the different observables and combining them with an actual detector simulation from the CMS experiment, which is applied to the raw collision data. This yields confidence intervals that show the probability of the higgs fraction being somewhere in the interval. They were created by Robert Schöfbeck and Lukas Lechner, using Delphes [4], with the details of the setup being the same as in [5] and [6]. These results will also soon be published in a separate paper [7].

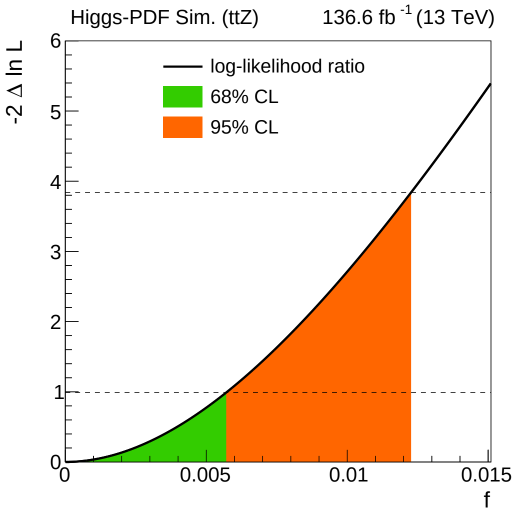

(a) Confidence interval for $t\bar{t}Z$ and higgs parameter $c = 0.01$

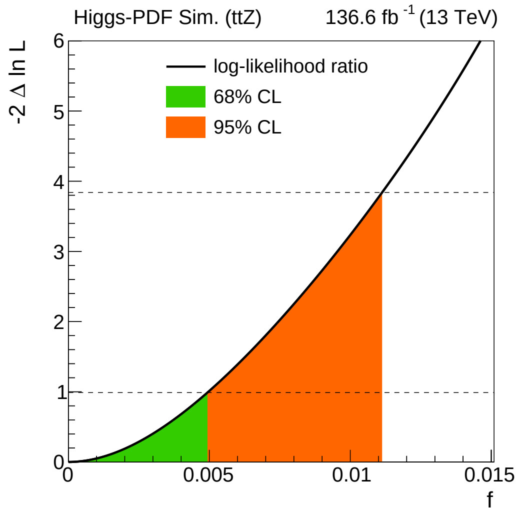

(b) Confidence interval for $t\bar{t}Z$ and higgs parameter $c = 0.1$

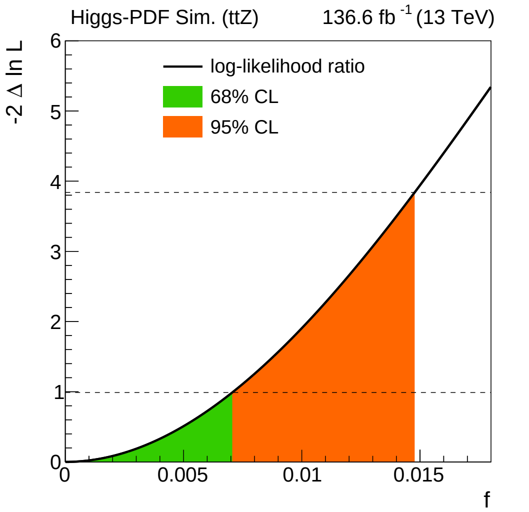

(c) Confidence interval for $t\bar{t}Z$ and higgs parameter $c = 1.0$

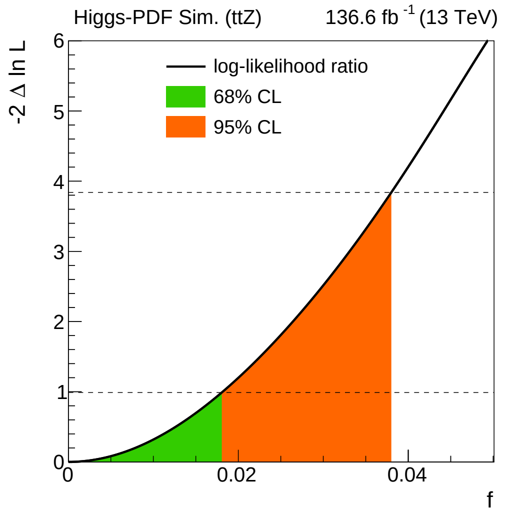

(d) Confidence interval for $t\bar{t}Z$ and higgs parameter $c = 10.0$

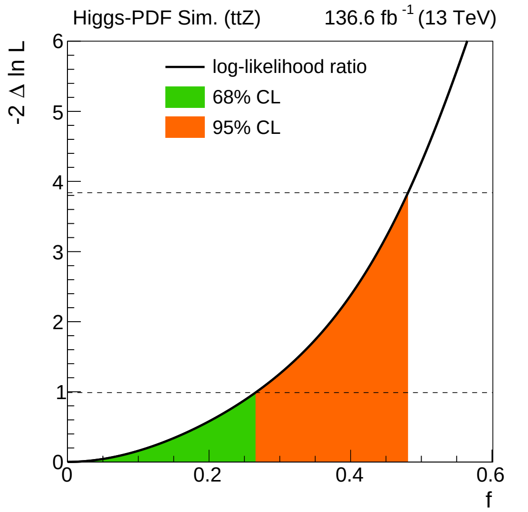

(e) Confidence interval for $t\bar{t}Z$ and higgs parameter $c = 100$

Fig. 6.12.: Confidence intervals for $t\bar{t}Z$, calculated with log-likelihood ratio test. Uses the information of the differential cross sections, together with a detector simulation provided by Robert Schöfbeck and Lukas Lechner (preliminary)

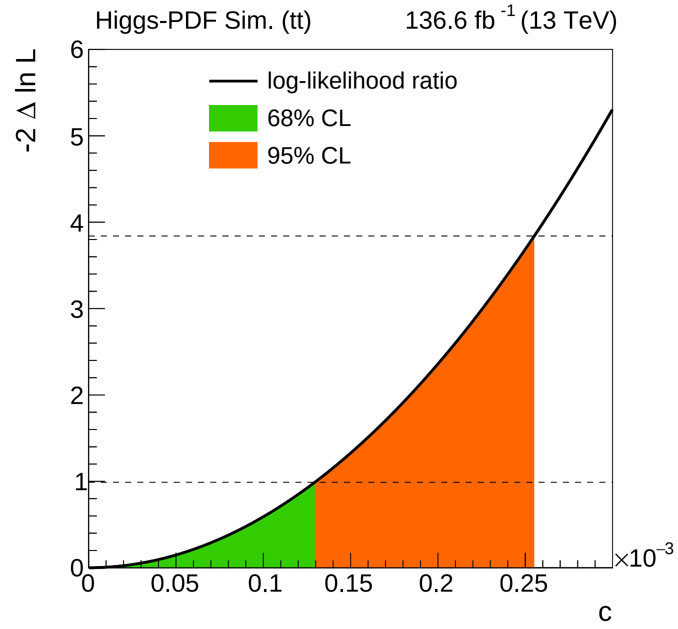

(a) Exclusion plot for $t\bar{t}$ and higgs parameter $c = 0.1$

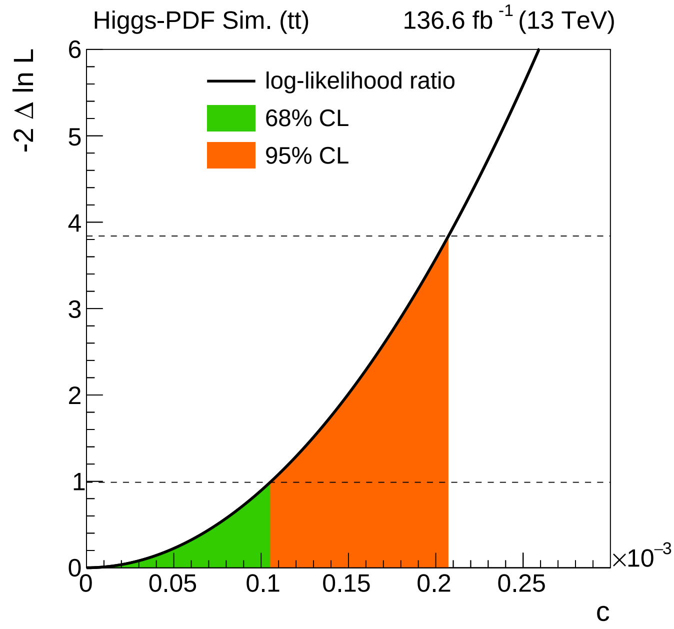

(b) Exclusion plot for $t\bar{t}$ and higgs parameter $c = 1.0$

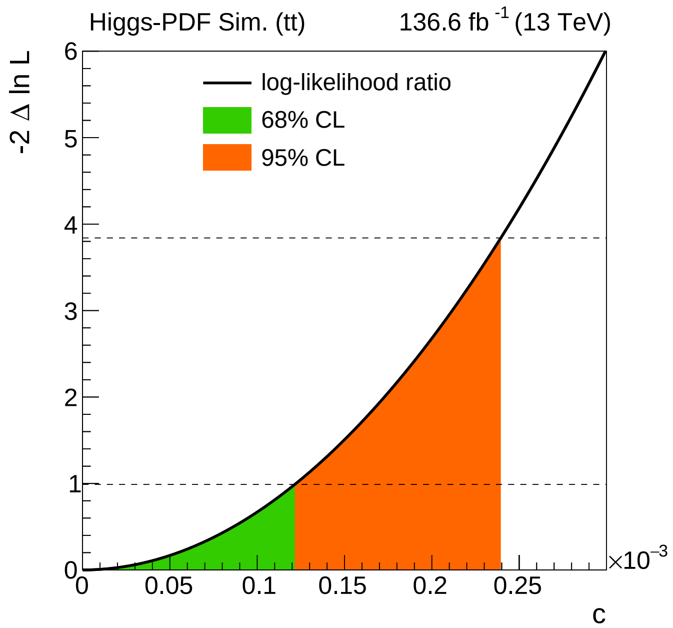

(c) Exclusion plot for $t\bar{t}$ and higgs parameter $c = 10.0$

Fig. 6.13.: Confidence intervals for $t\bar{t}$, calculated with log-likelihood ratio test. Uses the information of the differential cross sections, together with a detector simulation provided by Robert Schöfbeck and Lukas Lechner (preliminary)

6.8. Observables and partial cross sections

All evaluations of the raw scattering event data was done by Rivet, which is a C++ library and uses so called analysis files to reconstruct all kinds of final state observables. To quote from the manual: [8]

"Rivet is a C++ class library, which provides the infrastructure and calculational tools for particle level analyses for high energy collider experiments, enabling physicists to validate event generator models and tunings with minimal effort and maximum portability."

Rivet works with so called analysis files that book histograms, evaluate event data on a per event basis, such that there is no need to save all of the event records and finally fill the booked histograms with different observables, for the calculation of which Rivet provides a number of methods. The different Rivet analyses that were used can be found in App. B.

For the scattering processes $P'P' \to t\bar{t}$, $P'P' \to t\bar{t}Z$ and the di-leptonic decay channels of $P'P' \to t\bar{t}$, simply named $l\bar{l}$, the following observables were chosen:

$t\bar{t}$:

- η_t - Pseudorapidity of t
- $\eta_{\bar{t}}$ - Pseudorapidity of $\bar{t}$
- $\eta_{t,\bar{t}}$ - Pseudorapidity difference between t and $\bar{t}$
- $\hat{s}_t$ - invariant mass of t
- $\hat{s}_{\bar{t}}$ - invariant mass of $\bar{t}$
- $\hat{s}_{t\bar{t}}$ - invariant mass of the $t\bar{t}$-system
- Φ_t - azimuthal angle of t
- $\Phi_{\bar{t}}$ - azimuthal angle of $\bar{t}$
- $\Phi_{t,\bar{t}}$ - difference of azimuthal angle between t and $\bar{t}$
- pT_t - transverse momentum of t
- $pT_{\bar{t}}$ - transverse momentum of $\bar{t}$
- $pT_{t\bar{t}}$ - transverse momentum sum of t and $\bar{t}$

$t\bar{t}Z$:

- η_t - Pseudorapidity of t
- $\eta_{\bar{t}}$ - Pseudorapidity of $\bar{t}$
- η_Z - Pseudorapidity of Z
- $\eta_{t,\bar{t}}$ - Pseudorapidity difference between t and $\bar{t}$
- $\eta_{t\bar{t},Z}$ - Pseudorapidity difference between the $t\bar{t}$-system and Z
- $\hat{s}_t$ - invariant mass of t
- $\hat{s}_{\bar{t}}$ - invariant mass of $\bar{t}$
- $\hat{s}_Z$ - invariant mass of Z
- $\hat{s}_{t\bar{t}}$ - invariant mass of the $t\bar{t}$-system

- $\hat{s}_{t\bar{t}Z}$ - invariant mass of the $t\bar{t}Z$-system
- Φ_t - azimuthal angle of t
- $\Phi_{\bar{t}}$ - azimuthal angle of $\bar{t}$
- $\Phi_{\bar{t}}$ - azimuthal angle of Z
- $\Phi_{t,\bar{t}}$ - difference of azimuthal angle between t and $\bar{t}$
- $\Phi_{t\bar{t},Z}$ - difference of azimuthal angle between the $t\bar{t}$-system and Z
- pT_t - transverse momentum of t
- $pT_{\bar{t}}$ - transverse momentum of $\bar{t}$
- pT_Z - transverse momentum of Z
- $pT_{t\bar{t}}$ - transverse momentum sum of t and $\bar{t}$
- $pT_{t\bar{t}Z}$ - transverse momentum sum of t, $\bar{t}$ and Z

$l\bar{l}$:

- $\Phi_{l,\bar{l}}$ - difference of azimuthal angle between l and $\bar{l}$

(Here and in the following a comma separating particles always means the difference of the particle observables, while no comma with multiple particle subscripts means the observable of the whole system, i.e: the four-momenta of the particles are added and then the observable is calculated. Except in the case of transverse momentum, where the quantities are simply added)

The strongest effect was present in the process $P'P' \rightarrow t\bar{t}Z$ because of the additional Feynman diagrams, as already explained in Sec. 6.1. Thus differential cross sections for higgs PDF C6 and observables $\eta_{t,\bar{t}}$ and pT_t are shown in App. A.3 and compared in a ratio plot to the standard model results. Shown there are figures for the parameter values $c = (0.01, 10.0)$ as for $c = 100$ there was barely any effect visible at a higgs fraction of $f = 0.015$.

In App. A.2 the different higgs PDF values are compared for a particular higgs PDF model. For the process $l\bar{l}$ (Spin-correlation measurement) the azimuthal angle difference is shown Fig. A.1, in the process $t\bar{t}$ App. A.1.3 the observables η_t, $\eta_{t,\bar{t}}$ are shown and pT_t and in $t\bar{t}Z$ additionally the observable η_Z is also depicted.

The appendix App. A.2 shows figures comparing the different higgs PDFs to each other with the processes $l\bar{l}$ and $t\bar{t}$ having the same observables as the comparison among the higgs parameters.

7. Results

In general the bigger the higgs parameter the smaller the deviation among different PDFs, which is clear since there is less higgs PDF and the additional contributions due to the higgs are drowned out by the standard model contributions

$$\frac{d\sigma_{P'P'}}{d\Omega_f} = F_{PP}(\Omega_f) + F_{H,i}(c, \Omega_f) \tag{7.1}$$

where i labels the PDFs, $F_{H,i}(c, \Omega_f)$ are the summed up contributions due to the higgs and Ω_f stands for the final state kinematic variables which will be dropped in the following

Since $\lim_{c\to 0} F_{H,i}(c, \Omega_f) = 0$ this leads to the following ratio

$$\frac{\frac{d\sigma_{P'P',i}}{d\Omega_f}}{\frac{d\sigma_{P'P',j}}{d\Omega_f}} = \frac{F_{PP} + F_{H,i}(c, \Omega_f)}{F_{PP} + F_{H,j}(c, \Omega_f)} = \frac{1 + \frac{F_{H,i}}{F_{PP}}}{1 + \frac{F_{H,j}}{F_{PP}}} \underset{\lim_{c\to 0}}{=} 1 \tag{7.2}$$

Another general trend is that, for the higgs PDF $C34$ the shift in x of the peak becomes more important the narrower peaked the PDFs are, which is visible in Fig. A.13, Fig. A.16, Fig. A.17 and Fig. A.15. This means, the narrower the peak is, the more important the peak position becomes. The effects of a shifted peak position only become visible if the PDF is sufficiently narrow which is for large higgs parameters but then the effects become small and hard to see.

The modification $1 - x$ effectively reduces the cross sections everywhere as seen for example in Fig. A.21, Fig. A.20 and Fig. A.16. It is especially noticeable in the observable p_T, which is clear since it reduces the higgs PDF more for higher momentum fractions and thereby the amount of higgs colliding with a high momentum, leading to less particles with high transverse momentum.

The $\frac{1}{x}$ factor increases the cross section everywhere, since for $x \in (0, 1)$ it means multiplying the whole PDF by a factor greater than one. The divergence at $x \to 0$ does not seem to have a particularly strong effect on the cross sections and in general the low x behaviour seems to have little influence in the final cross sections.

In Fig. A.25 and Fig. A.26 one can see, that for η_t and in Fig. A.29 for η_Z, the cross section is diminshed compared to the standard model prediction. This means that the added higgs would reduce the number of particles that are emitted at a high angle to the beam axis. It appears that this effect becomes stronger the greater the higgs PDF, since for C1, which is the largest PDF, the effect is greater than for C6, which is the smallest PDF. The effect vanishes however in $t\bar{t}Z$ for all PDFs but C2 and C34. It is also only visible for $c \leq 0.1$.

<table>
<tr><td colspan="2" rowspan="2">$f\,\%$</td><td>0.01</td><td>0.1</td><td>1.0</td><td>10.0</td><td>100.0</td></tr>
<tr><td colspan="5">c</td></tr>
<tr><td>C1</td><td rowspan="5">PDF</td><td>0.24</td><td>0.25</td><td>0.33</td><td>1.2</td><td>2.5</td></tr>
<tr><td>C2</td><td>0.44</td><td>0.48</td><td>0.76</td><td>2.2</td><td>1.6</td></tr>
<tr><td>C34</td><td>0.45</td><td>0.47</td><td>0.6</td><td>2.4</td><td>2.0</td></tr>
<tr><td>C5</td><td>0.54</td><td>0.55</td><td>0.65</td><td>1.7</td><td>2.3</td></tr>
<tr><td>C6</td><td>1.6</td><td>1.7</td><td>2.4</td><td>2.0</td><td>1.6</td></tr>
</table>

Tab. 7.1.: Maximally allowed higgs fraction f for different PDFs and parameter values, calculated with *ExclusionPlots.py* given in App. B.5

For η_t, $\eta_{\bar{t}}$ and η_Z all higgs PDFs increase the cross section at high η values. The $\frac{1}{x}$ factor increases the cross section for intermediate values of η and slightly decreases it for low η. The inverse can be said about the $1 - x$ factor, it increases the cross section for low and decreases it for high η values. In the higgs PDF C5 a mixture of both is found. What can be seen at high values of the higgs parameter c is that the shift in x of the peak grows in importance, which can be seen for example at $c \geq 10$ at high η values.

Looking at the observable pT one can see, that the (1-x) factor diminshes more and more going to high p_T but for $pT_{t\bar{t}Z}$ Fig. A.22 it also boosts below $p_T \approx 200GeV$. The factor $\frac{1}{x}$ behaves once again contrarily, decreasing the cross section at p_T below 200 GeV and increasing it above. At the maximum point of the $pT_{t\bar{t}Z}$ cross section all the different higgs PDFs almost meet at a point.

All in all it is hard to extract any kind of particular behaviour out of the cross sections, that can be attributed to a specific shape of the PDFs. The most important factor seems to be the width of the PDF followed by the modifications $(1 - x), x$ to the PDF. Least important is the peak position, the effects of which only really become visible for large higgs parameter i.e: narrow peaks.

The main goal of this thesis is however to establish a bound to the allowable higgs content in the proton as well as the parameter range for a given PDF and higgs fraction, for which the exclusion plots can serve as a first restriction. The raw data used in the exclusion plots is shown in Tab. 7.1 for the analyzed parameter range $c = (0.01, 0.1, 1.0, 10.0, 100.0)$. From there it can be seen, that for the favoured PDF C6 the maximum higgs fraction for the whole parameter range is $> 1.6\%$.

No matter what the higgs PDF and parameters are at some point for hard events the deviation from the standard model prediction necessarily becomes incompatible with the experiment, which can be seen in Fig. A.23 to Fig. A.30. The question then is, at what value of the observable one whishes to make a cut-off and neglect anything above/below. This depends on the particular observable considered. For the transverse momentum p_T the cutoff was chosen at 400 GeV, such that anything above can be ignored. In the case of the pseudorapidity η the bounds chosen are $\eta = (-5, 5)$. The results are considered incompatible with the experiment, if the deviation of the differential cross section for the higgs modified process to the standard model process exceeds 20%.

In the comparison of the differential cross section to the standard model the most restricting observable is η_Z. So it is sufficient to analyze this observable to see at which higgs parameter value the results exceed the error threshold. From Fig. 7.1 and Fig. 7.2, the limits given in Tab. 7.2, on the higgs parameter, for a given higgs fraction of $f = 1.5\%$, can be determined. The threshold value of the higgs pa-

PDF:	C1	C2	C34	C5	C6
c:	> 10.0	> 10.0	> 10.0	> 10.0	> 10.0

Tab. 7.2.: Limits on the higgs parameter c for the higgs fraction $f = 1.5\%$

c:	0.01	0.1	1.0	10.0	100.0
$f\,(95\%\,CI)$:	1.2%	1.1%	1.5%	3.75%	47.5%
f (exclusion plots):	1.6%	1.7%	2.4%	2.0%	1.6%

Tab. 7.3.: Limits on the higgs fraction, for PDF C6, from confidence intervals (CI) in Fig. 6.12 and from the exclusion plots Tab. 7.1

rameter, at which the cross sections start exceeding the standard model prediction, is somewhere in the interval $c = (10.0, 100.0)$.

Comparing this data with the exclusion plots it is clear, that even in this crude approach the differential cross sections restrict the Higgs content much more tightly. The higgs PDF C6 for example, at a higgs fraction $f = 1.5\%$, has the whole parameter range allowed in the exclusion plot Fig. 6.11. With the information from the differential cross sections, the higgs parameter can be limited to a range $c > 10.0$ for this and all others PDF.

From the 95% confidence intervals in Fig. 6.12 for the higgs PDF C6 it can be seen, that even for the process $t\bar{t}Z$, which showed the strongest effects of an additional higgs contribution, the confidence interval includes higgs fractions as high as $f = 1.2\%$ for a higgs parameter of $c = 0.01$. This is a much higher higgs fraction than would have been expected, by using the differential cross sections naively with the cutoff method outlined above. The exclusion plots allow for a maximum higgs fraction of $f = 1.6\%$ at that value of the higgs parameter, so the allowed fraction was constrained further. The higgs parameter values $c = (0.1, 1.0)$ could be narrowed down further as well, from $(1.7\%, 2.4\%)$ to $(1.1\%, 1.5\%)$. For a parameter value of $c = 10.0$ and above the confidence intervals essentially do not constrain the allowable higgs fraction.

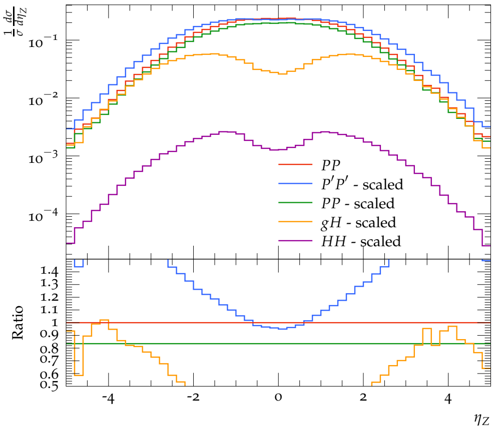

(a) η_Z for higgs PDF C1

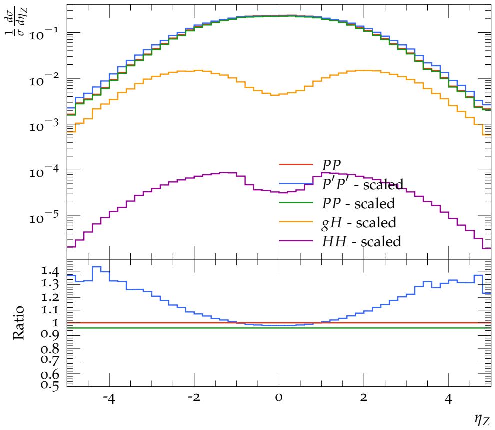

(b) η_Z for higgs PDF C2

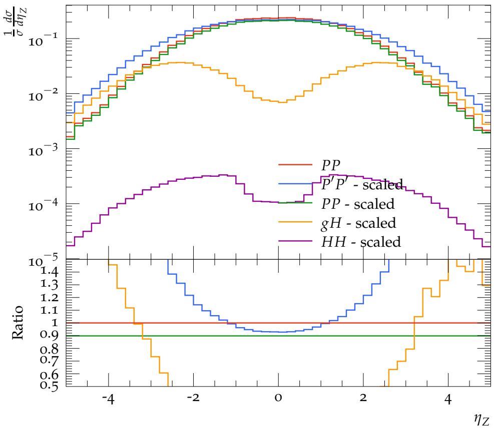

(c) η_Z for higgs PDF C34

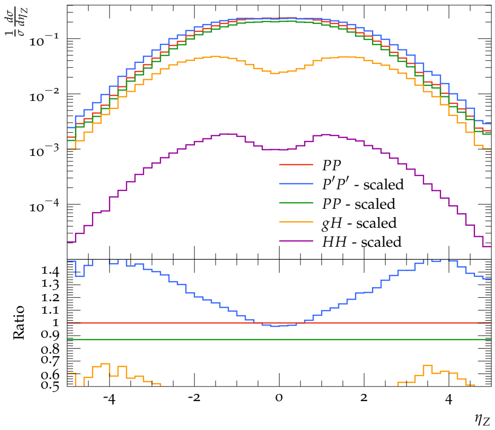

(d) η_Z for higgs PDF C5

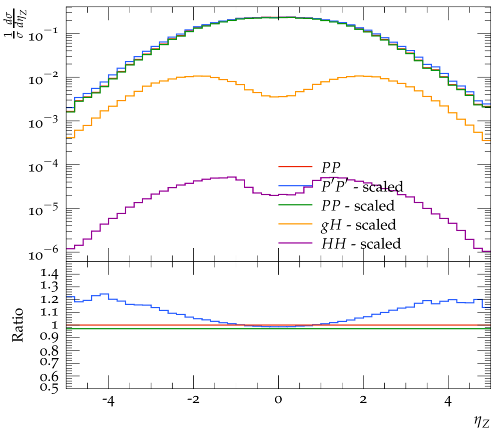

(e) η_Z for higgs PDF C6

Fig. 7.1.: Comparison to standard model cross section for η_Z in $t\bar{t}Z$, all higgs PDFs and $c = 10.0$

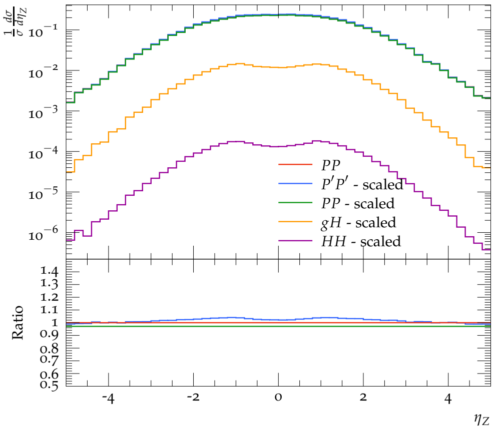

(a) η_Z for higgs PDF C1

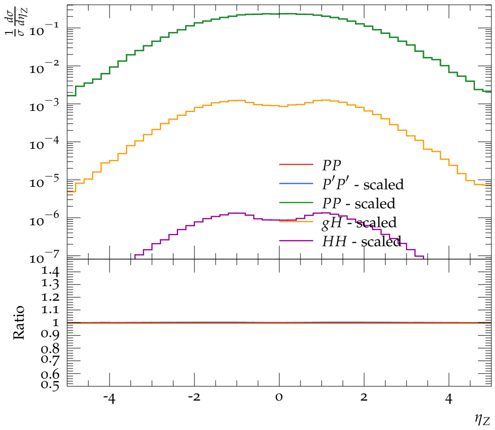

(b) η_Z for higgs PDF C2

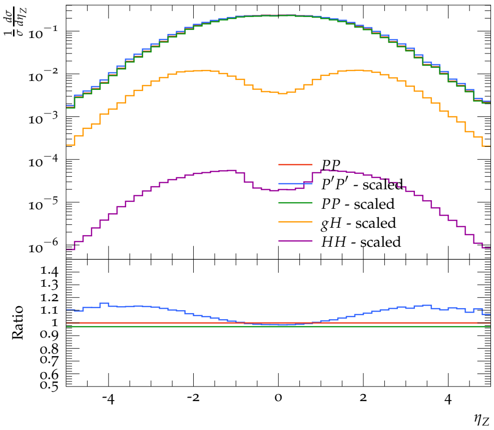

(c) η_Z for higgs PDF C34

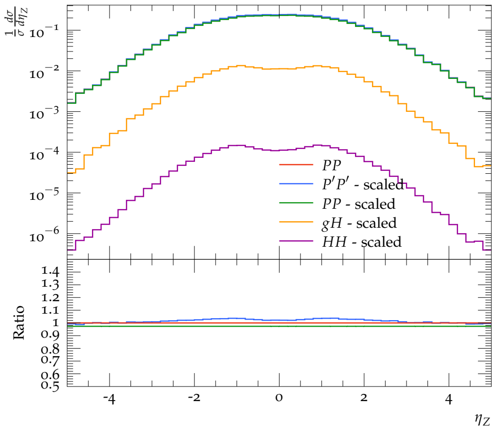

(d) η_Z for higgs PDF C5

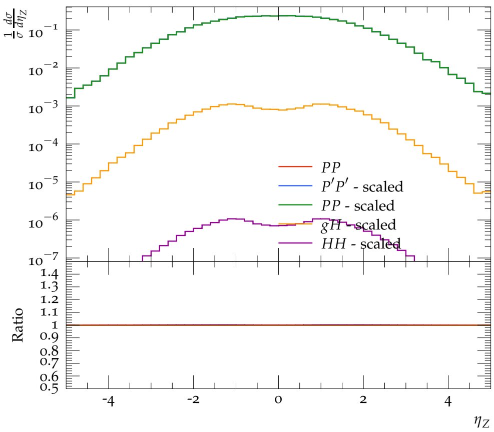

(e) η_Z for higgs PDF C6

Fig. 7.2.: Comparison to standard model cross section for η_Z in $t\bar{t}Z$, all higgs PDFs and $c = 100.0$

8. Summary

The higgs content in the proton, which is demanded by strict non-perturbative gauge invariance and group theoretical arguments and which is taken account of by the way of a higgs parton distribution function of the proton, was studied in proton-proton collisions. For that purpose a Monte-Carlo event generator, called Herwig was used to obtain cross sections for different processes and observables, that are argued to show the biggest impact of said higgs contribution. From the results it can be concluded, that there is quite a bit of room for the higgs PDF in the proton, without it actually changing the cross sections beyond the current experimental error bounds. The method used to determine the allowed higgs fraction was however quite crude and it can be expected, that the maximum higgs fraction will be considerably smaller in the confidence intervals calculated with the log-likelihood ratio test, that is to come, in the paper following this thesis. In general if the higgs parameter is big enough and thus the PDF narrowly peaked, the higgs fraction can be seemingly arbitrarily big. The width had the biggest impact, followed by the factor $\frac{1}{x}$, which greatly increased the cross sections and $1 - x$, which overall dimished the cross sections. Least impactful was the peak position in the PDF C34 but this changes the larger the higgs parameter and thus the narrower the peaks become. For higgs parameters above $c > 10$ the peak position dominated the behaviour of the cross sections. From the exclusion plot data the higgs fraction can be limited to $f < 1.6\%$ for the PDF C6, which is the smallest one and and $f < 0.24\%$ for C1, the biggest one. Using the differential cross sections, it was possible to further restrict all PDFs, at $f = 1.5\%$, to a higgs parameter $c > 10$. Using a log-likelihood ratio test it was possible to create confidence intervals Fig. 6.12, that restrict the higgs paramters $c < 10.0$ further. However the confidence intervals are preliminary results and the final version will be found in [7].

Looking forward, further improvements that need to be made in order to get more substantial quantitative results, are first of all a global refit of all the PDFs in the proton including the higgs, since most likely some of the effects of the higgs, are hidden in other PDFs. Second, to implement a Q^2-evolution for the higgs. Thirdly use generalized parton distribution functions with on- and on-shell contributions because the higgs is heavy enough to not always be on-shell, even at high CM energies. Finally calculate the results at NLO, to be able to directly compare them to measured cross sections. In conclusion, there are many ways this study can be improved, given the time and resources, as this thesis is merely a first exploration of the topic. The goal was to get first estimates on the size of the higgs contribution, it's effects on cross sections and limits on the parameter space.

A. Plots

Of the observables listed in Sec. 6.8 only those are shown, that show significantly different behaviour. For example observables like η_t, $\eta_{\bar{t}}$ are nearly identical so only η_t is shown, the same goes for pT_t and $pT_{\bar{t}}$, etc... Also the azimuthal angle observables were left out since they did not show any particularly interesting behaviour. The differential cross sections were created by calculating the individual initial state contributions to the complete scattering processes $P'P' \rightarrow t\bar{t}, t\bar{t}Z$, which are PP, gH and HH as described in Sec. 6.1, scaling them according to the prefactors in Eq. 6.8 and merging the histogram files with *yodamerge*, a routine for combining similar histograms provided by Rivet. All differential cross sections depicted are for a higgs fraction of $f = 0.015$.

There are two kinds of comparison plots that were made for each of the processes $t\bar{t}$ and $t\bar{t}Z$ and the spin-correlation observable $l\bar{l}$:

- a comparison of different parameter values for one higgs PDF model App. A.1
- a comparison between different higgs PDF models for a particular parameter value App. A.2

In App. A.3 the differential cross section for the observables pT_Z, η_t, η_Z and $\eta_{t,\bar{t}}$ is compared to the standard model prediction for higgs PDF C6, which allows for the biggest higgs fraction, at parameter values $c = (0.01, 10.0)$.

A.1. Comparing differential cross sections for different higgs parameters

A.1.1. $P'P' \to l\bar{l}$

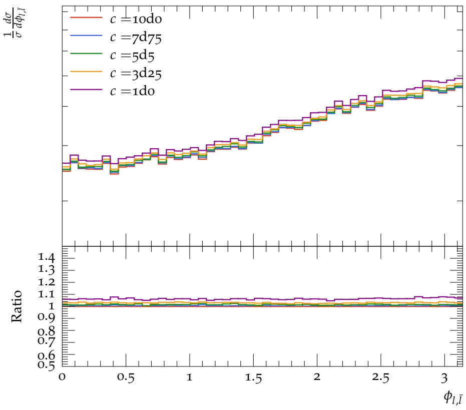

(a) $\phi_{l,\bar{l}}$ for higgs PDF C1: $\frac{1}{x}\exp(-cx^2)$

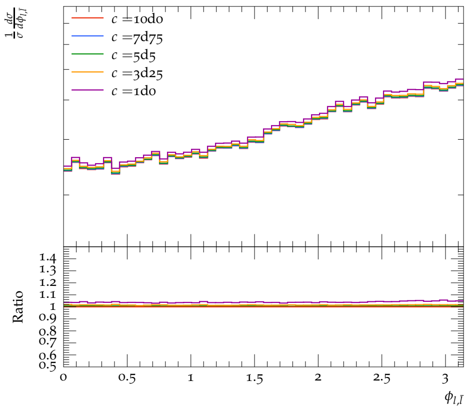

(b) $\phi_{l,\bar{l}}$ for higgs PDF C2: $\exp(-cx^2)$

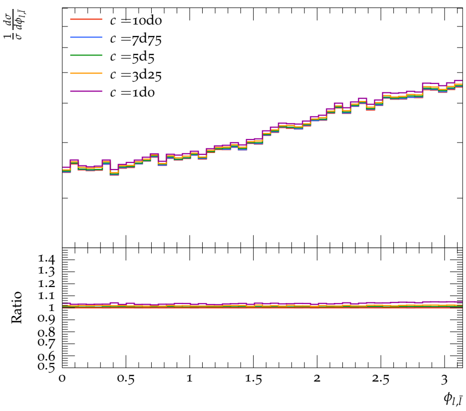

(c) $\phi_{l,\bar{l}}$ for higgs PDF C34: $\exp(-c(x-0.2)^2)$

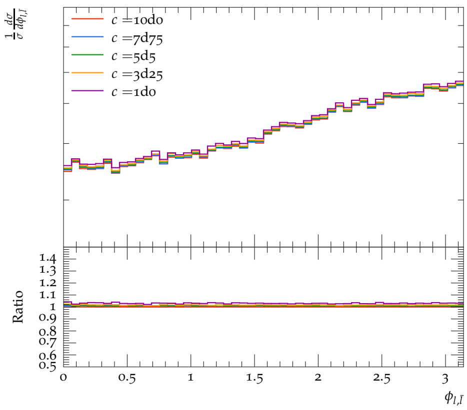

(d) $\phi_{l,\bar{l}}$ for higgs PDF C5: $\frac{(1-x)}{x}\exp(-cx^2)$

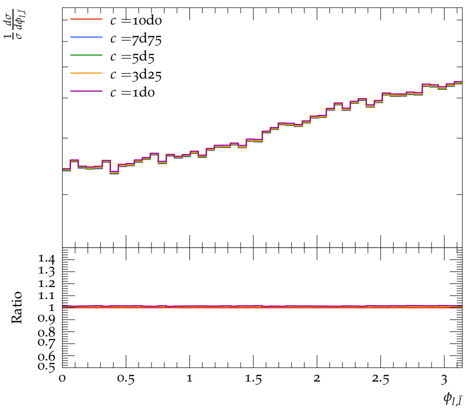

(e) $\phi_{l,\bar{l}}$ for higgs PDF C6: $(1-x)\exp(-cx^2)$

Fig. A.1.: Comparing $\phi_{l,\bar{l}}$ for higgs parameter values $c = (1, 3.25, 5.5, 7.75, 10)$

A.1.2. $P'P' \to t\bar{t}$

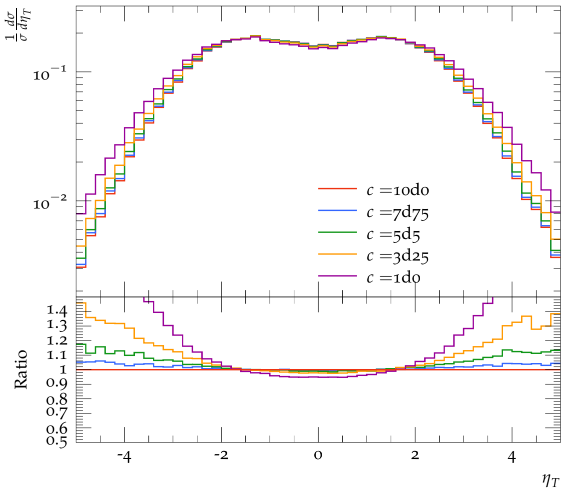

(a) η_t for higgs PDF C1: $\frac{1}{x}\exp(-cx^2)$

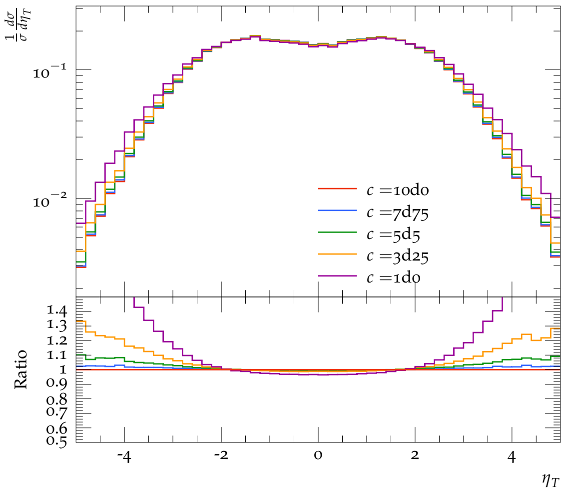

(b) η_t for higgs PDF C2: $\exp(-cx^2)$

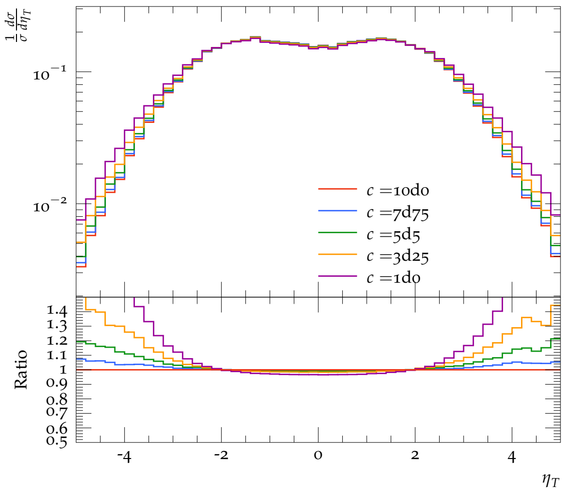

(c) η_t for higgs PDF C34: $\exp(-c(x-0.2)^2)$

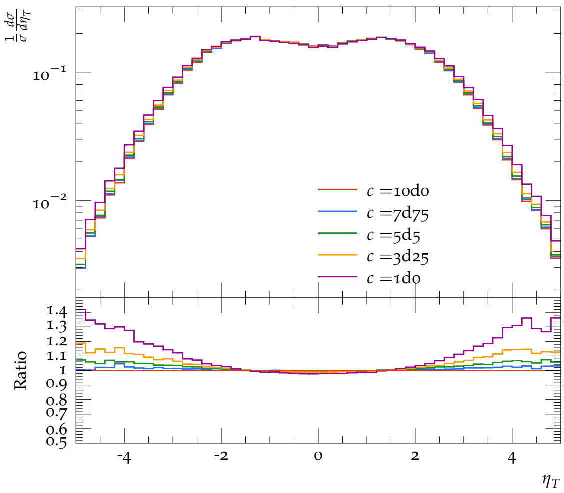

(d) η_t for higgs PDF C5: $\frac{(1-x)}{x}\exp(-cx^2)$

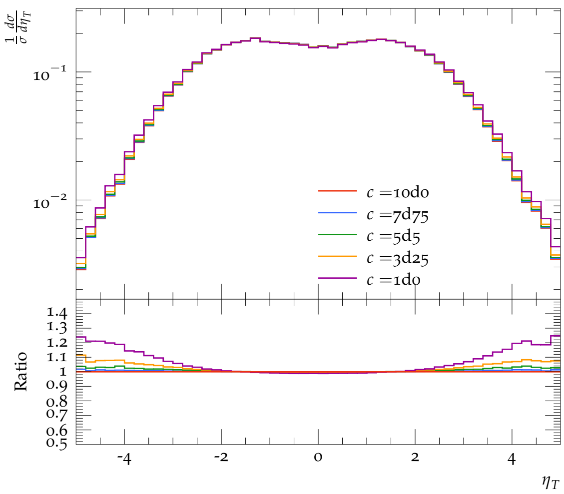

(e) η_t for higgs PDF C6: $(1-x)\exp(-cx^2)$

Fig. A.2.: Comparing η_t for higgs parameter values $c = (1, 3.25, 5.5, 7.75, 10)$

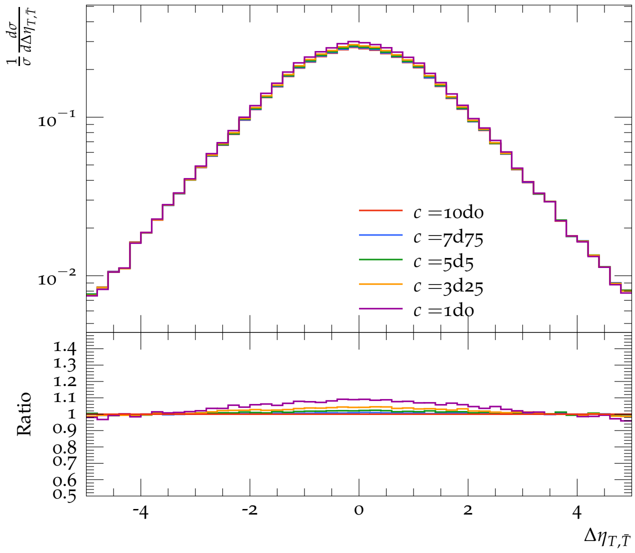

(a) $\eta_{t,\bar{t}}$ for higgs PDF C1: $\frac{1}{x}\exp(-cx^2)$

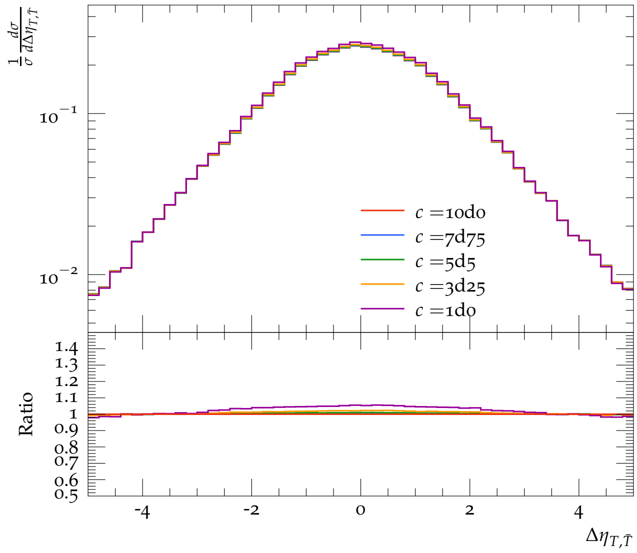

(b) $\eta_{t,\bar{t}}$ for higgs PDF C2: $\exp(-cx^2)$

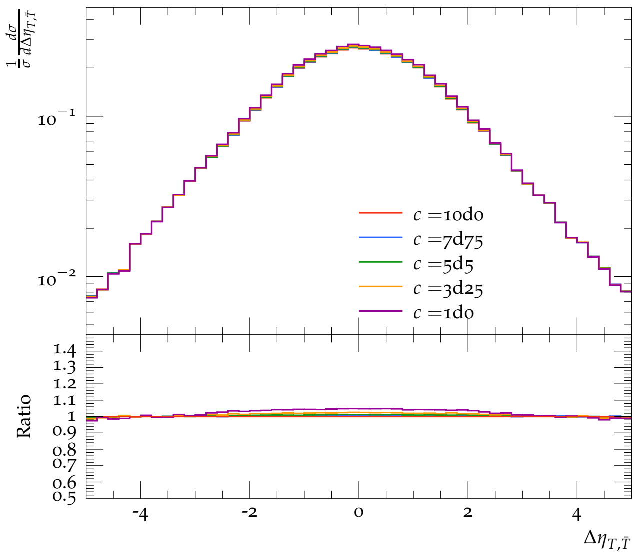

(c) $\eta_{t,\bar{t}}$ for higgs PDF C34: $\exp(-c(x-0.2)^2)$

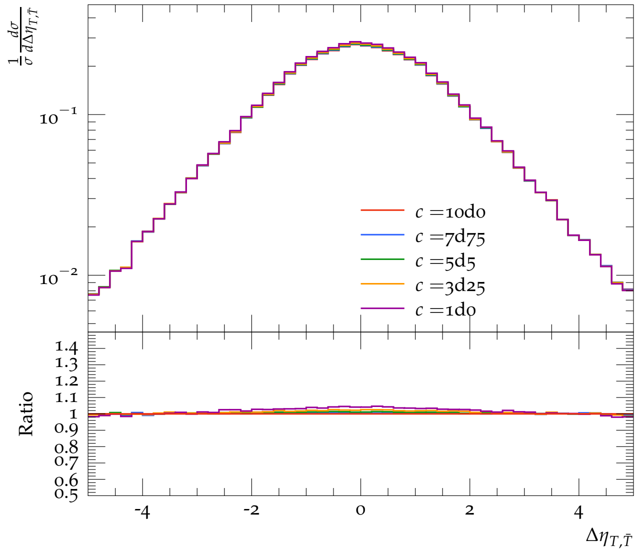

(d) $\eta_{t,\bar{t}}$ for higgs PDF C5: $\frac{(1-x)}{x}\exp(-cx^2)$

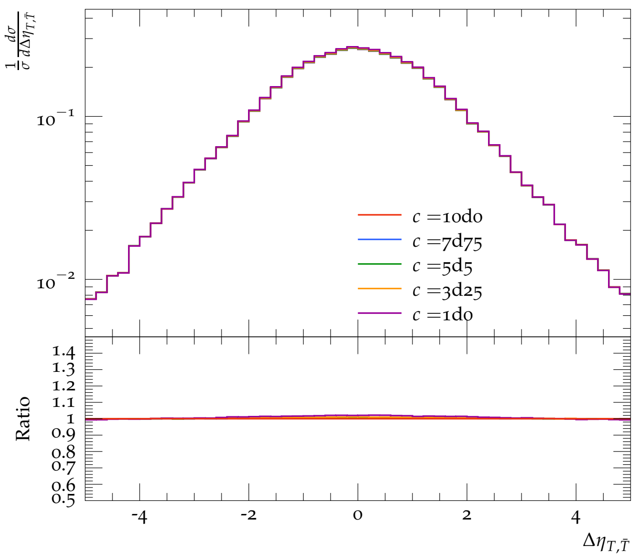

(e) $\eta_{t,\bar{t}}$ for higgs PDF C6: $(1-x)\exp(-cx^2)$

Fig. A.3.: Comparing $\eta_{t,\bar{t}}$ for higgs parameter values $c = (1, 3.25, 5.5, 7.75, 10)$

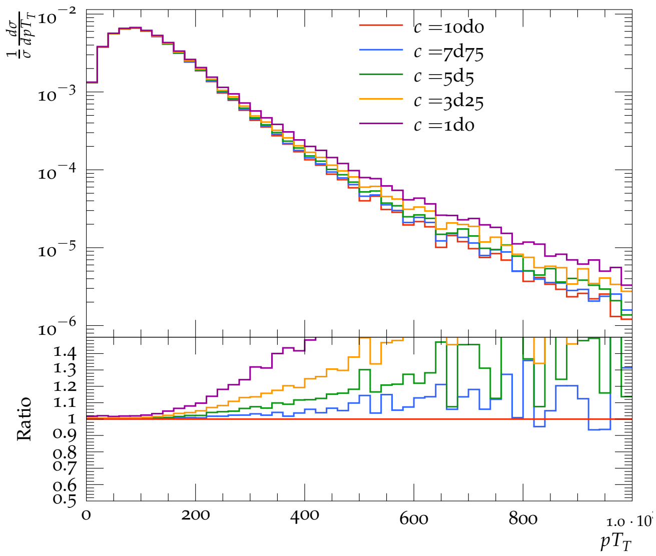

(a) pT_t for higgs PDF C1: $\frac{1}{x}\exp(-cx^2)$

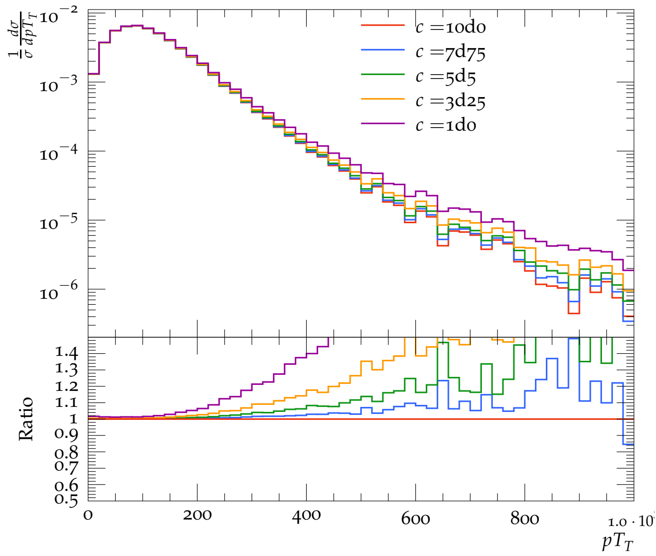

(b) pT_t for higgs PDF C2: $\exp(-cx^2)$

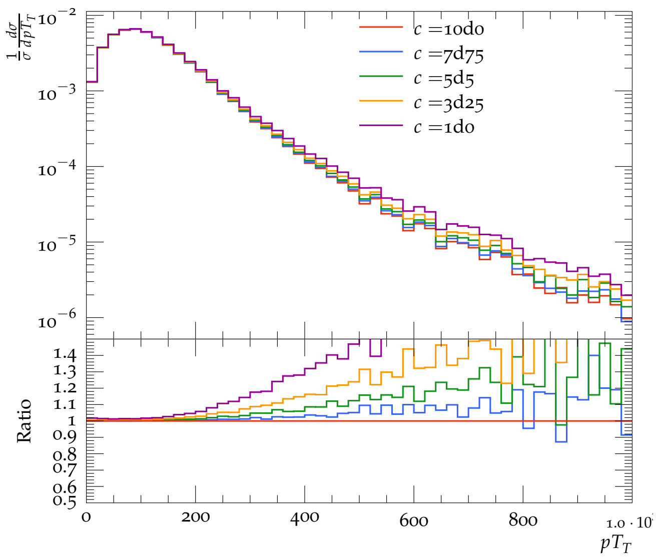

(c) pT_t for higgs PDF C34: $\exp(-c(x-0.2)^2)$

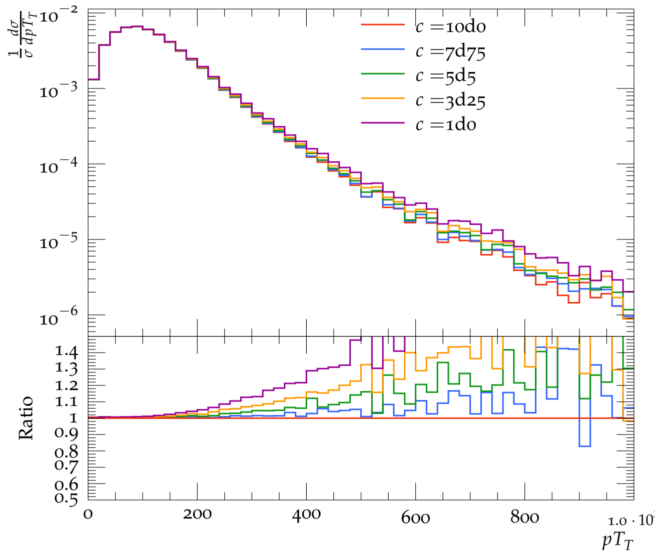

(d) pT_t for higgs PDF C5: $\frac{(1-x)}{x}\exp(-cx^2)$

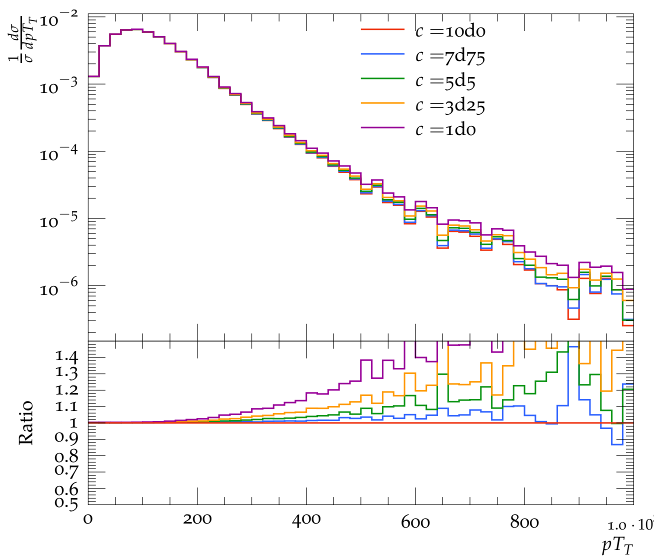

(e) pT_t for higgs PDF C6: $(1-x)\exp(-cx^2)$

Fig. A.4.: Comparing pT_t for higgs parameter values $c = (1, 3.25, 5.5, 7.75, 10)$

A.1.3. $P'P' \to t\bar{t}Z$

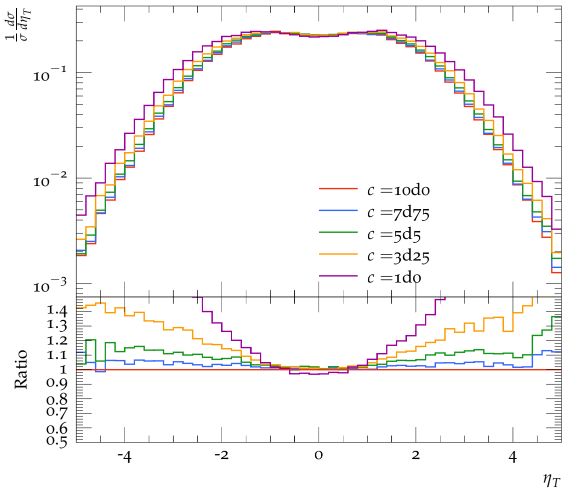

(a) η_t for higgs PDF C1: $\frac{1}{x}\exp(-cx^2)$

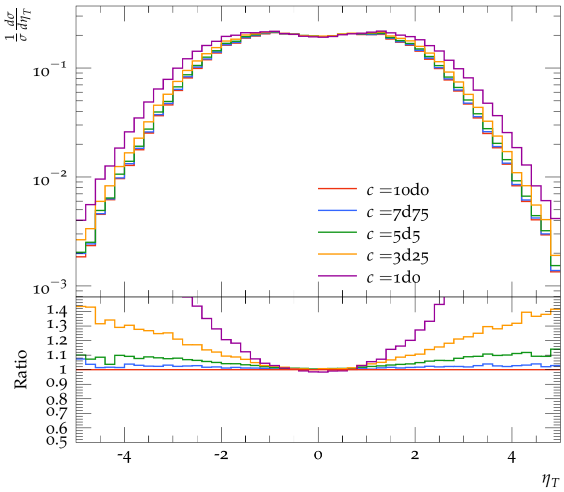

(b) η_t for higgs PDF C2: $\exp(-cx^2)$

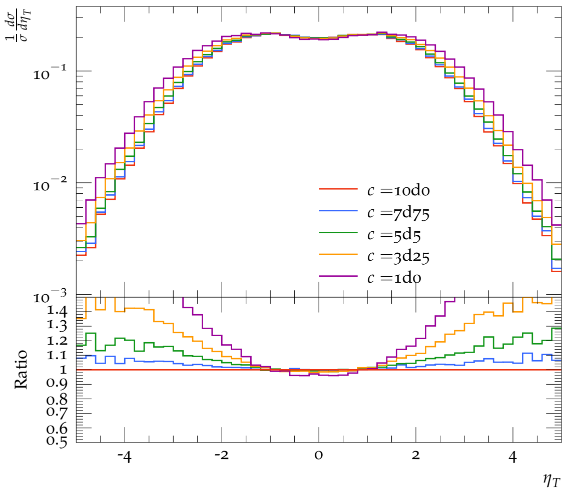

(c) η_t for higgs PDF C34: $\exp(-c(x-0.2)^2)$

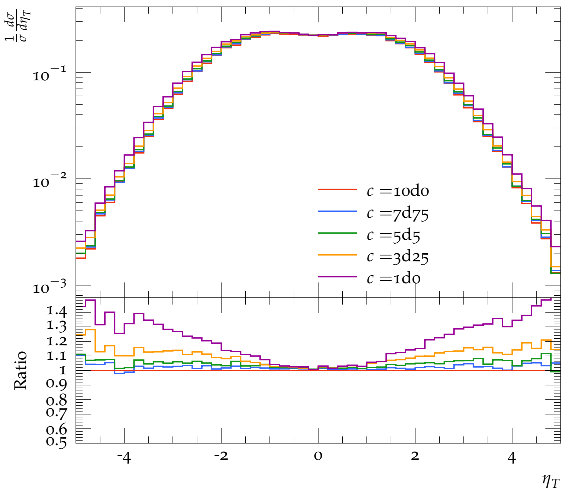

(d) η_t for higgs PDF C5: $\frac{(1-x)}{x}\exp(-cx^2)$

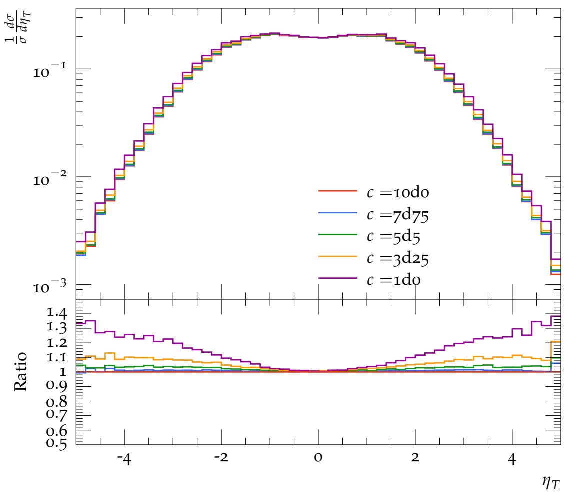

(e) η_t for higgs PDF C6: $(1-x)\exp(-cx^2)$

Fig. A.5.: Comparing η_t for higgs parameter values $c = (1, 3.25, 5.5, 7.75, 10)$

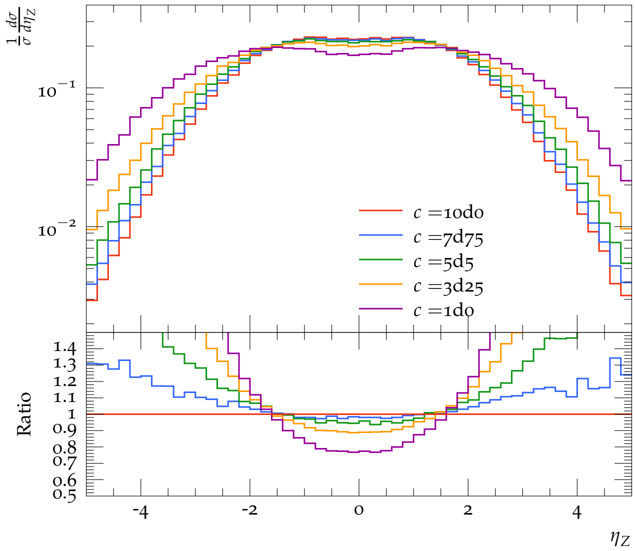

(a) η_Z for higgs PDF C1: $\frac{1}{x}\exp(-cx^2)$

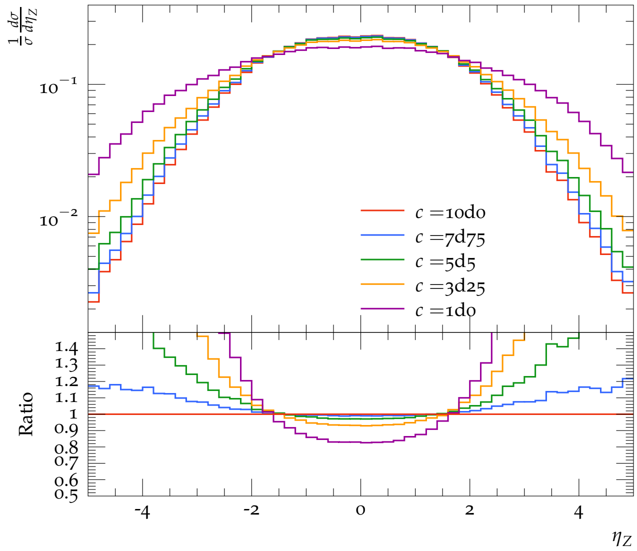

(b) η_Z for higgs PDF C2: $\exp(-cx^2)$

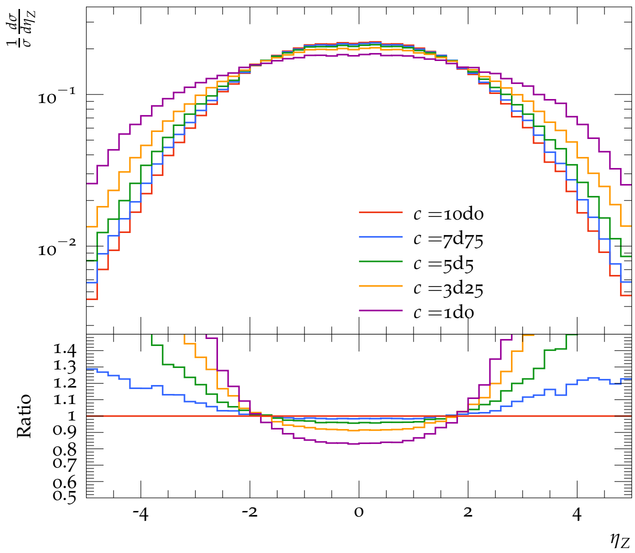

(c) η_Z for higgs PDF C34: $\exp(-c(x-0.2)^2)$

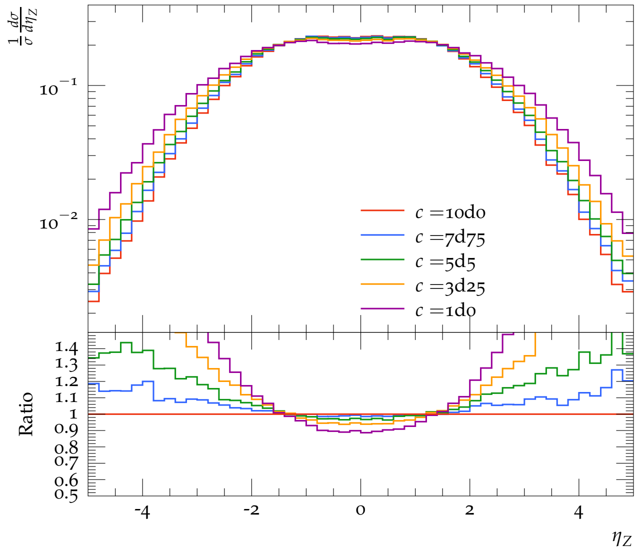

(d) η_Z for higgs PDF C5: $\frac{(1-x)}{x}\exp(-cx^2)$

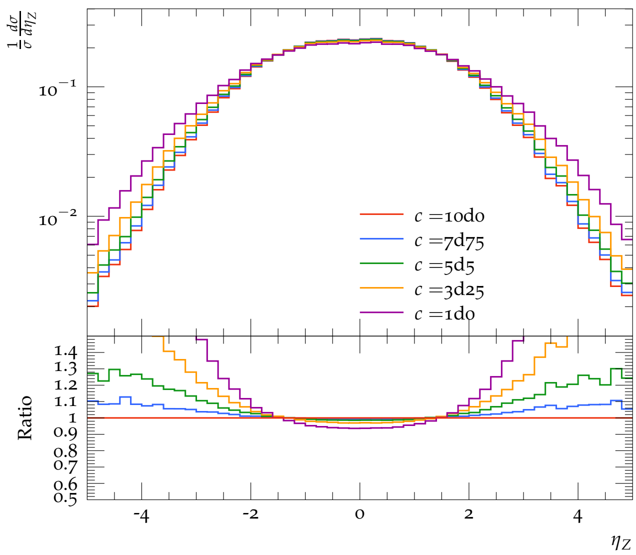

(e) η_Z for higgs PDF C6: $(1-x)\exp(-cx^2)$

Fig. A.6.: Comparing η_Z for higgs parameter values $c = (1, 3.25, 5.5, 7.75, 10)$

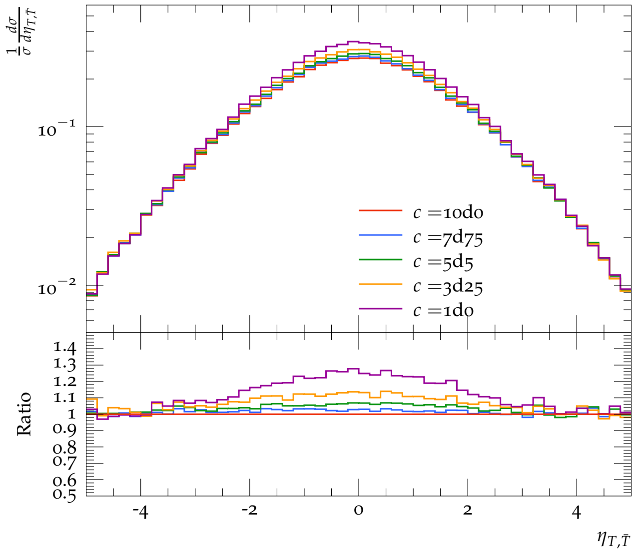

(a) $\eta_{t,\bar{t}}$ for higgs PDF C1: $\frac{1}{x}\exp(-cx^2)$

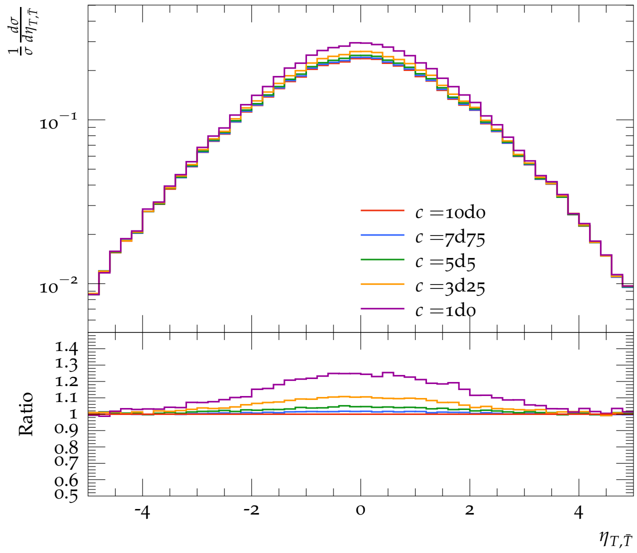

(b) $\eta_{t,\bar{t}}$ for higgs PDF C2: $\exp(-cx^2)$

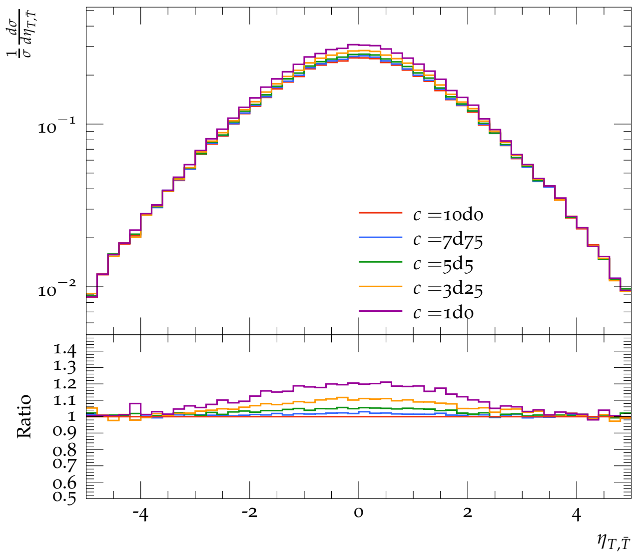

(c) $\eta_{t,\bar{t}}$ for higgs PDF C34: $\exp(-c(x-0.2)^2)$

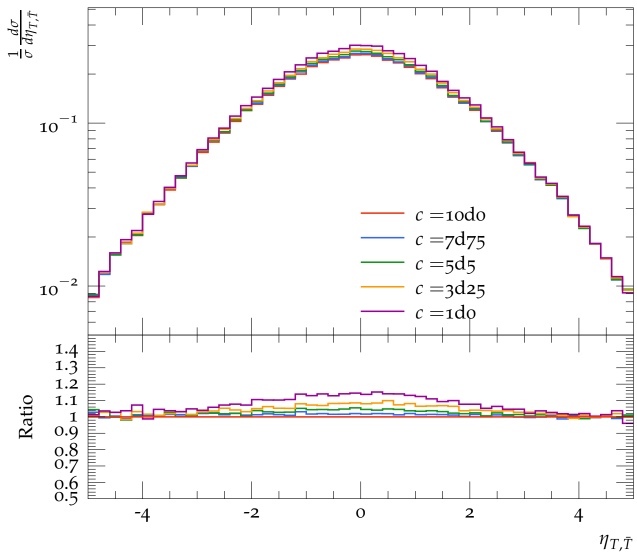

(d) $\eta_{t,\bar{t}}$ for higgs PDF C5: $\frac{(1-x)}{x}\exp(-cx^2)$

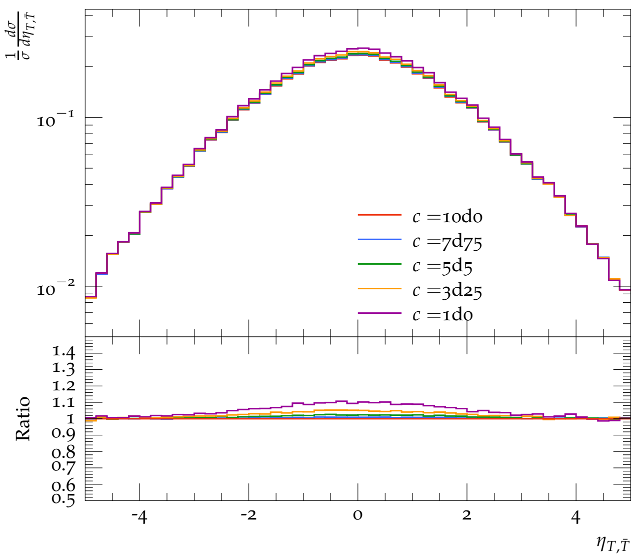

(e) $\eta_{t,\bar{t}}$ for higgs PDF C6: $(1-x)\exp(-cx^2)$

Fig. A.7.: Comparing $\eta_{t,\bar{t}}$ for higgs parameter values $c = (1, 3.25, 5.5, 7.75, 10)$

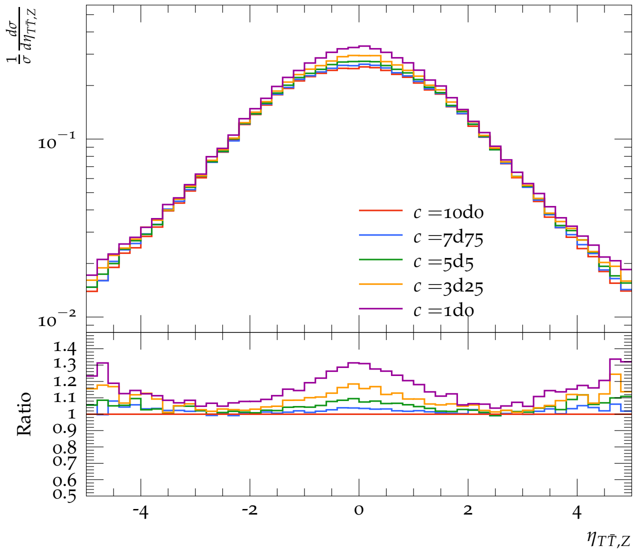

(a) $\eta_{t\bar{t},Z}$ for higgs PDF C1: $\frac{1}{x}\exp(-cx^2)$

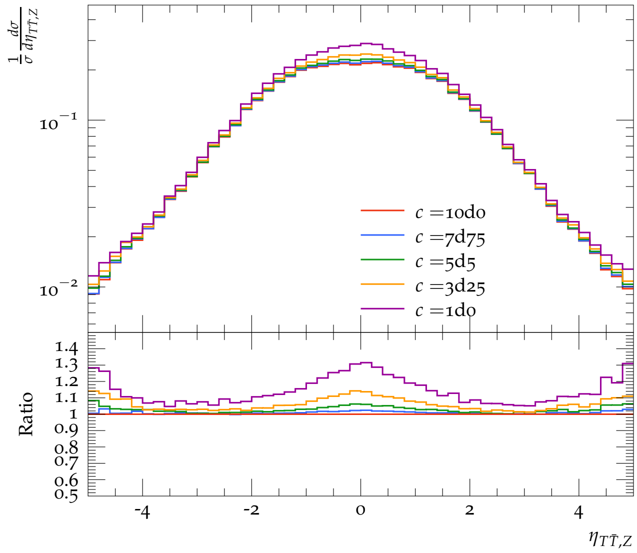

(b) $\eta_{t\bar{t},Z}$ for higgs PDF C2: $\exp(-cx^2)$

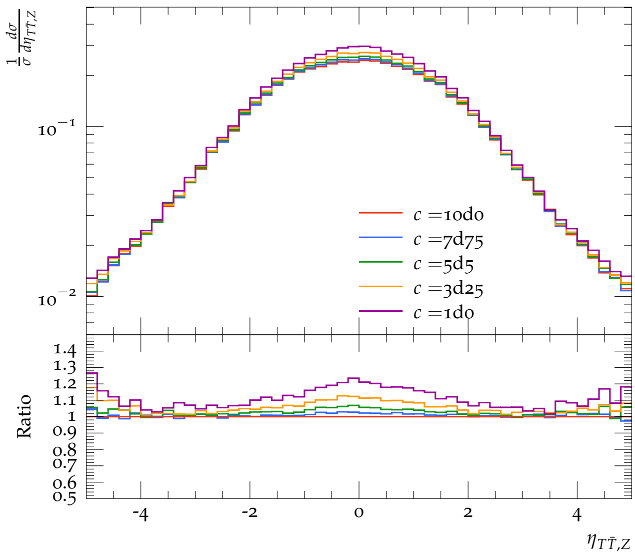

(c) $\eta_{t\bar{t},Z}$ for higgs PDF C34: $\exp(-c(x-0.2)^2)$

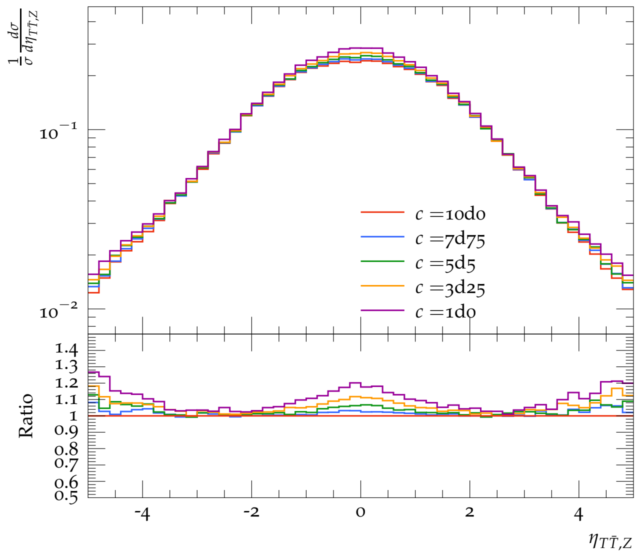

(d) $\eta_{t\bar{t},Z}$ for higgs PDF C5: $\frac{(1-x)}{x}\exp(-cx^2)$

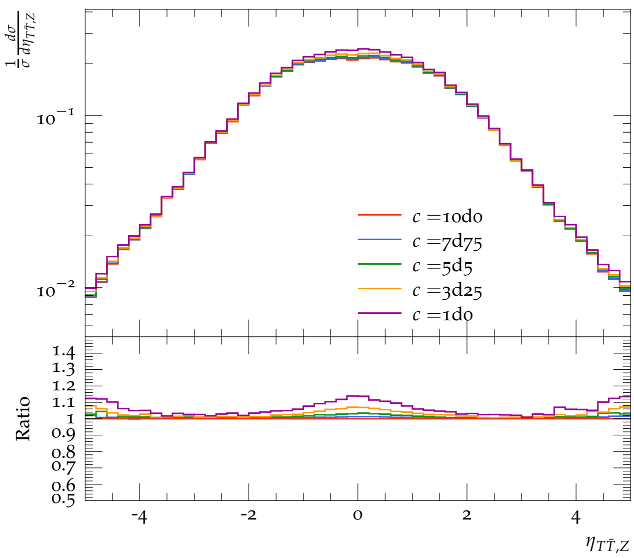

(e) $\eta_{t\bar{t},Z}$ for higgs PDF C6: $(1-x)\exp(-cx^2)$

Fig. A.8.: Comparing $\eta_{t\bar{t},Z}$ for higgs parameter values $c = (1, 3.25, 5.5, 7.75, 10)$

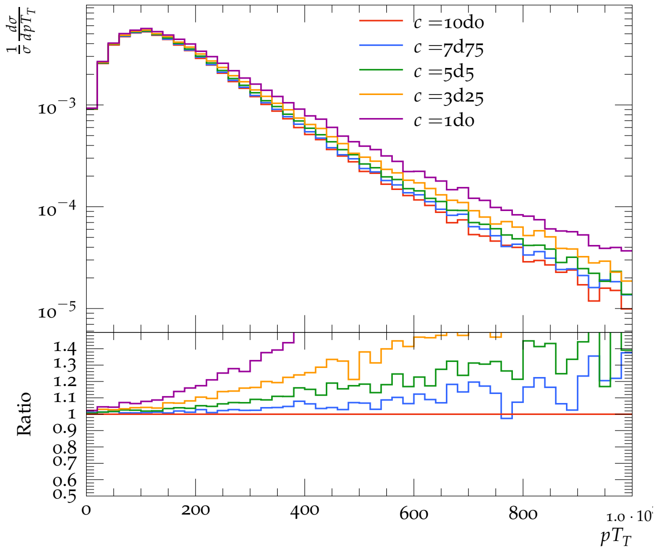

(a) pT_t for higgs PDF C1: $\frac{1}{x}\exp(-cx^2)$

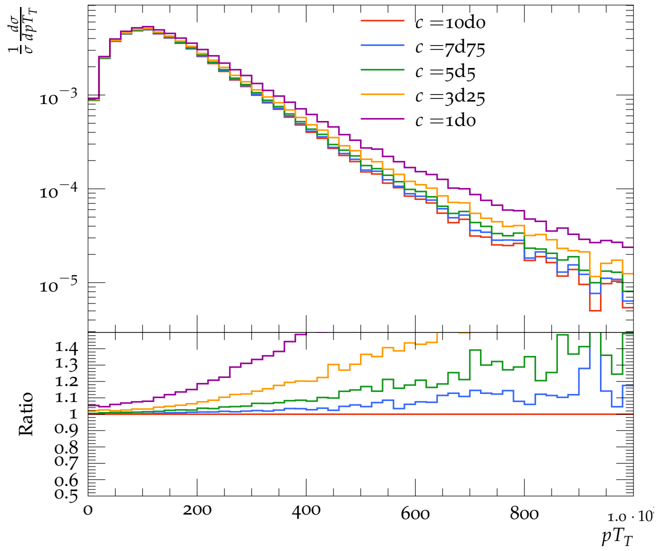

(b) pT_t for higgs PDF C2: $\exp(-cx^2)$

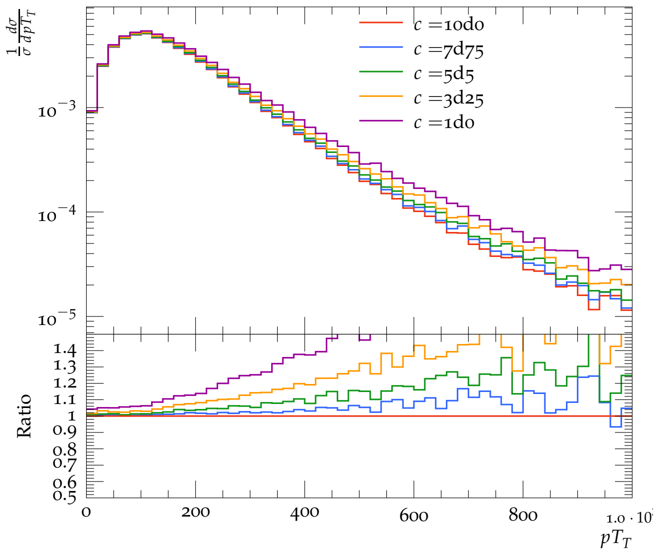

(c) pT_t for higgs PDF C34: $\exp(-c(x-0.2)^2)$

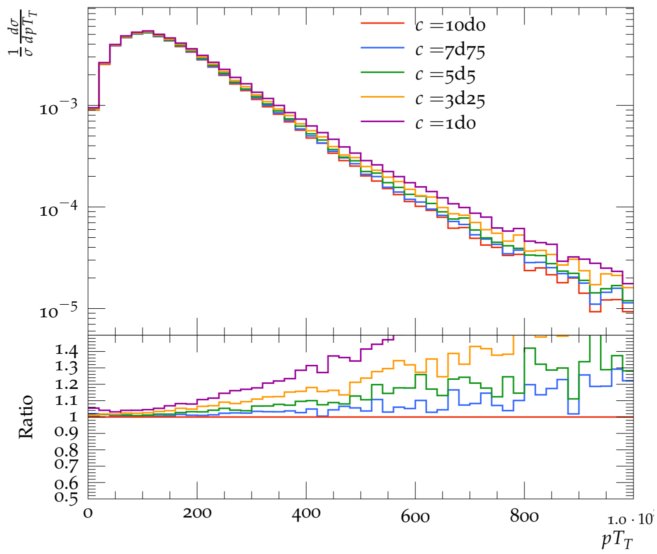

(d) pT_t for higgs PDF C5: $\frac{(1-x)}{x}\exp(-cx^2)$

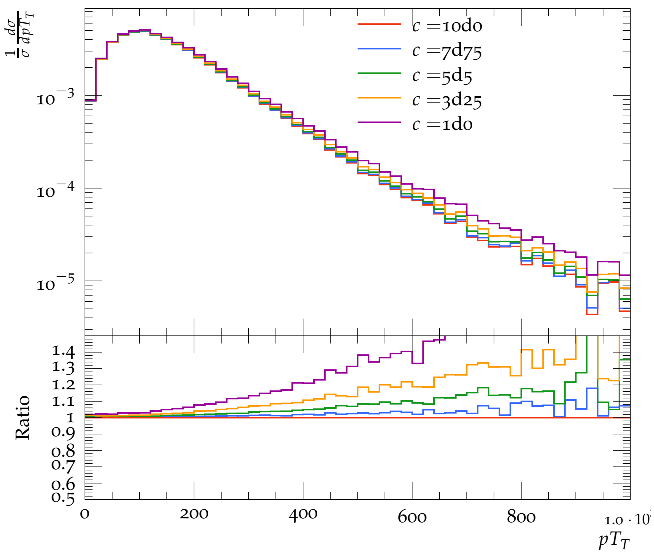

(e) pT_t for higgs PDF C6: $(1-x)\exp(-cx^2)$

Fig. A.9.: Comparing pT_t for higgs parameter values $c = (1, 3.25, 5.5, 7.75, 10)$

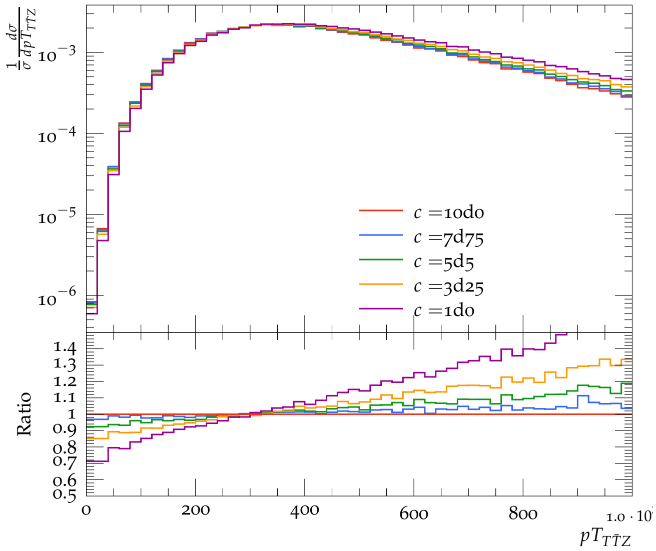

(a) $pT_{t\bar{t}Z}$ for higgs PDF C1: $\frac{1}{x}\exp(-cx^2)$

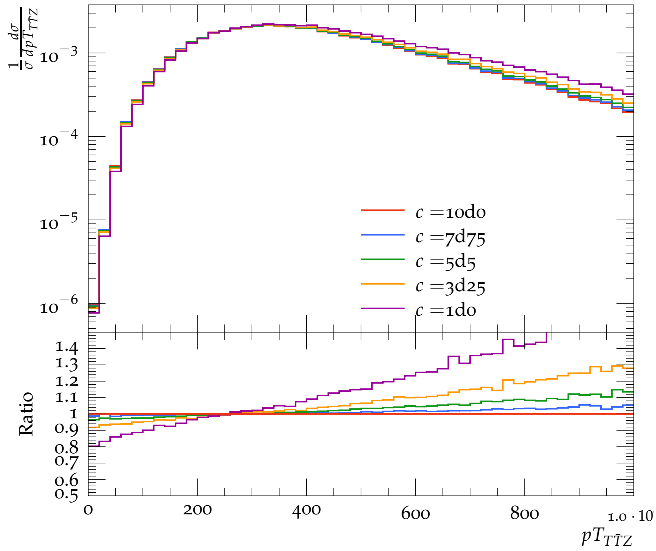

(b) $pT_{t\bar{t}Z}$ for higgs PDF C2: $\exp(-cx^2)$

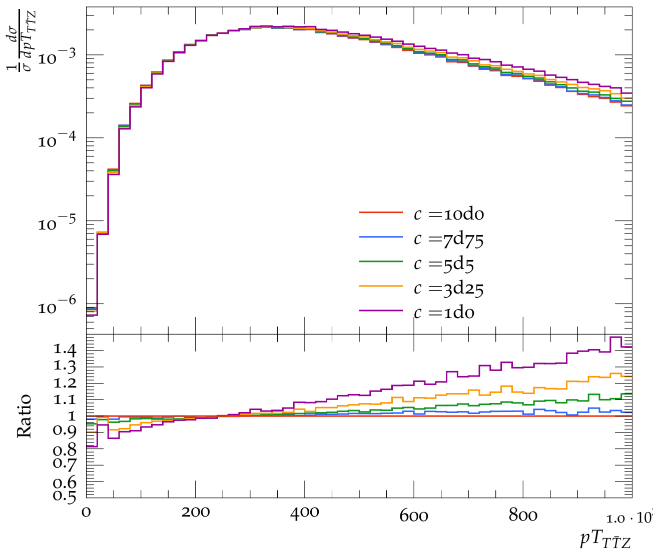

(c) $pT_{t\bar{t}Z}$ for higgs PDF C34: $\exp(-c(x-0.2)^2)$

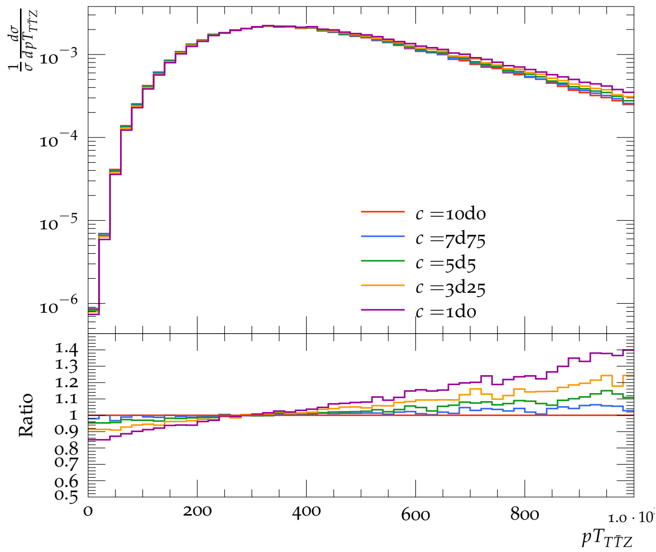

(d) $pT_{t\bar{t}Z}$ for higgs PDF C5: $\frac{(1-x)}{x}\exp(-cx^2)$

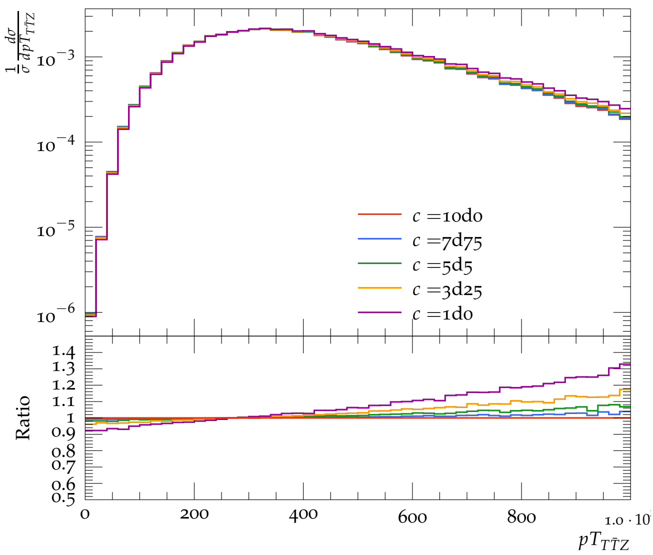

(e) $pT_{t\bar{t}Z}$ for higgs PDF C6: $(1-x)\exp(-cx^2)$

Fig. A.10.: Comparing $pT_{t\bar{t}Z}$ for higgs parameter values $c = (1, 3.25, 5.5, 7.75, 10)$

A.2. Comparing differential cross sections for different higgs PDF models

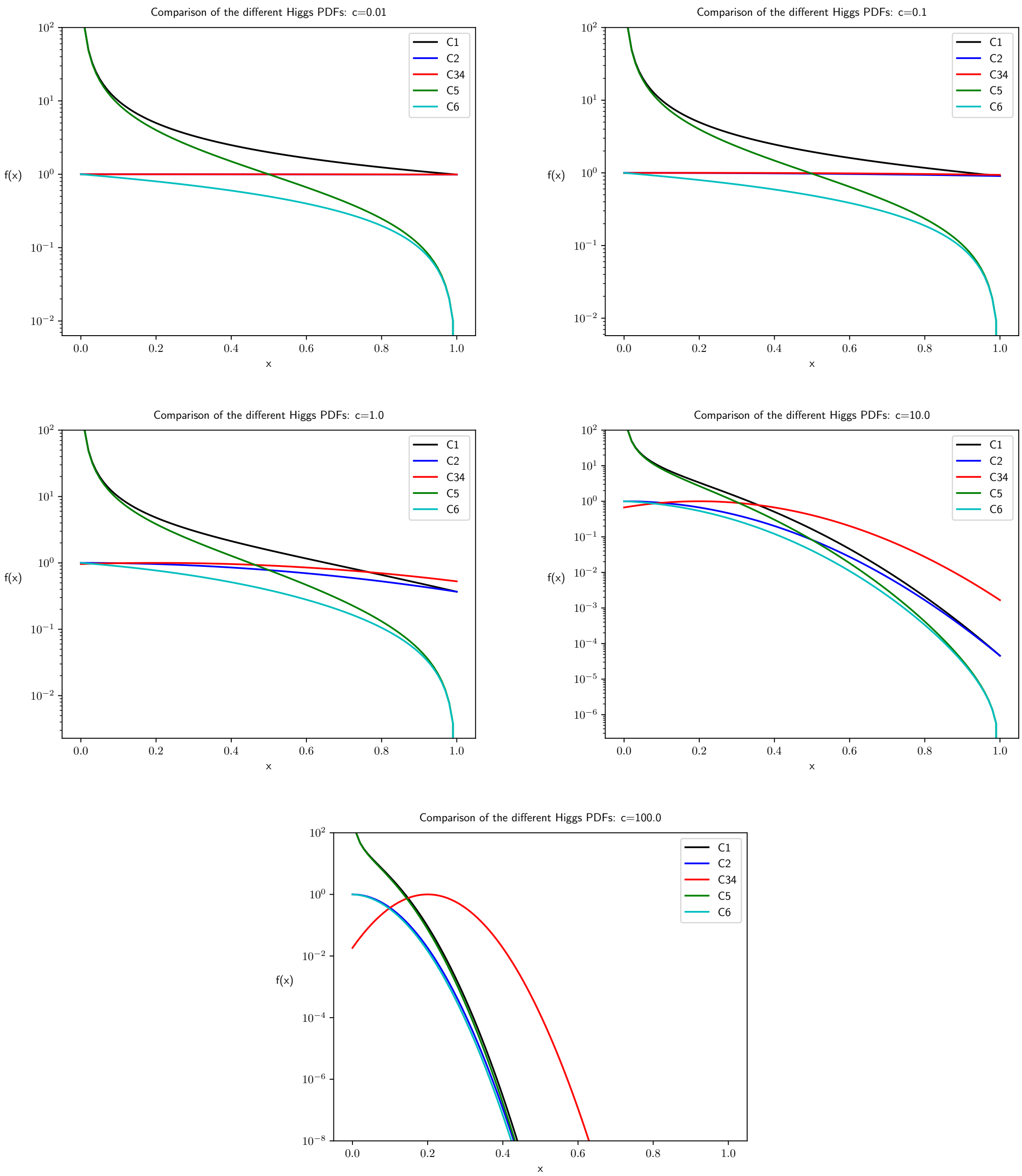

Fig. A.11.: Overview of the different higgs PDFs

A.2.1. $P'P' \to l\bar{l}$

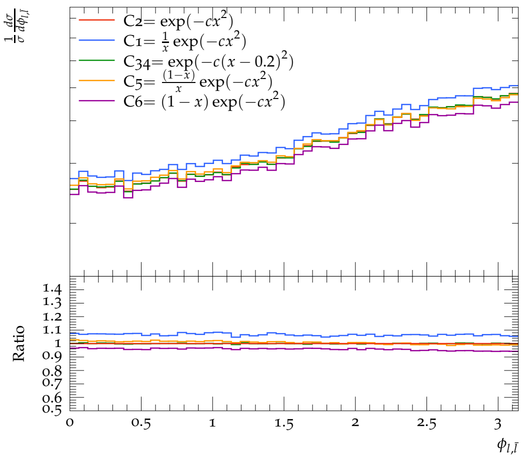

(a) $\phi_{l,\bar{l}}$ for different higgs PDFs and $c = 0.01$

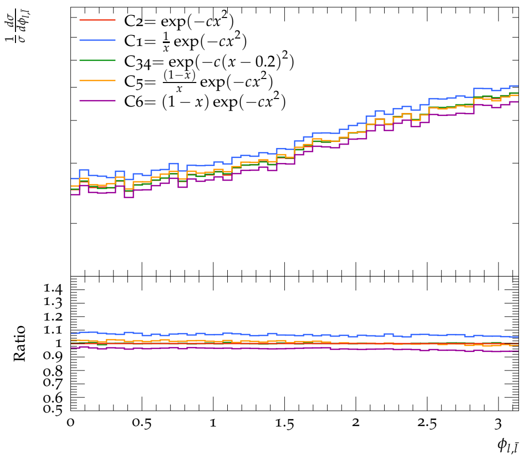

(b) $\phi_{l,\bar{l}}$ for different higgs PDFs and $c = 0.1$

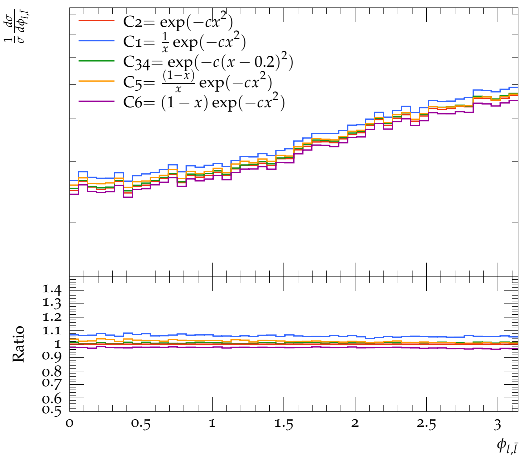

(c) $\phi_{l,\bar{l}}$ for different higgs PDFs and $c = 1.0$

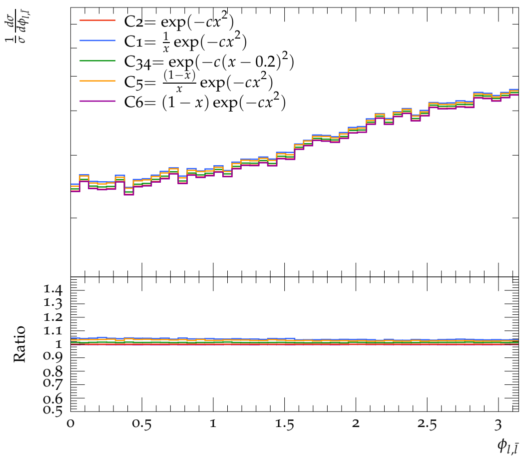

(d) $\phi_{l,\bar{l}}$ for different higgs PDFs and $c = 100.0$

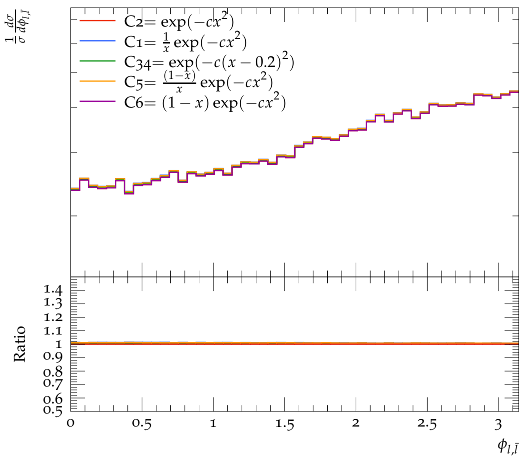

(e) $\phi_{l,\bar{l}}$ for different higgs PDFs and $c = 100.0$

Fig. A.12.: Comparing $\phi_{l,\bar{l}}$ for higgs PDFs C1, C2, C34, C5, C6 for parameters $c = (0.01, 0.1, 1.0, 10.0, 100.0)$

A.2.2. $P'P' \to t\bar{t}$

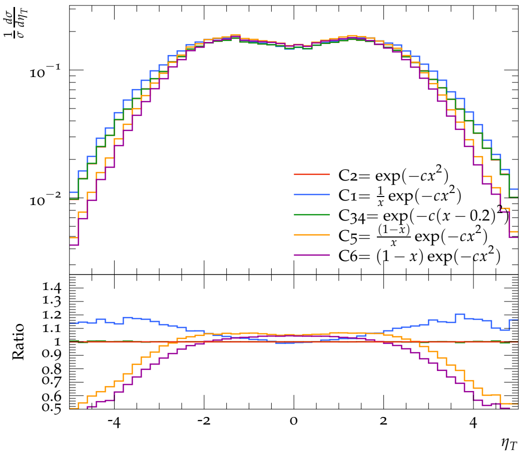

(a) η_t for different higgs PDFs and $c = 0.01$

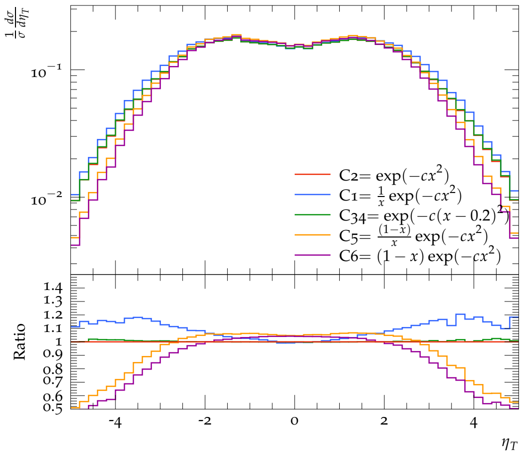

(b) η_t for different higgs PDFs and $c = 0.1$

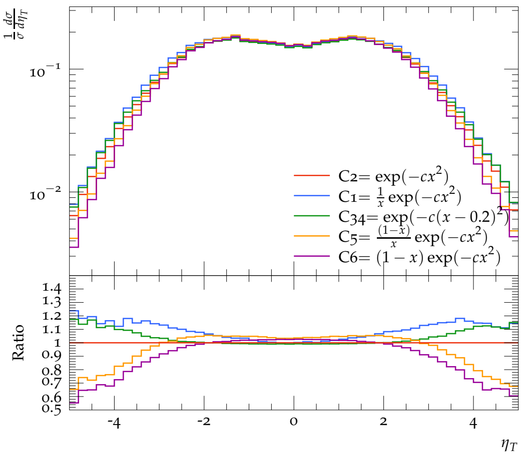

(c) η_t for different higgs PDFs and $c = 1.0$

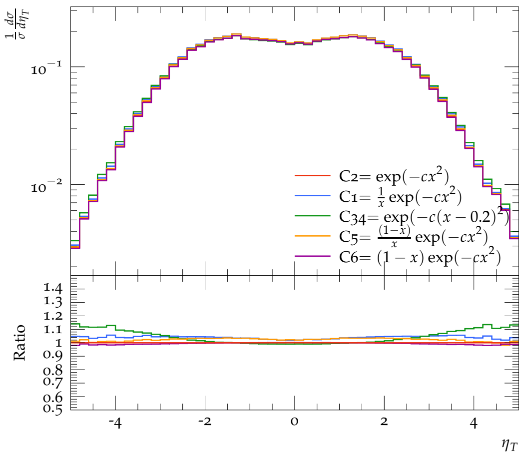

(d) η_t for different higgs PDFs and $c = 100.0$

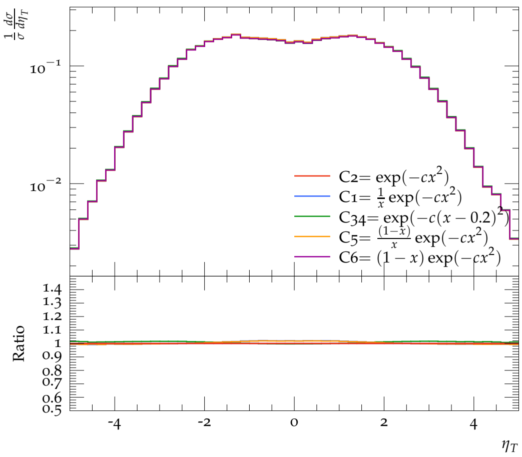

(e) η_t for different higgs PDFs and $c = 100.0$

Fig. A.13.: Comparing η_t for higgs PDFs C1, C2, C34, C5, C6 for parameters $c = (0.01, 0.1, 1.0, 10.0, 100.0)$

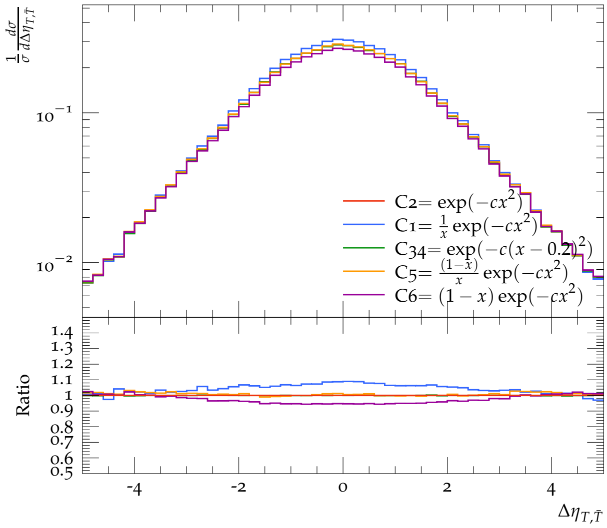

(a) $\eta_{t,\bar{t}}$ for different higgs PDFs and $c = 0.01$

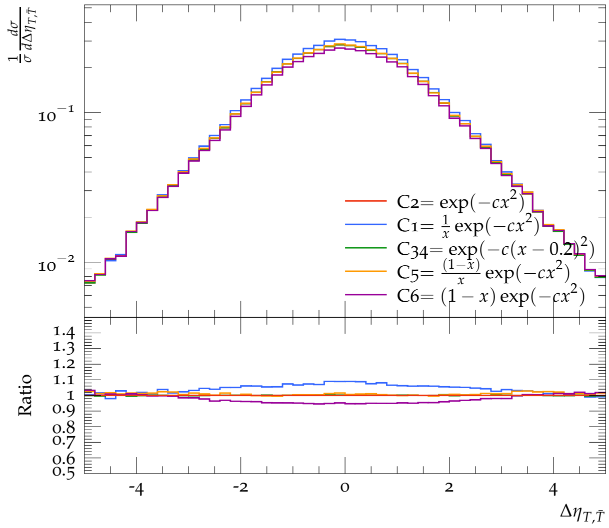

(b) $\eta_{t,\bar{t}}$ for different higgs PDFs and $c = 0.1$

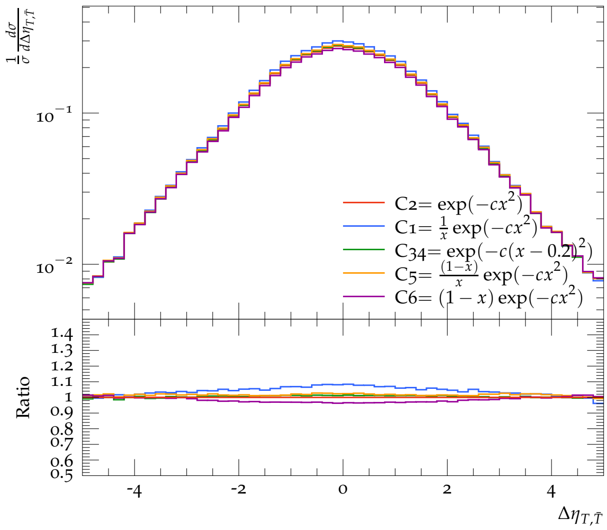

(c) $\eta_{t,\bar{t}}$ for different higgs PDFs and $c = 1.0$

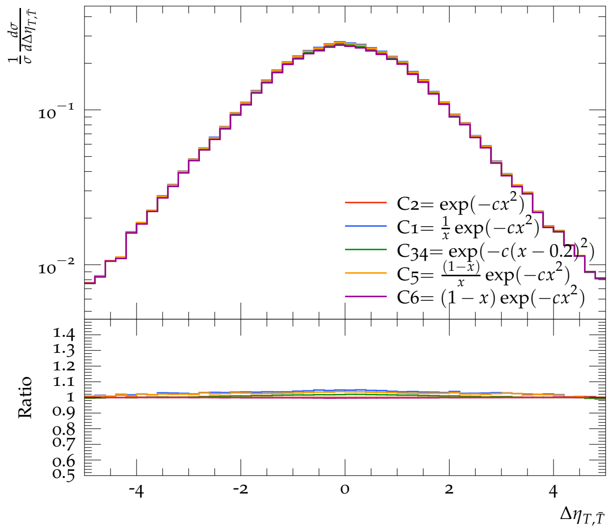

(d) $\eta_{t,\bar{t}}$ for different higgs PDFs and $c = 100.0$

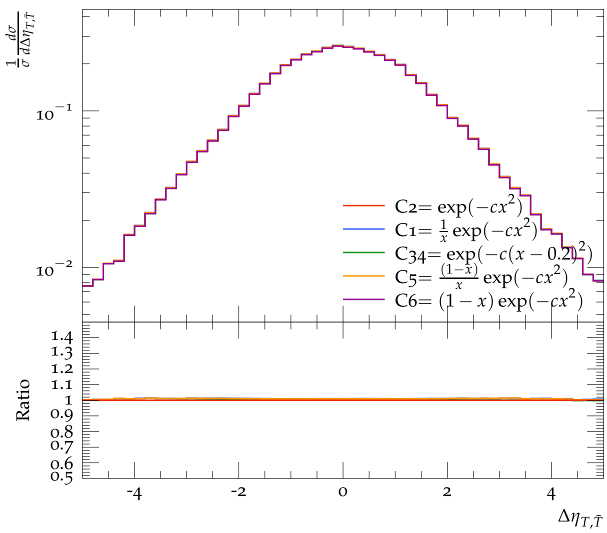

(e) $\eta_{t,\bar{t}}$ for different higgs PDFs and $c = 100.0$

Fig. A.14.: Comparing $\eta_{t,\bar{t}}$ for higgs PDFs C1, C2, C34, C5, C6 for parameters $c = (0.01, 0.1, 1.0, 10.0, 100.0)$

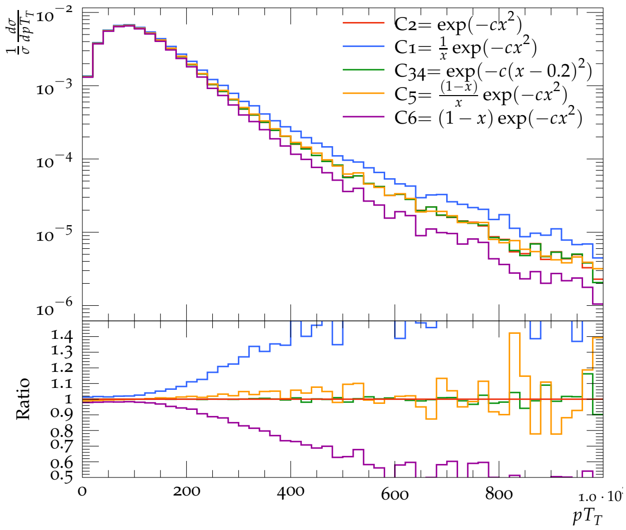

(a) pT_t for different higgs PDFs and $c = 0.01$

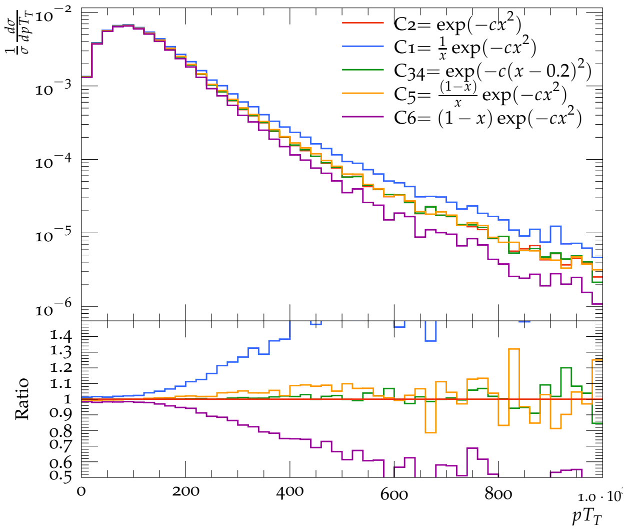

(b) pT_t for different higgs PDFs and $c = 0.1$

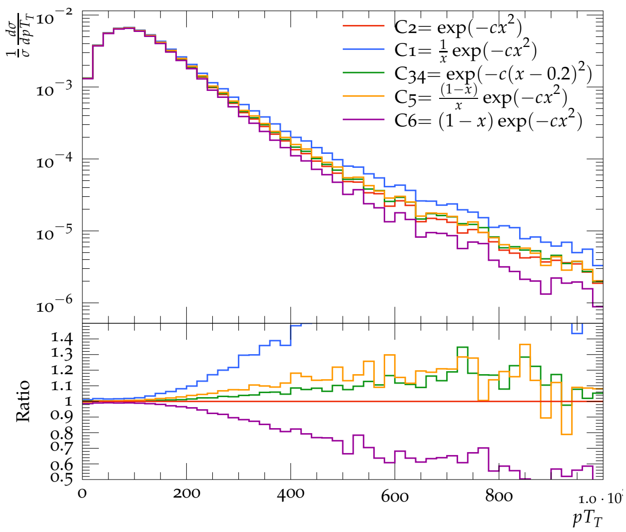

(c) pT_t for different higgs PDFs and $c = 1.0$

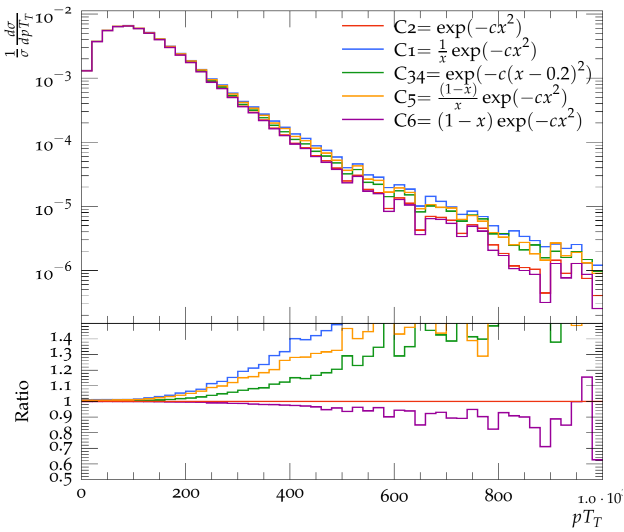

(d) pT_t for different higgs PDFs and $c = 100.0$

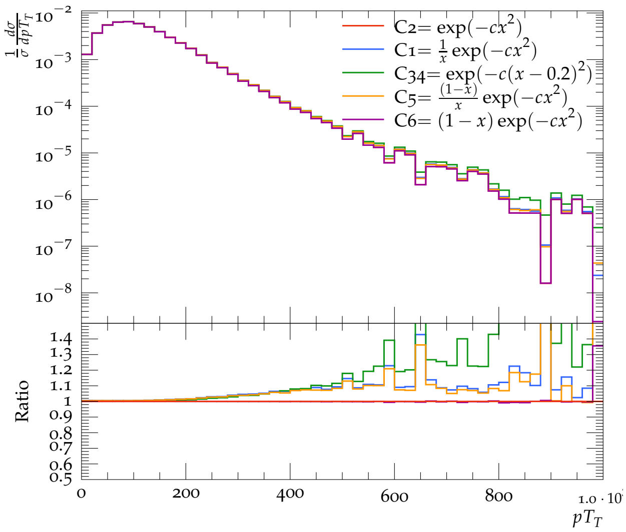

(e) pT_t for different higgs PDFs and $c = 100.0$

Fig. A.15.: Comparing pT_t for higgs PDFs C1, C2, C34, C5, C6 for parameters $c = (0.01, 0.1, 1.0, 10.0, 100.0)$

A.2.3. $P'P' \to t\bar{t}Z$

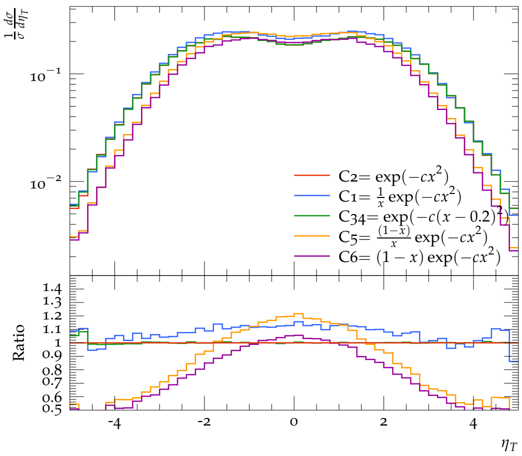

(a) η_t for different higgs PDFs and $c = 0.01$

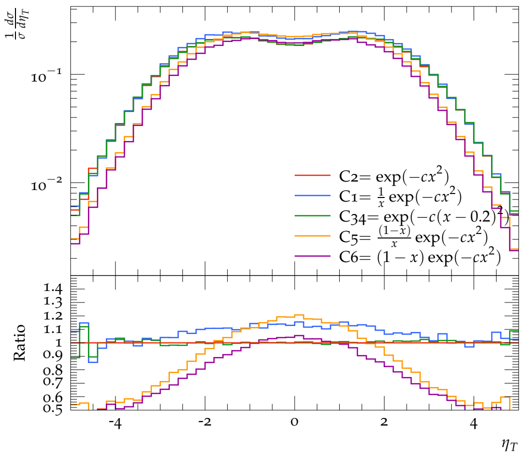

(b) η_t for different higgs PDFs and $c = 0.1$

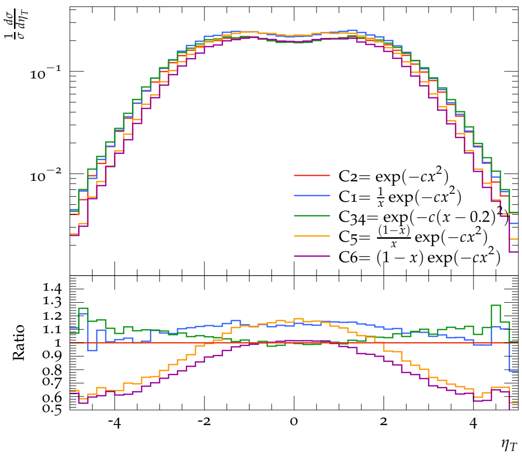

(c) η_t for different higgs PDFs and $c = 1.0$

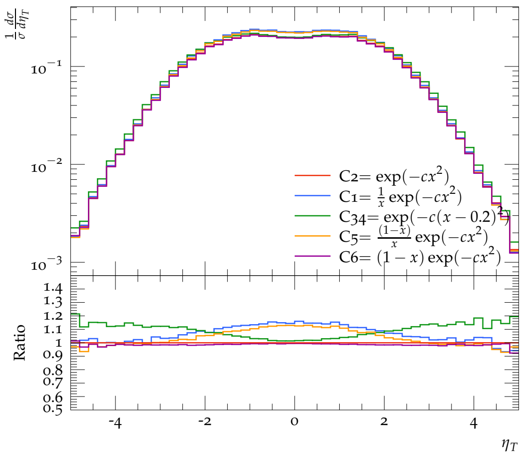

(d) η_t for different higgs PDFs and $c = 10.0$

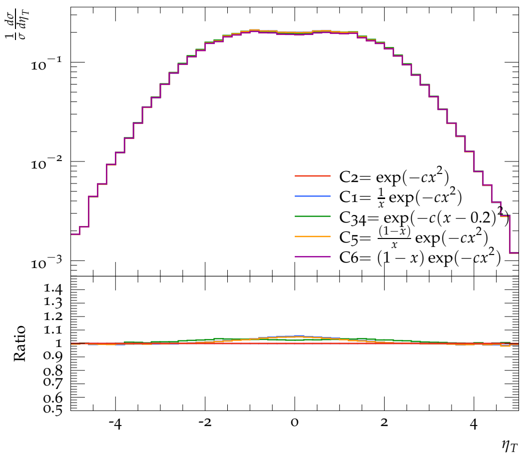

(e) η_t for different higgs PDFs and $c = 100.0$

Fig. A.16.: Comparing η_t for higgs PDFs C1, C2, C34, C5, C6 for parameters $c = (0.01, 0.1, 1.0, 10.0, 100.0)$

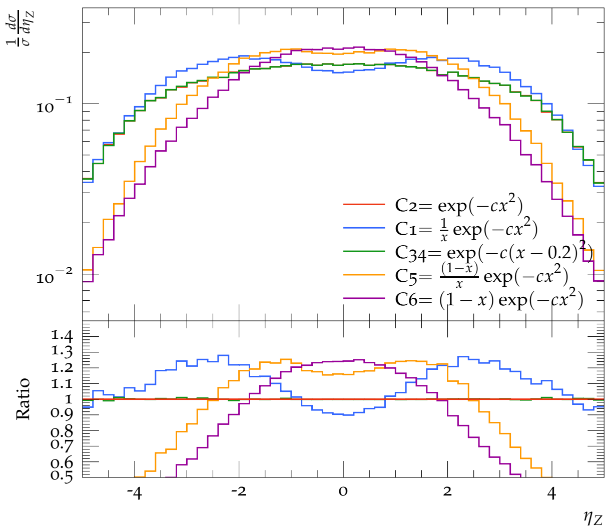

(a) η_Z for different higgs PDFs and $c = 0.01$

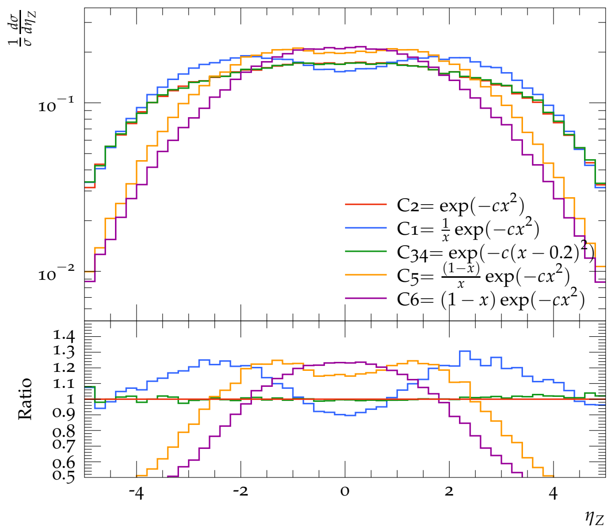

(b) η_Z for different higgs PDFs and $c = 0.1$

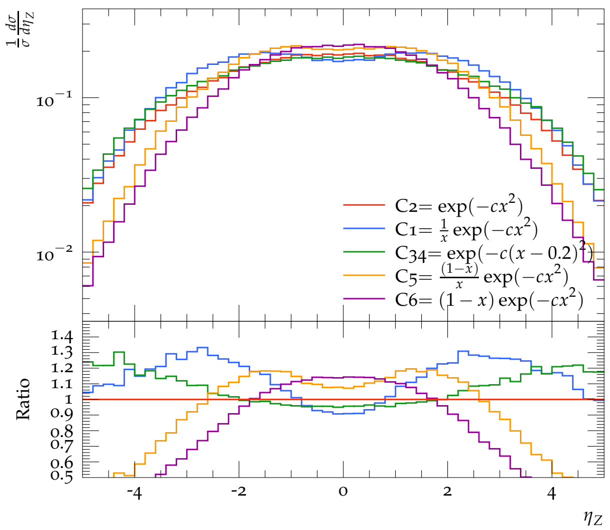

(c) η_Z for different higgs PDFs and $c = 1.0$

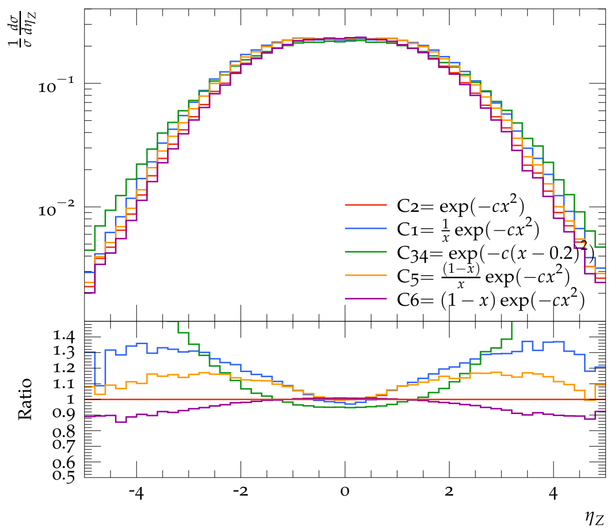

(d) η_Z for different higgs PDFs and $c = 10.0$

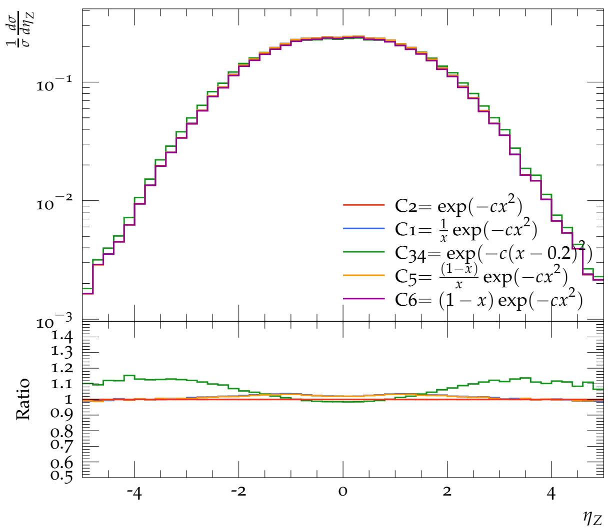

(e) η_Z for different higgs PDFs and $c = 100.0$

Fig. A.17.: Comparing η_Z for higgs PDFs C1, C2, C34, C5, C6 for parameters $c = (0.01, 0.1, 1.0, 10.0, 100.0)$

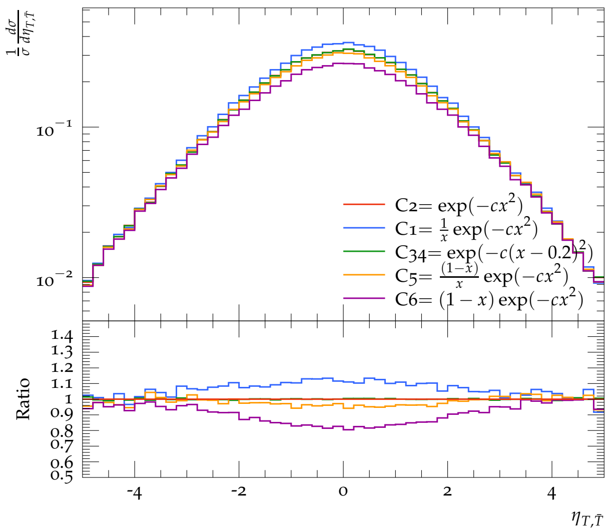

(a) $\eta_{t,\bar{t}}$ for different higgs PDFs and $c = 0.01$

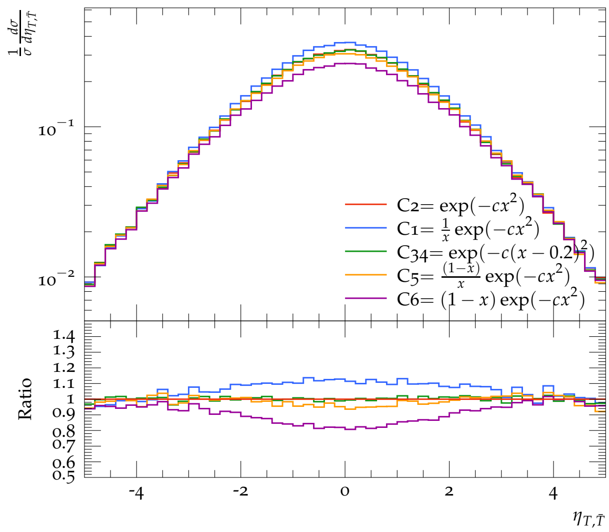

(b) $\eta_{t,\bar{t}}$ for different higgs PDFs and $c = 0.1$

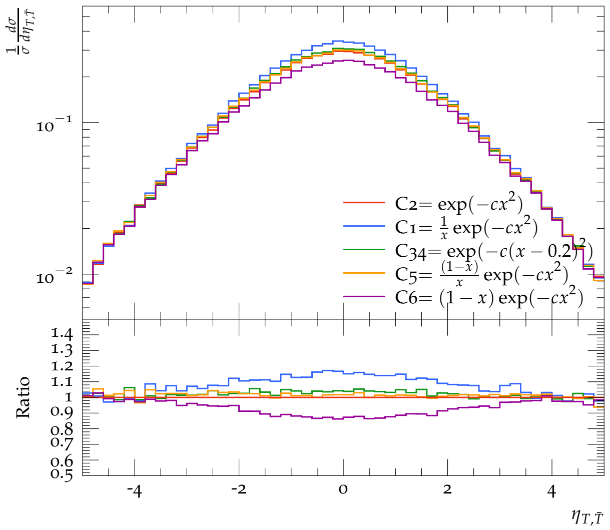

(c) $\eta_{t,\bar{t}}$ for different higgs PDFs and $c = 1.0$

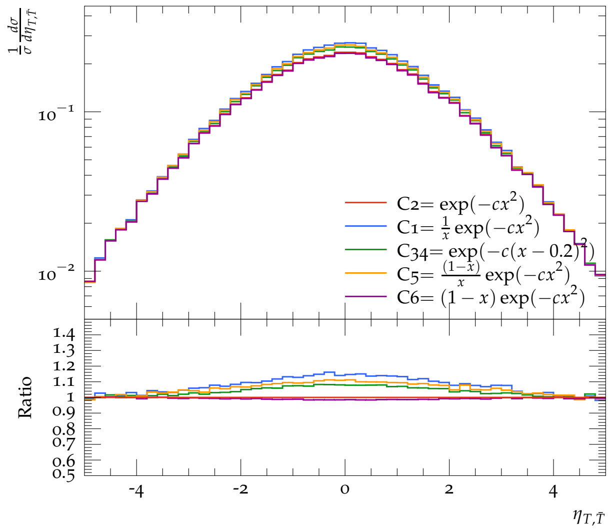

(d) $\eta_{t,\bar{t}}$ for different higgs PDFs and $c = 10.0$

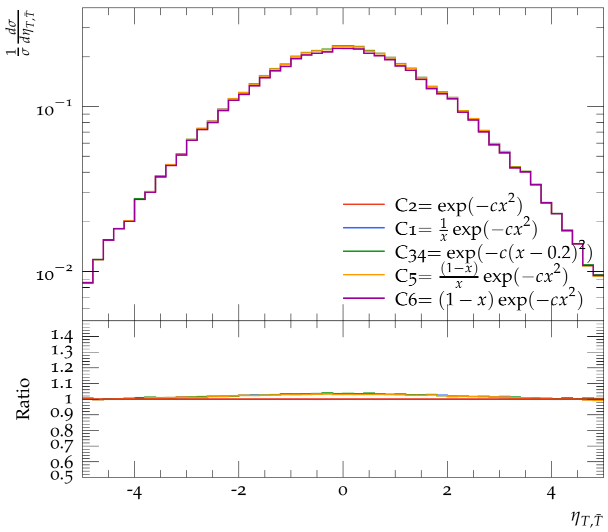

(e) $\eta_{t,\bar{t}}$ for different higgs PDFs and $c = 100.0$

Fig. A.18.: Comparing $\eta_{t,\bar{t}}$ for higgs PDFs C1, C2, C34, C5, C6 for parameters $c = (0.01, 0.1, 1.0, 10.0, 100.0)$

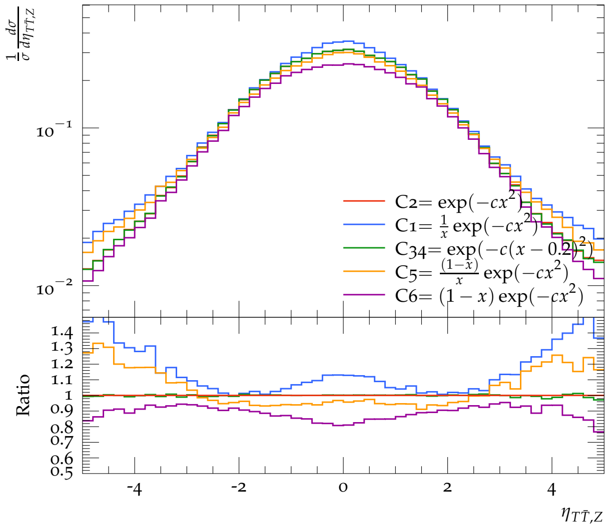

(a) $\eta_{t\bar{t},Z}$ for different higgs PDFs and $c = 0.01$

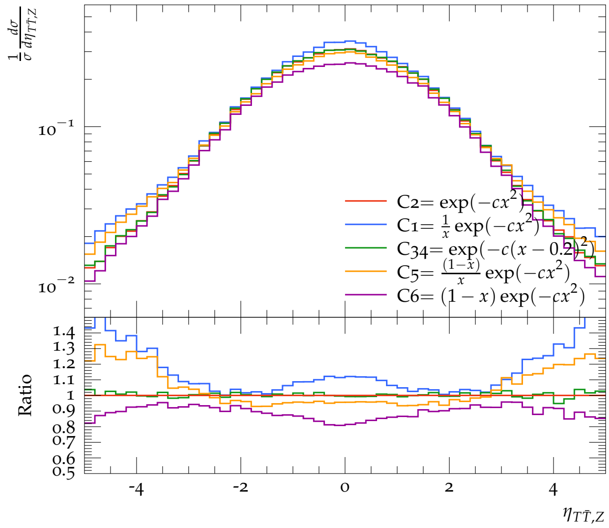

(b) $\eta_{t\bar{t},Z}$ for different higgs PDFs and $c = 0.1$

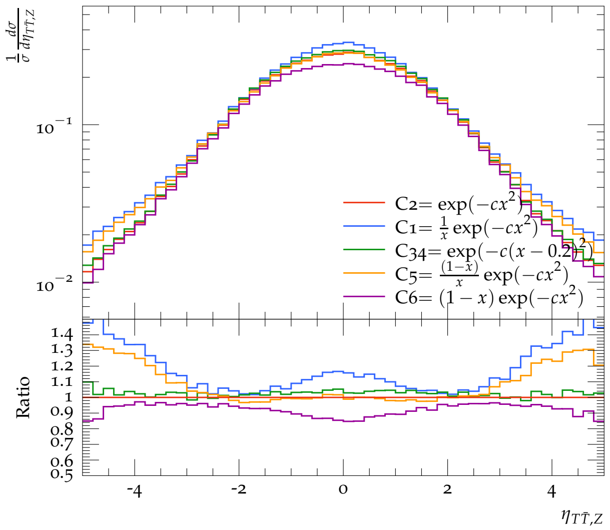

(c) $\eta_{t\bar{t},Z}$ for different higgs PDFs and $c = 1.0$

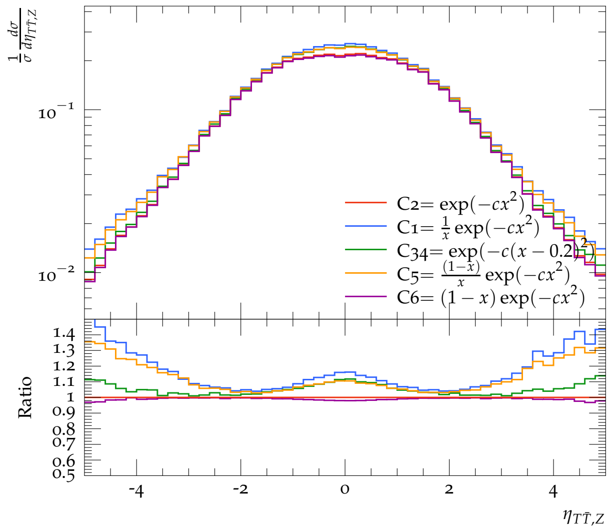

(d) $\eta_{t\bar{t},Z}$ for different higgs PDFs and $c = 10.0$

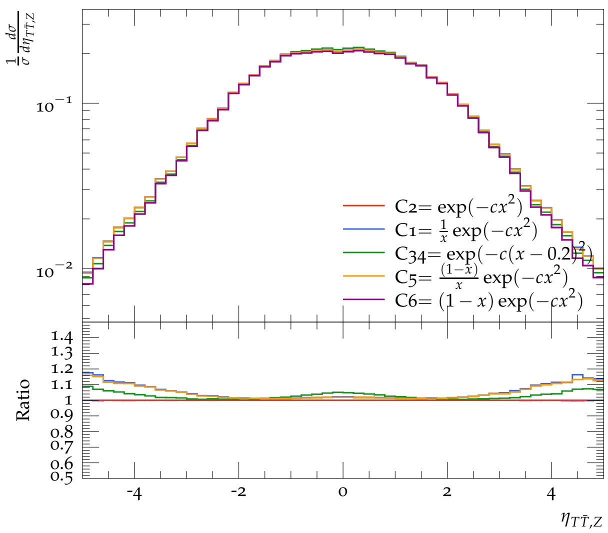

(e) $\eta_{t\bar{t},Z}$ for different higgs PDFs and $c = 100.0$

Fig. A.19.: Comparing $\eta_{t\bar{t},Z}$ for higgs PDFs C1, C2, C34, C5, C6 for parameters $c = (0.01, 0.1, 1.0, 10.0, 100.0)$

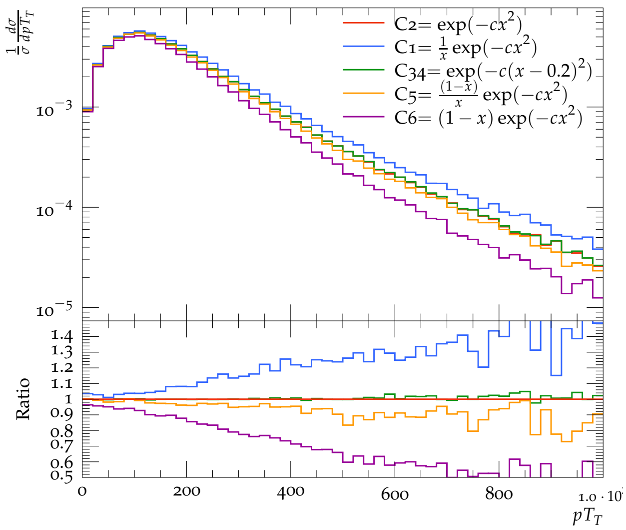

(a) pT_t for different higgs PDFs and $c = 0.01$

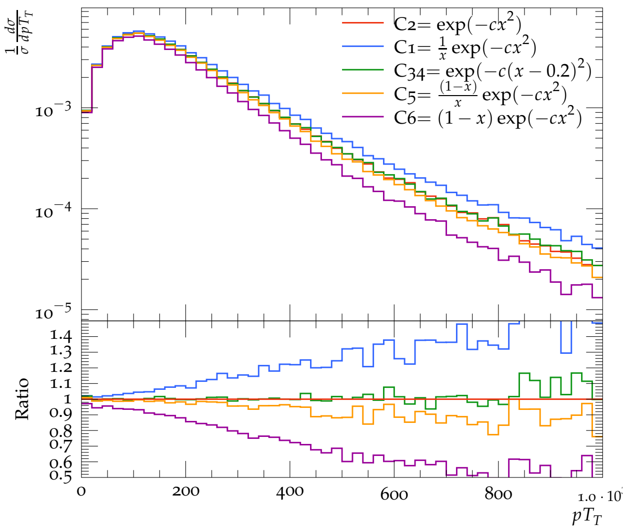

(b) pT_t for different higgs PDFs and $c = 0.1$

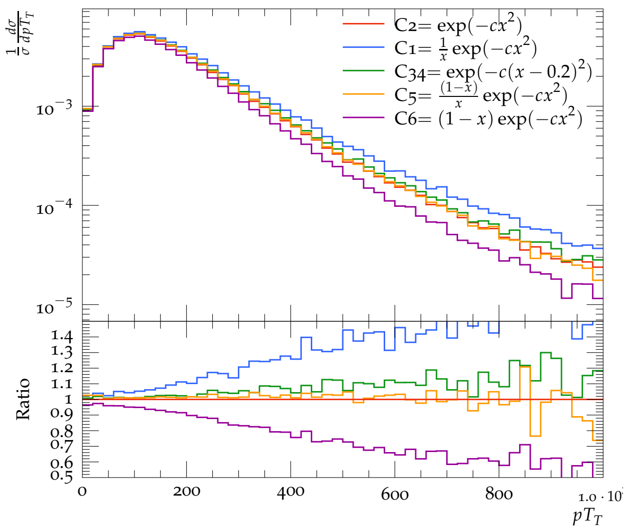

(c) pT_t for different higgs PDFs and $c = 1.0$

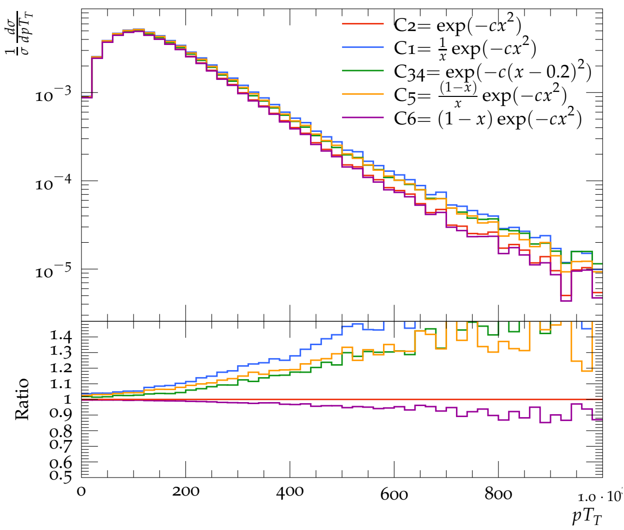

(d) pT_t for different higgs PDFs and $c = 10.0$

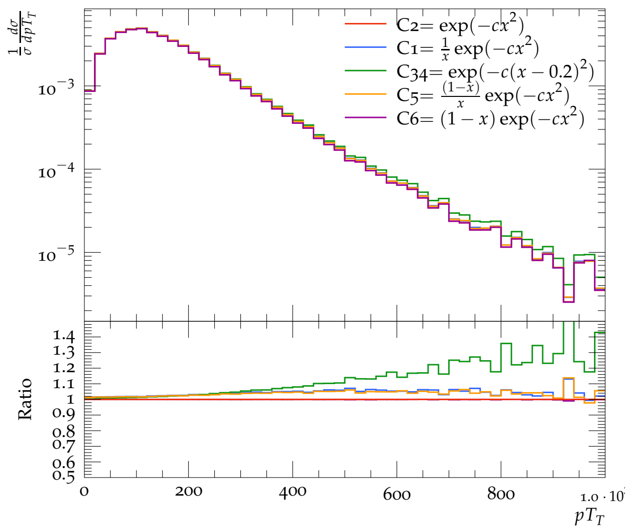

(e) pT_t for different higgs PDFs and $c = 100.0$

Fig. A.20.: Comparing pT_t for higgs PDFs C1, C2, C34, C5, C6 for parameters $c = (0.01, 0.1, 1.0, 10.0, 100.0)$

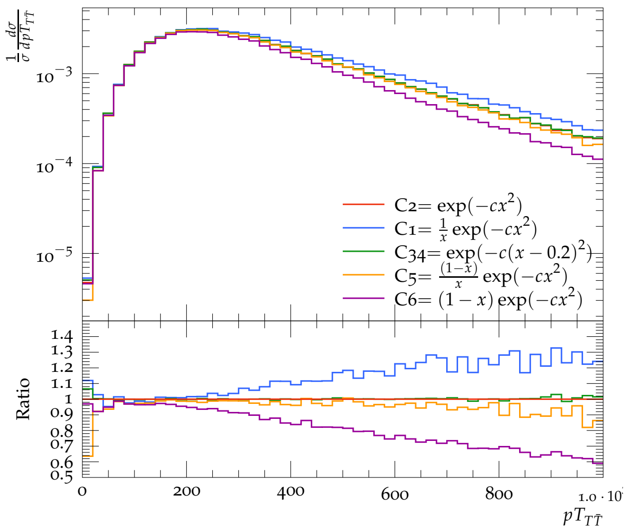

(a) $pT_{t\bar{t}}$ for different higgs PDFs and $c = 0.01$

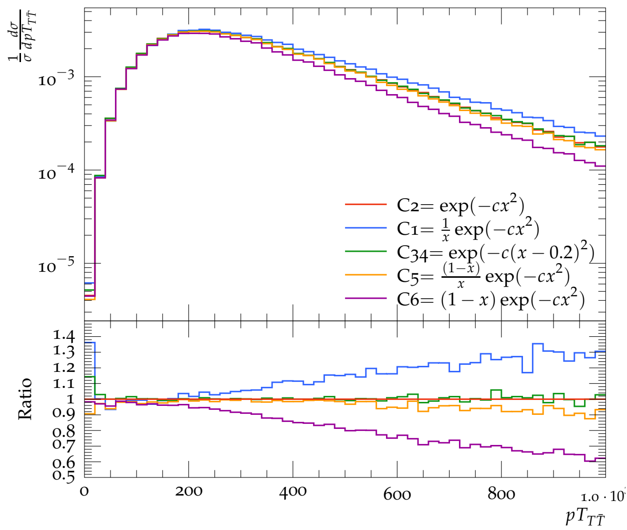

(b) $pT_{t\bar{t}}$ for different higgs PDFs and $c = 0.1$

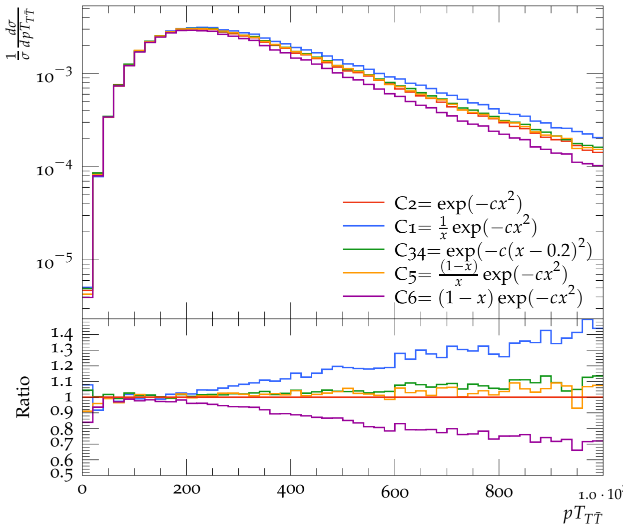

(c) $pT_{t\bar{t}}$ for different higgs PDFs and $c = 1.0$

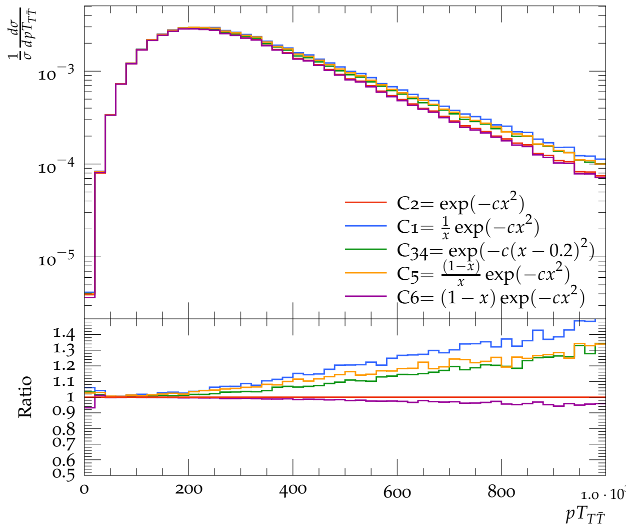

(d) $pT_{t\bar{t}}$ for different higgs PDFs and $c = 10.0$

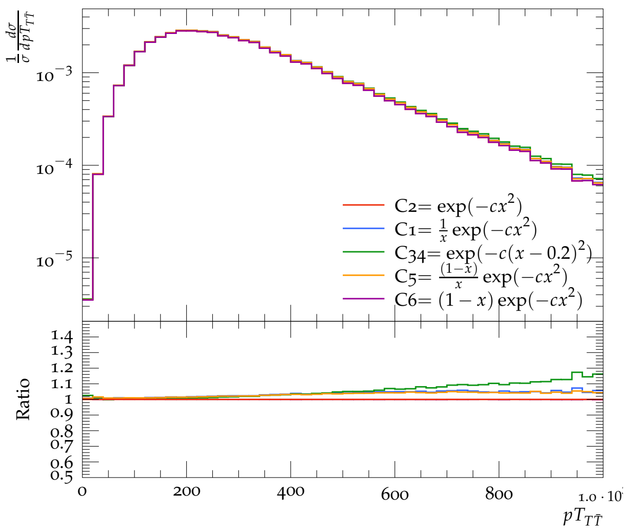

(e) $pT_{t\bar{t}}$ for different higgs PDFs and $c = 100.0$

Fig. A.21.: Comparing $pT_{t\bar{t}}$ for higgs PDFs C1, C2, C34, C5, C6 for parameters $c = (0.01, 0.1, 1.0, 10.0, 100.0)$

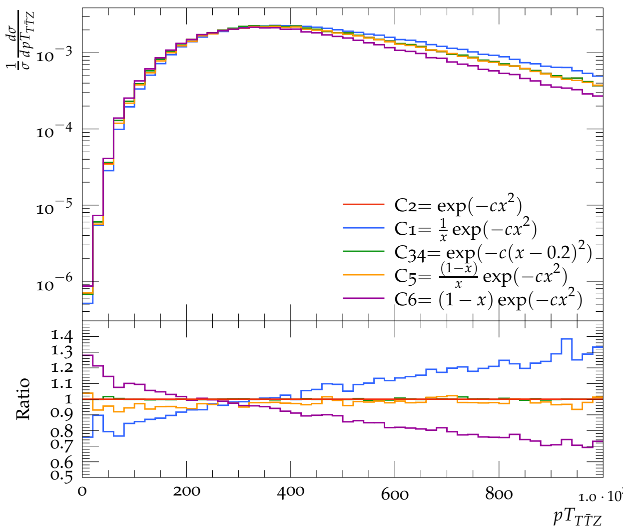

(a) $pT_{t\bar{t}Z}$ for different higgs PDFs and $c = 0.01$

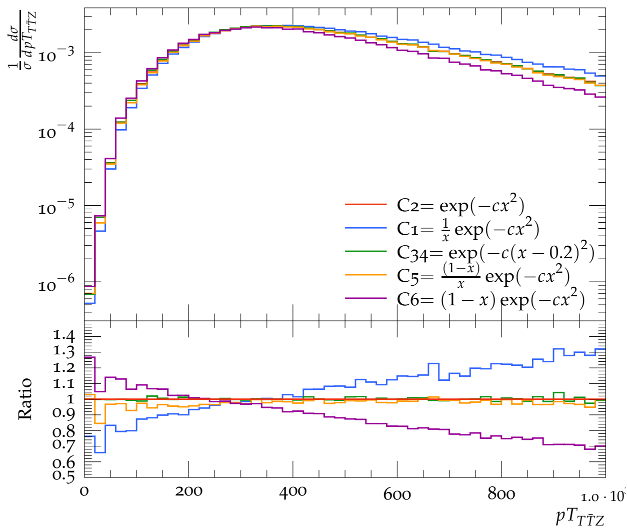

(b) $pT_{t\bar{t}Z}$ for different higgs PDFs and $c = 0.1$

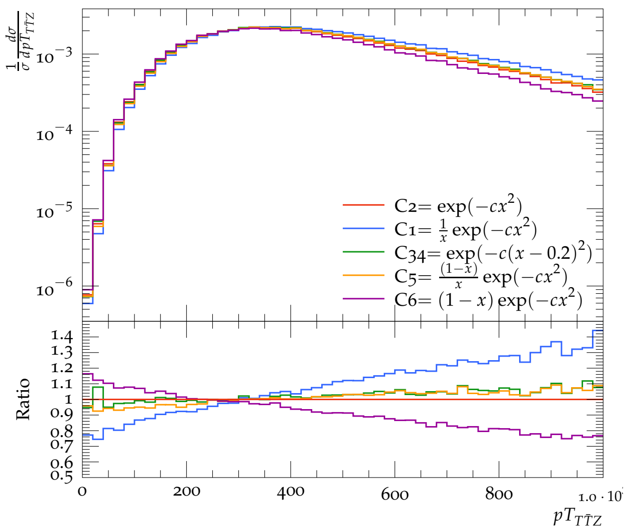

(c) $pT_{t\bar{t}Z}$ for different higgs PDFs and $c = 1.0$

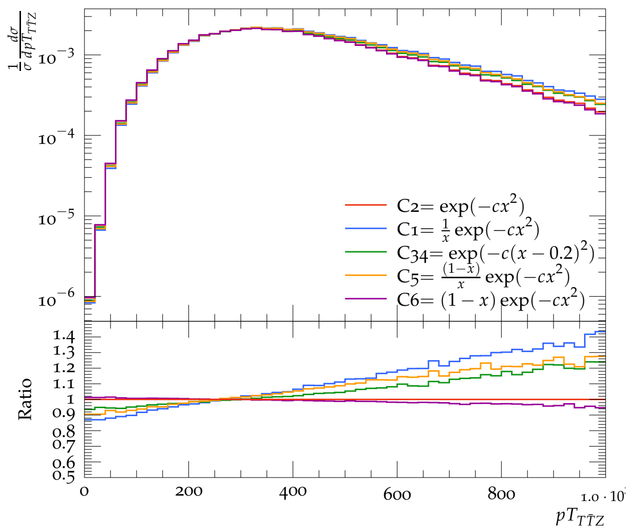

(d) $pT_{t\bar{t}Z}$ for different higgs PDFs and $c = 10.0$

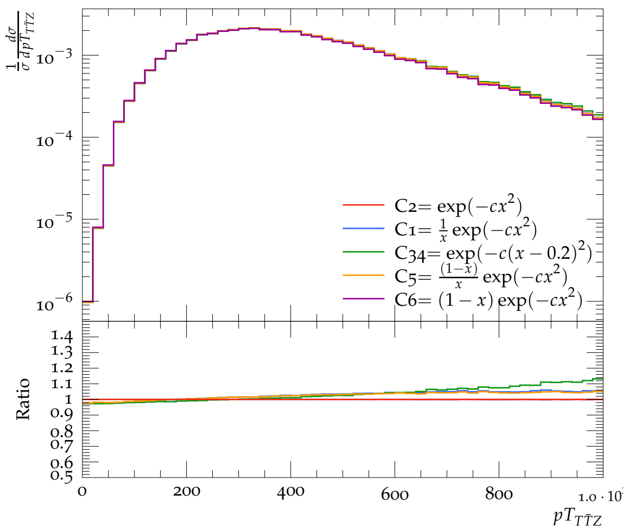

(e) $pT_{t\bar{t}Z}$ for different higgs PDFs and $c = 100.0$

Fig. A.22.: Comparing $pT_{t\bar{t}Z}$ for higgs PDFs C1, C2, C34, C5, C6 for parameters $c = (0.01, 0.1, 1.0, 10.0, 100.0)$

A.3. Comparing the higgs-modified cross sections to the calculated standard model cross sections

The plots show the contributions of the different initial states in the modified proton P', which are PP, gH and HH as well as the sum, scaled with the weights of Eq. 6.8 in the left figure and unscaled in the right. Also shown are the proton quark and gluon PDFs together with the higgs PDF, with logarithmic y-axis scaling on the left and linear scaling on the right. The differential cross sections are compared to the standard model cross section $\frac{d\sigma_{PP\to f}}{d\Omega_f}$ labeled PP, in a ratio plot, to show how big the deviation from the standard model result is. Also shown are all the PDFs involved in the calculation with linear y-axis scaling and with logarithmic scaling. The non-higgs PDFs involved were taken from the LHAPDF python module [52] and the specific set used is called MMHT2014, which is the same one used for the calculations with Herwig. The figures are shown for a higgs parameter value $c = (0.01, 10.0)$ and for the observables pT_Z, η_t, η_Z and $\eta_{t,\bar{t}}$

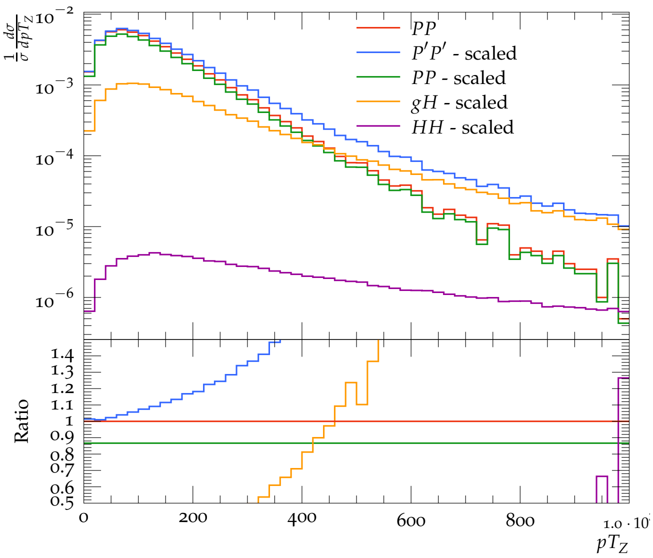

(a) pT_Z for higgs PDF C6 and $c = 0.01$

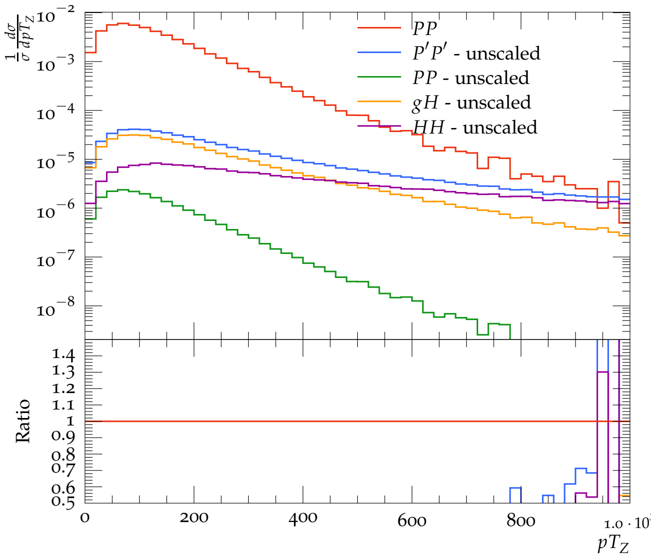

(b) pT_Z for higgs PDF C6 and $c = 0.01$

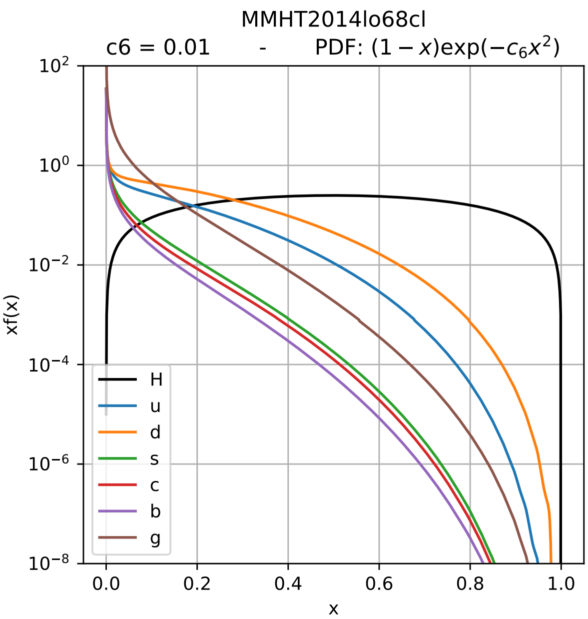

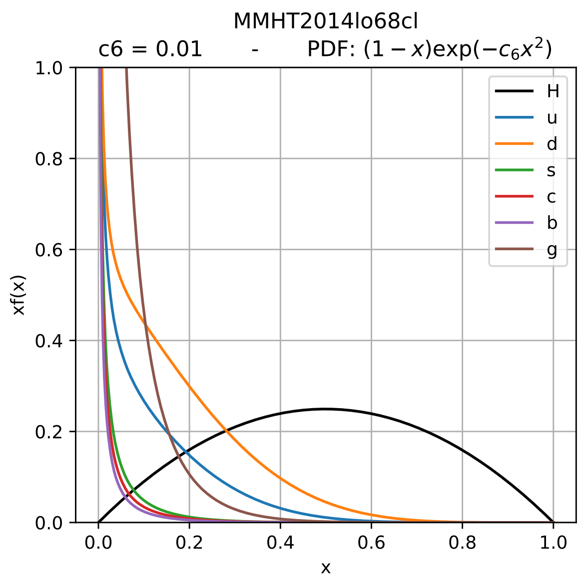

Fig. A.23.: Comparison to standard model cross section for pT_Z in $t\bar{t}Z$, higgs PDF C6 and $c = 0.01$

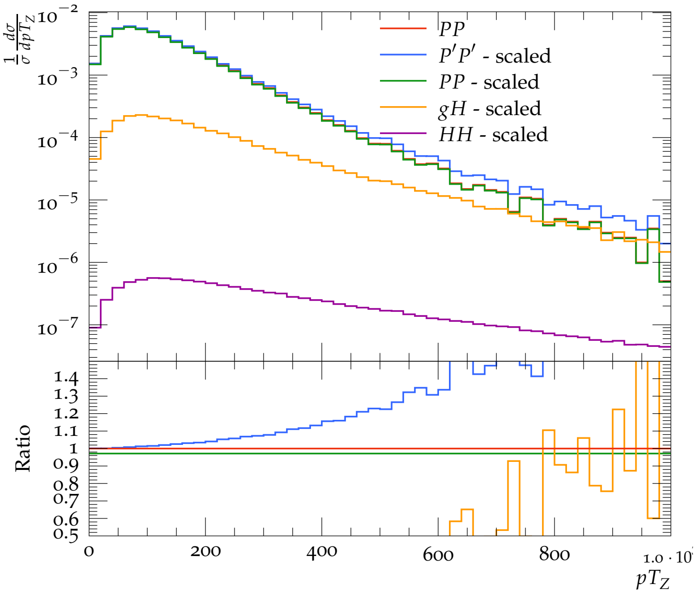

(a) pT_Z for higgs PDF C6 and $c = 10.0$

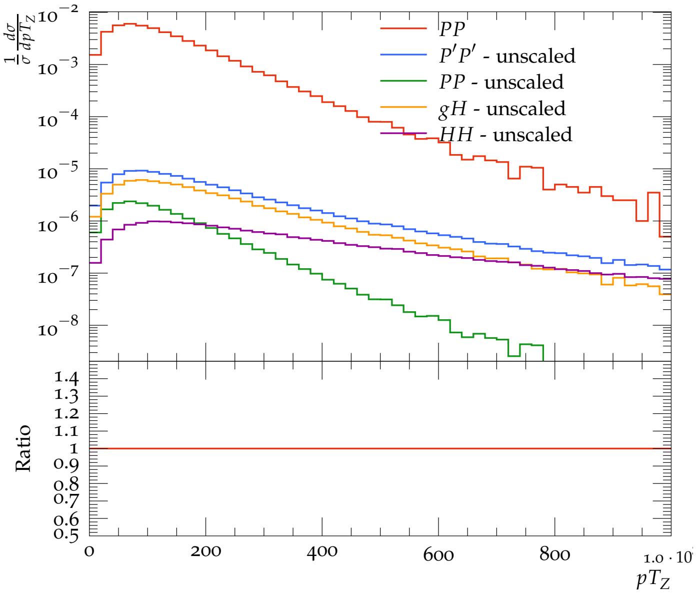

(b) pT_Z for higgs PDF C6 and $c = 10.0$

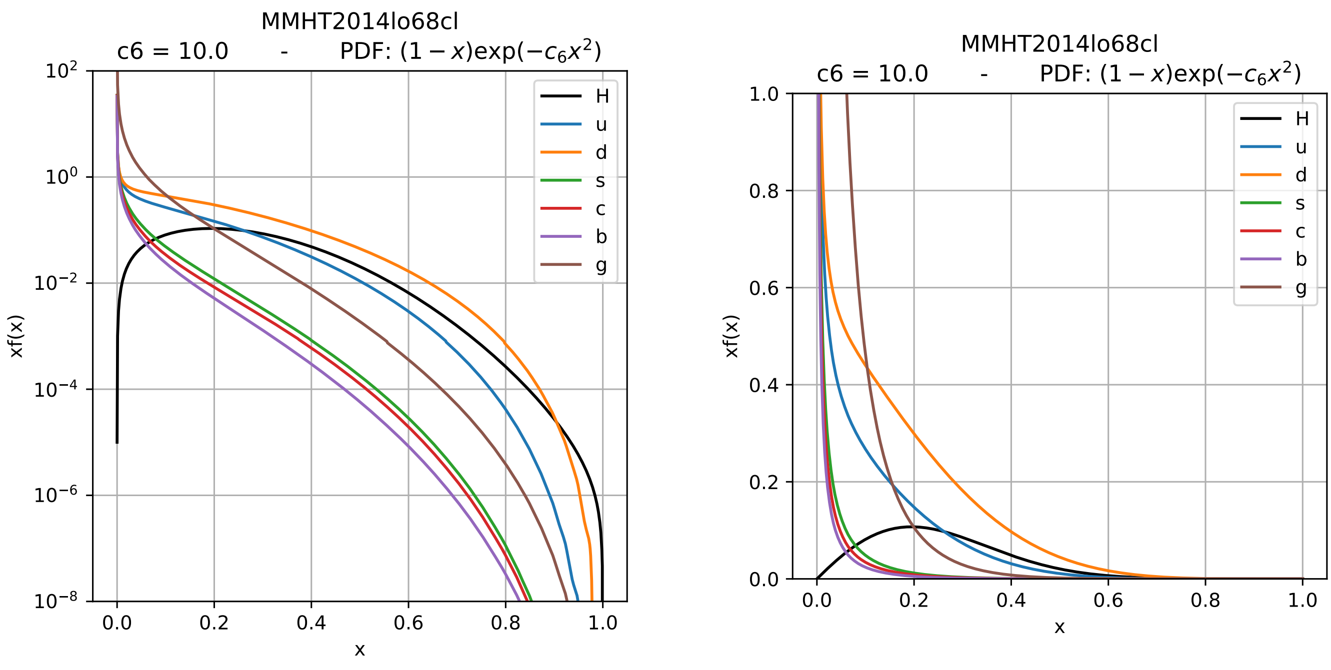

Fig. A.24.: Comparison to standard model cross section for pT_Z in $t\bar{t}Z$, higgs PDF C6 and $c = 10.0$

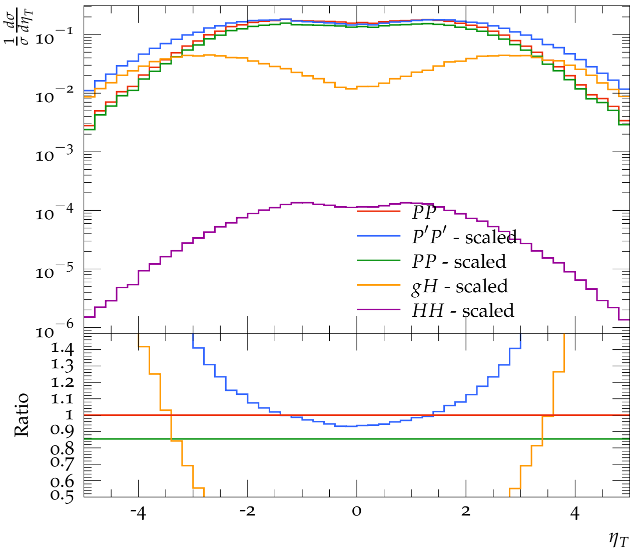

(a) η_t for higgs PDF C1 and $c = 0.01$ weighted with prefactors in (6.8)

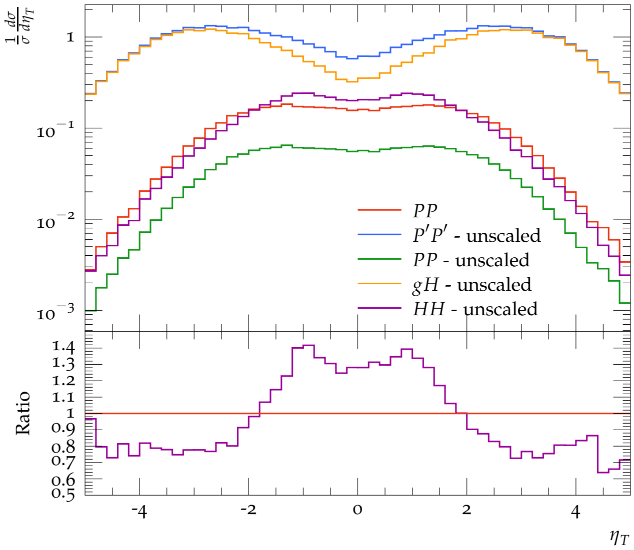

(b) η_t for higgs PDF C1 and $c = 0.01$

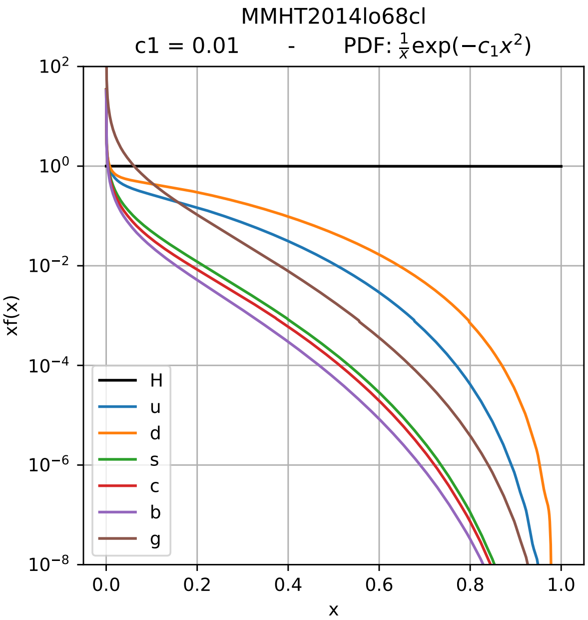

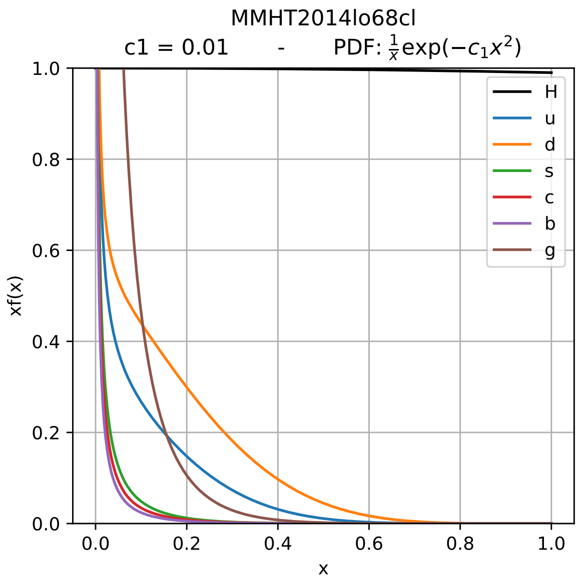

Fig. A.25.: Comparison to standard model cross section for η_t in $t\bar{t}$, higgs PDF C1 and $c = 0.01$

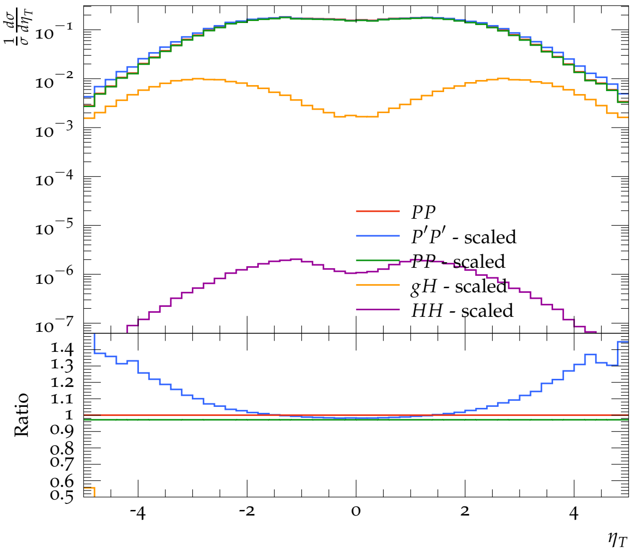

(a) η_t for higgs PDF C6 and $c = 0.01$ weighted with prefactors in (6.8)

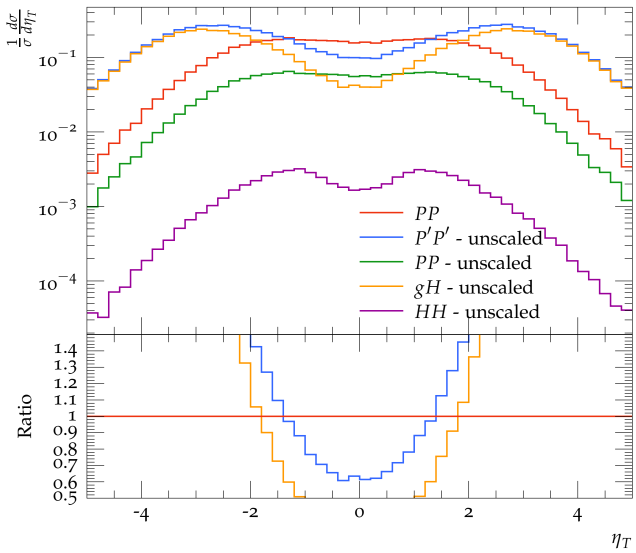

(b) η_t for higgs PDF C6 and $c = 0.01$

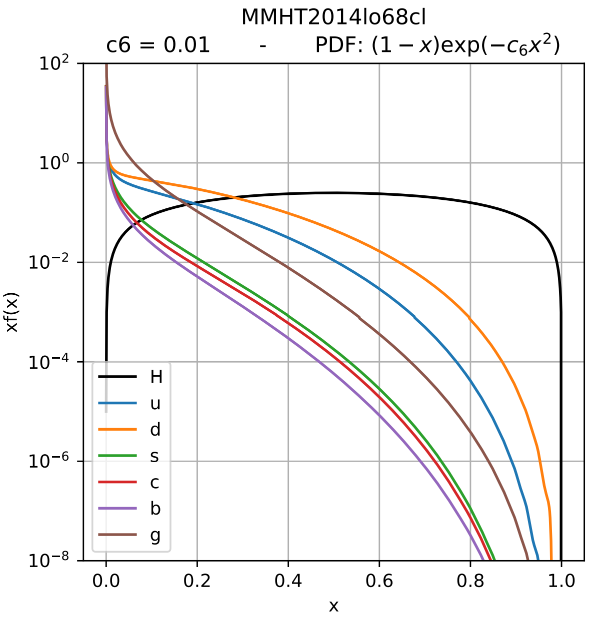

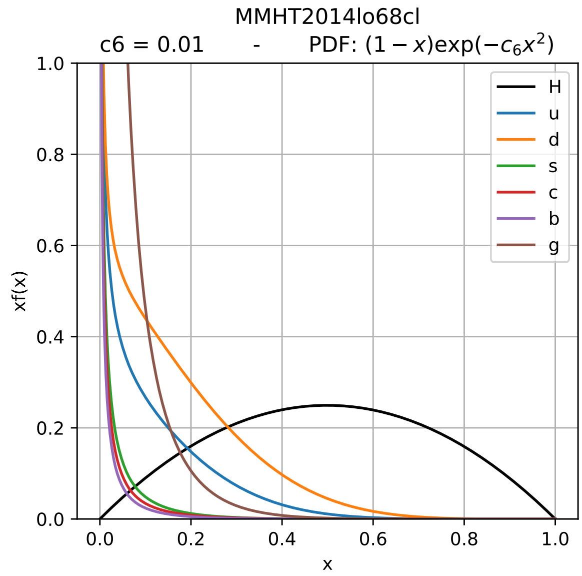

Fig. A.26.: Comparison to standard model cross section for η_t in $t\bar{t}$, higgs PDF C6 and $c = 0.01$

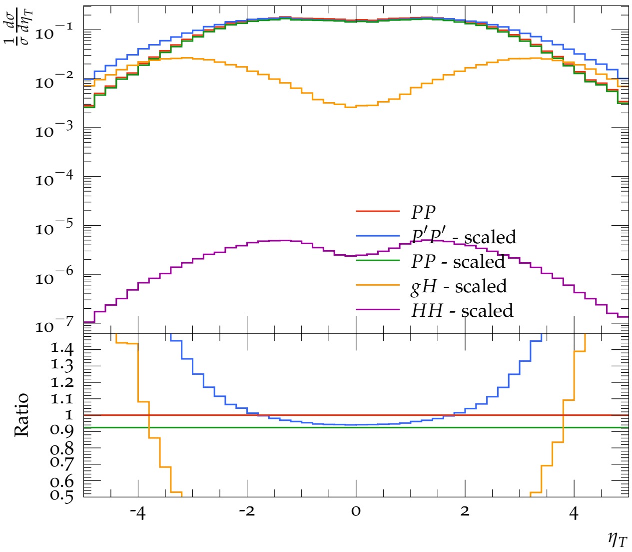

(a) η_t for higgs PDF C2 and $c = 0.01$ weighted with prefactors in (6.8)

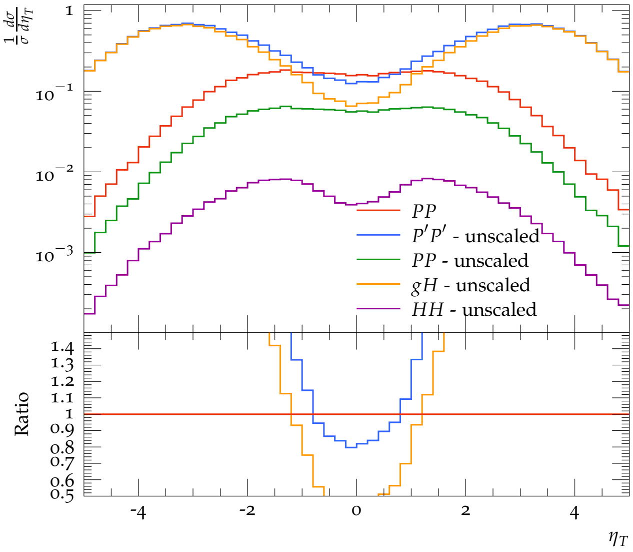

(b) η_t for higgs PDF C2 and $c = 0.01$

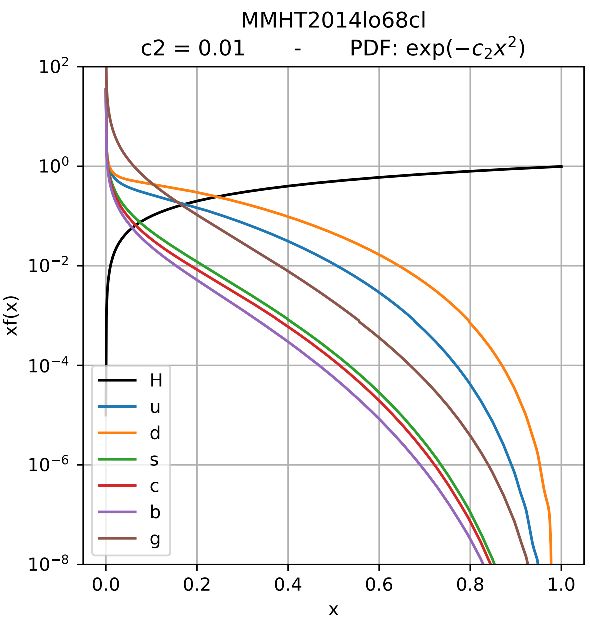

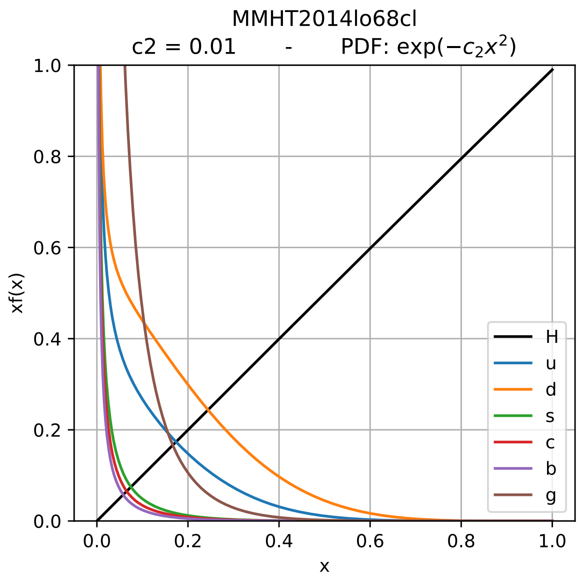

Fig. A.27.: Comparison to standard model cross section for η_t in $t\bar{t}$, higgs PDF C2 and $c = 0.01$

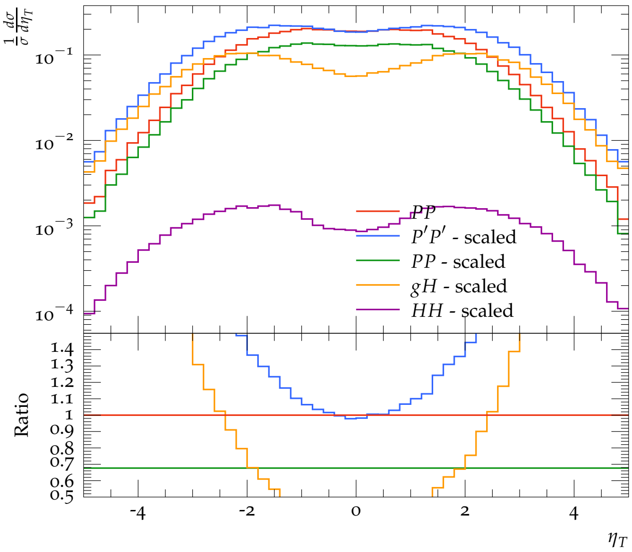

(a) η_t for higgs PDF C2 and $c = 0.01$ weighted with prefactors in (6.8)

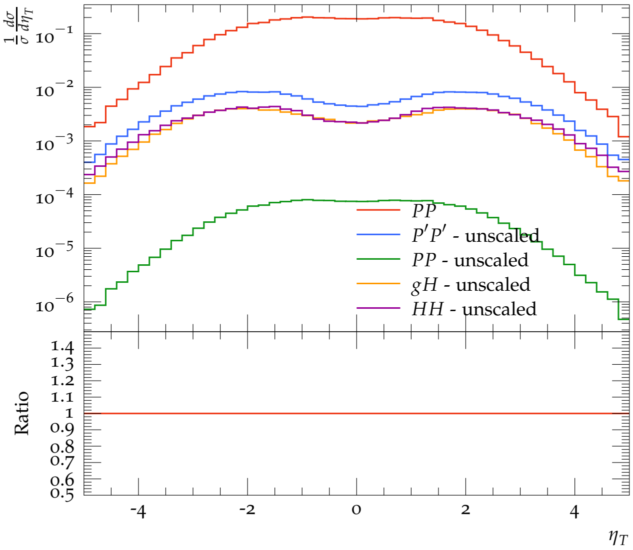

(b) η_t for higgs PDF C2 and $c = 0.01$

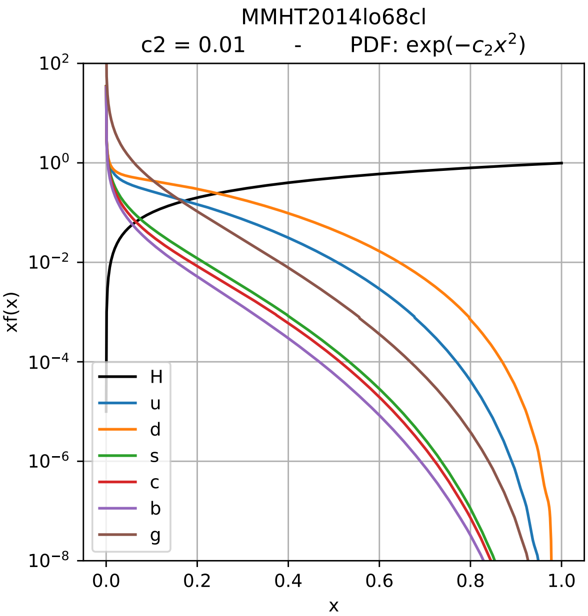

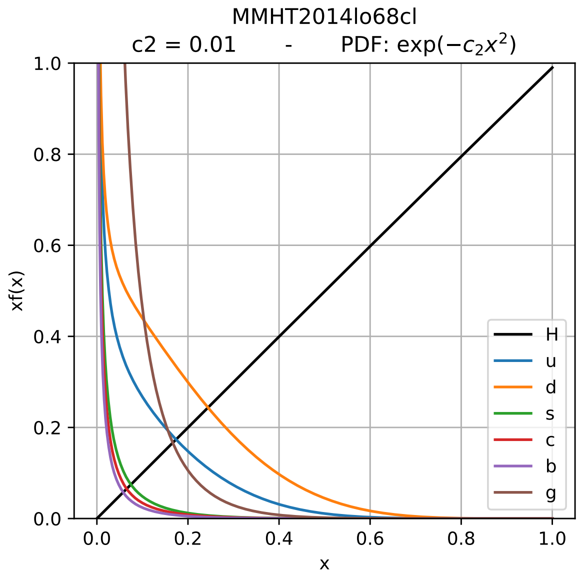

Fig. A.28.: Comparison to standard model cross section for η_t in $t\bar{t}Z$, higgs PDF C2 and $c = 0.01$

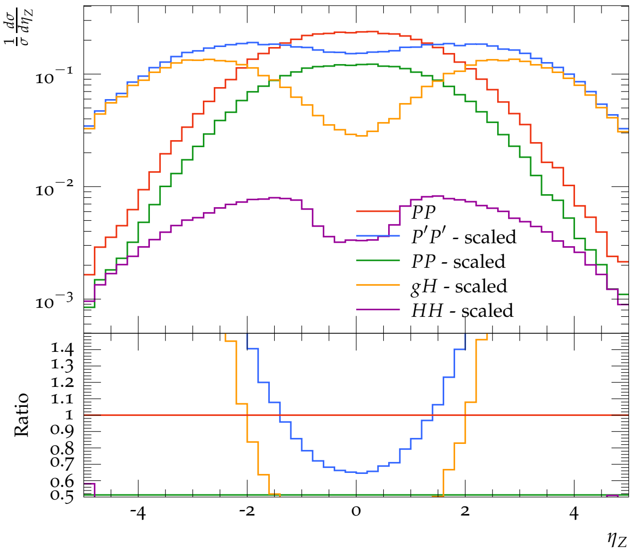

(a) η_Z for higgs PDF C1 and $c = 0.01$ weighted with prefactors in (6.8)

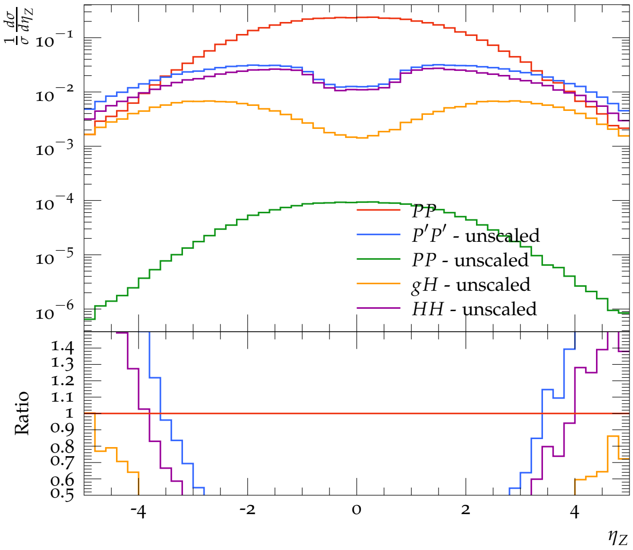

(b) η_Z for higgs PDF C1 and $c = 0.01$

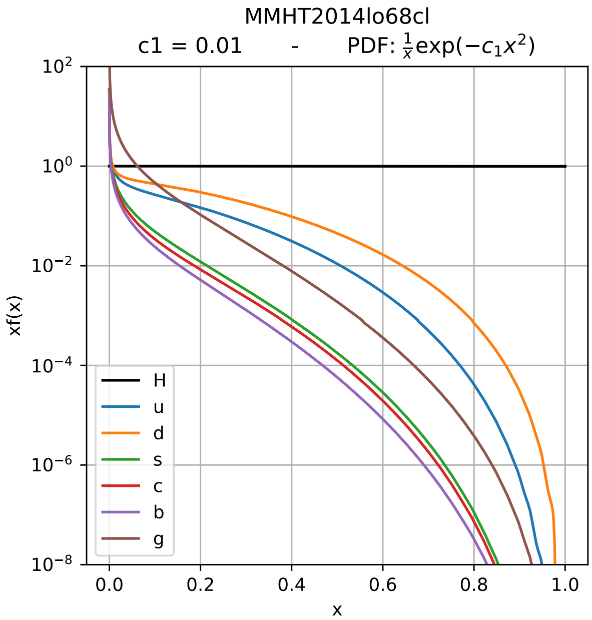

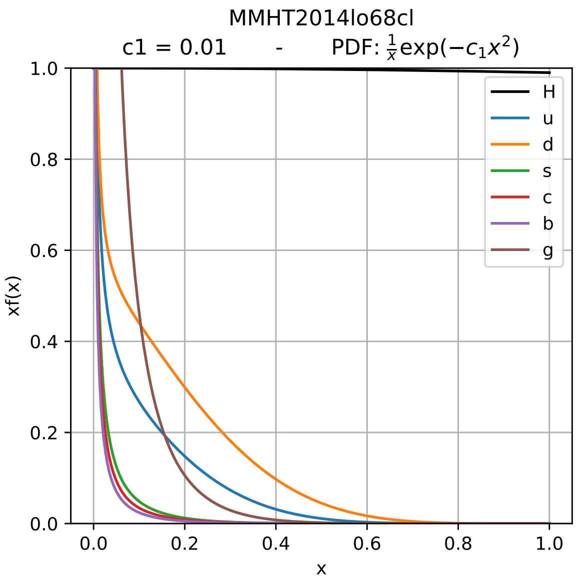

Fig. A.29.: Comparison to standard model cross section for η_Z in $t\bar{t}Z$, higgs PDF C1 and $c = 0.01$

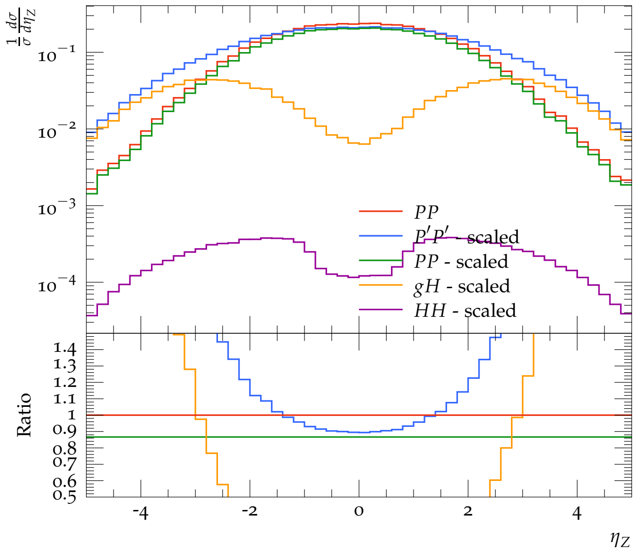

(a) η_Z for higgs PDF C6 and $c = 0.01$ weighted with prefactors in (6.8)

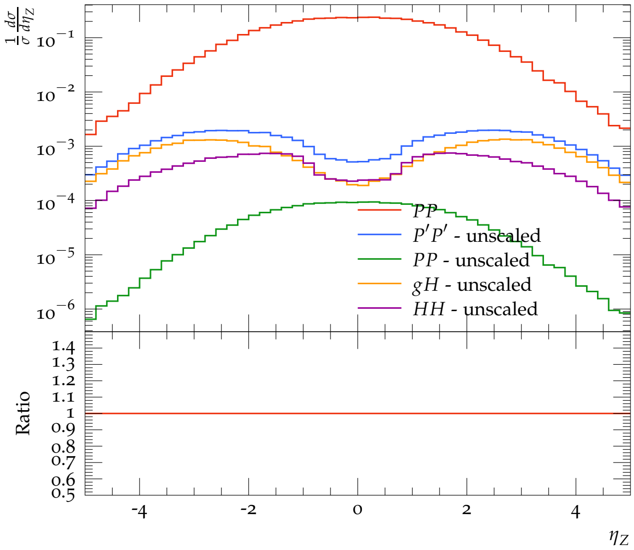

(b) η_Z for higgs PDF C6 and $c = 0.01$

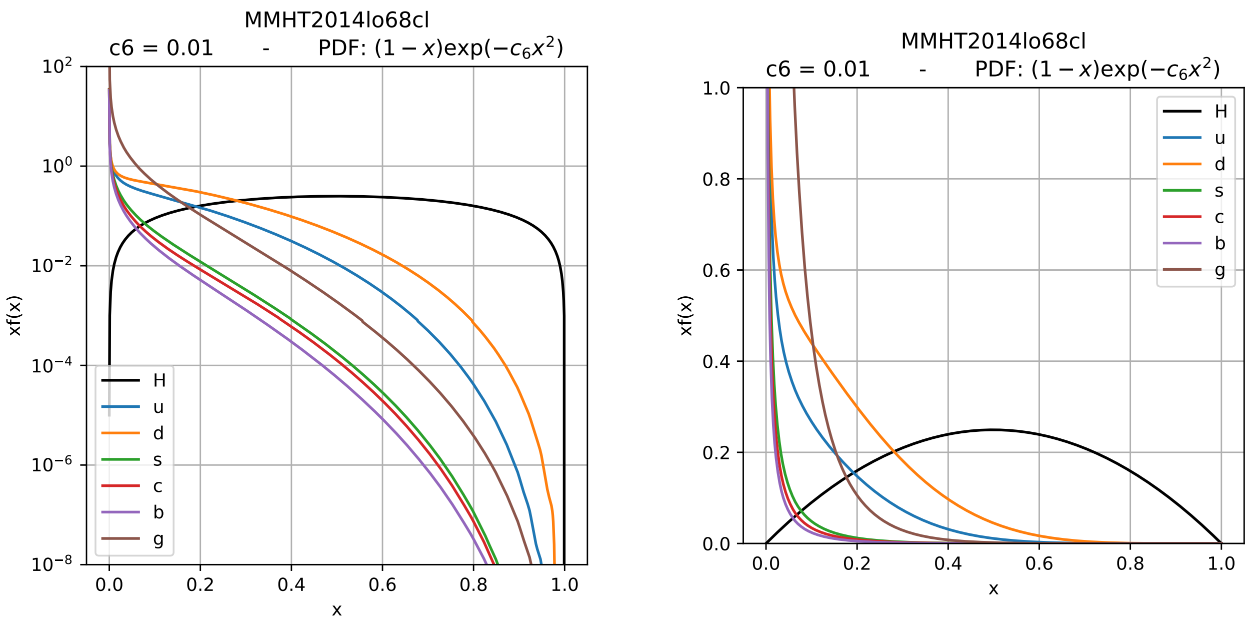

Fig. A.30.: Comparison to standard model cross section for η_Z in $t\bar{t}Z$, higgs PDF C6 and $c = 0.01$

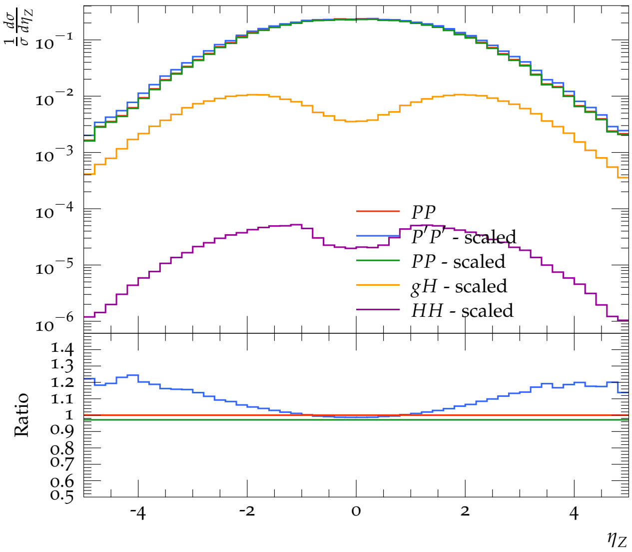

(a) η_Z for higgs PDF C6 and $c = 10.0$ weighted with prefactors in (6.8)

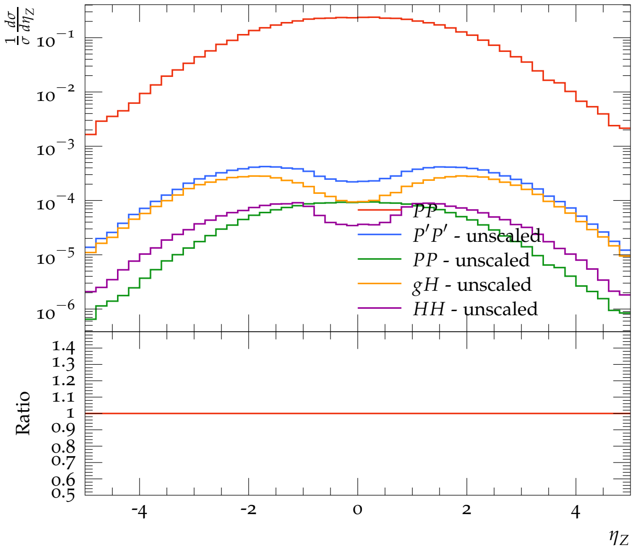

(b) η_Z for higgs PDF C6 and $c = 10.0$

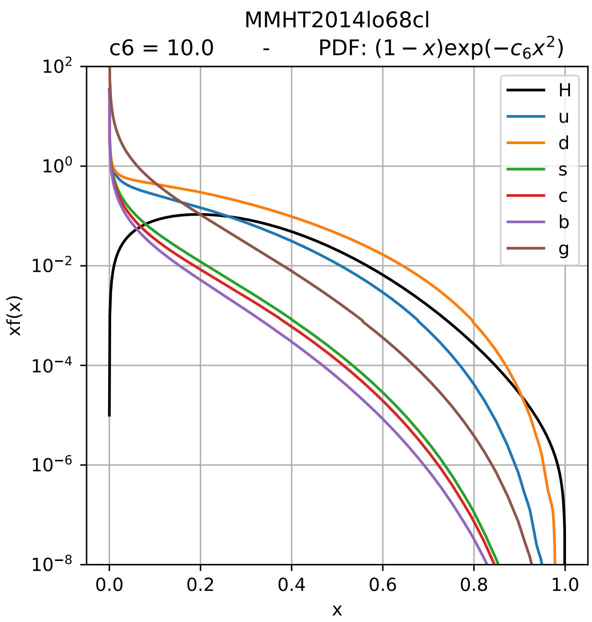

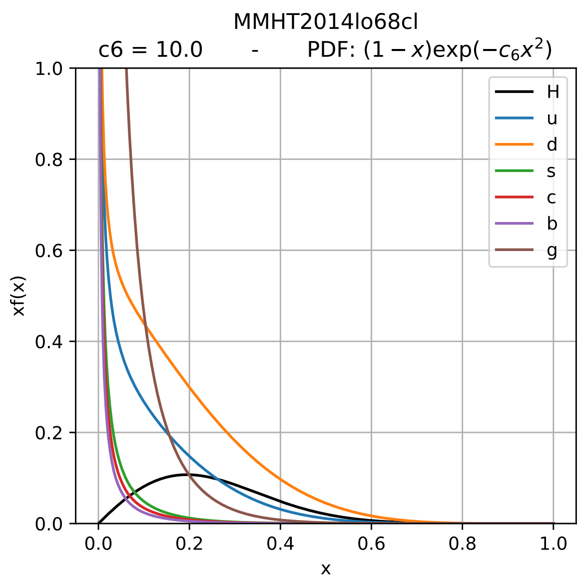

Fig. A.31.: Comparison to standard model cross section for η_Z in $t\bar{t}Z$, higgs PDF C6 and $c = 10.0$

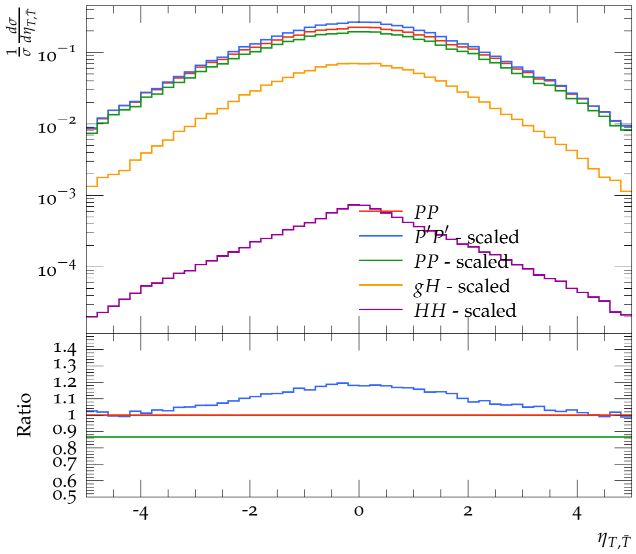

(a) $\eta_{t,\bar{t}}$ for higgs PDF C6 and $c = 0.01$ weighted with prefactors in (6.8)

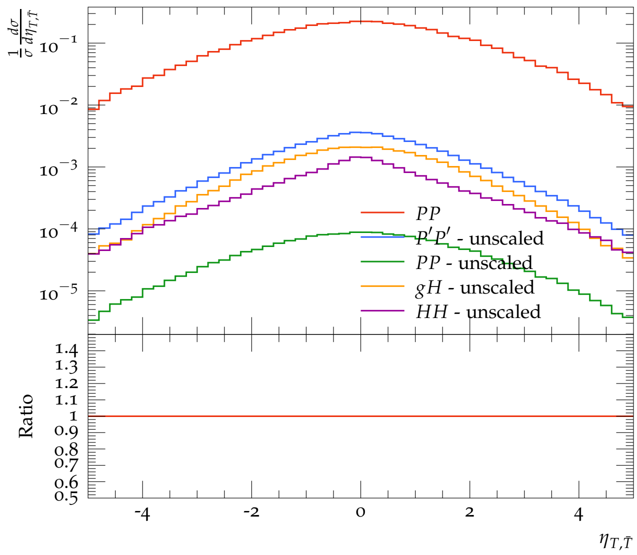

(b) $\eta_{t,\bar{t}}$ for higgs PDF C6 and $c = 0.01$

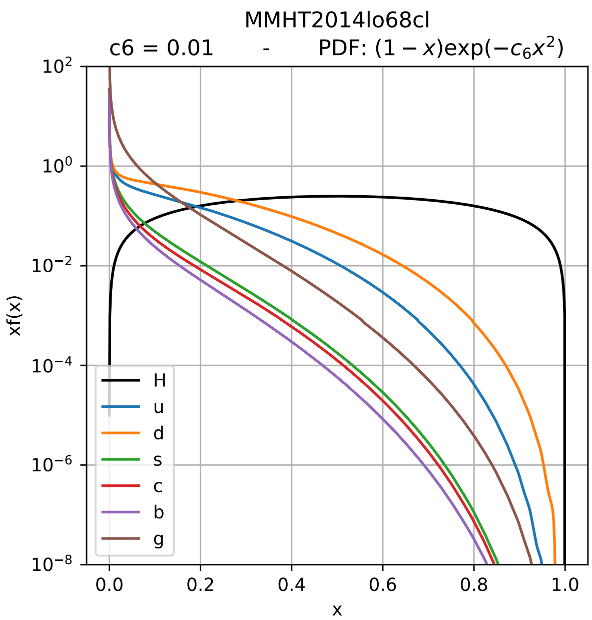

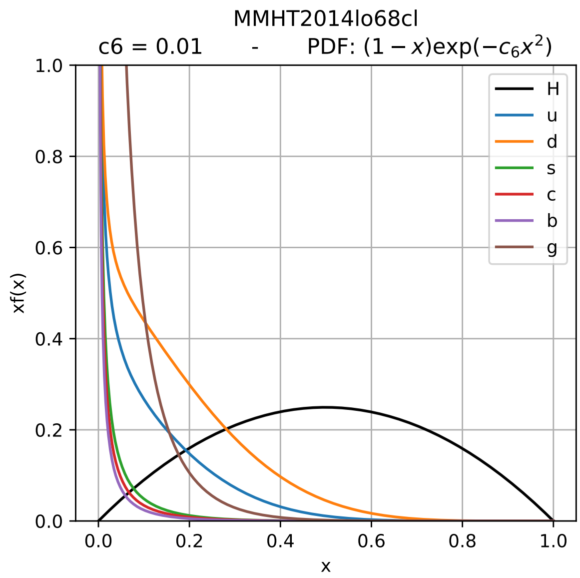

Fig. A.32.: Comparison to standard model cross section for $\eta_{t,\bar{t}}$ in $t\bar{t}Z$, higgs PDF C6 and $c = 0.01$

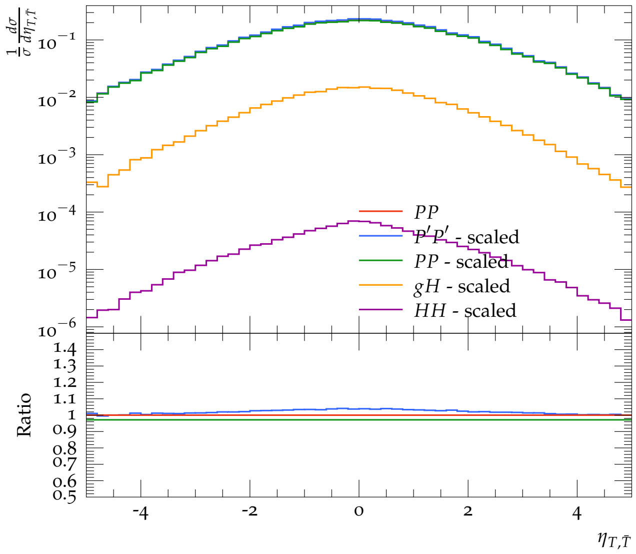

(a) $\eta_{t,\bar{t}}$ for higgs PDF C6 and $c = 10.0$ weighted with prefactors in (6.8)

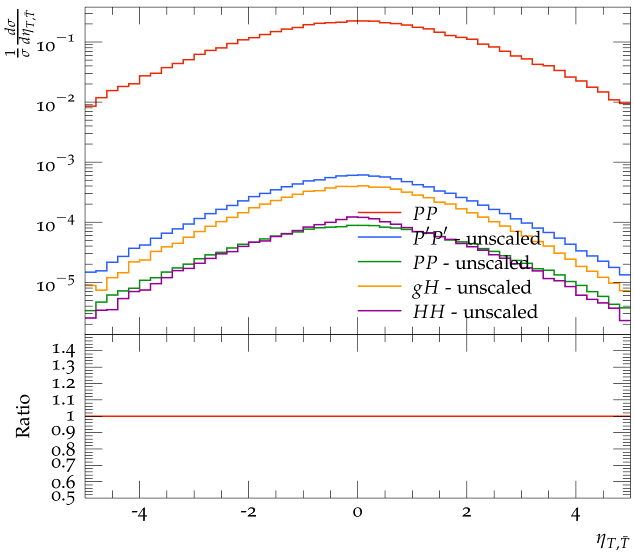

(b) $\eta_{t,\bar{t}}$ for higgs PDF C6 and $c = 10.0$

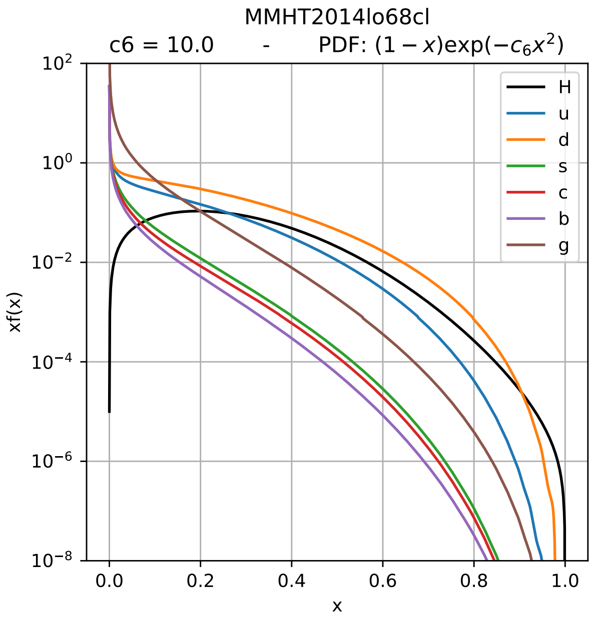

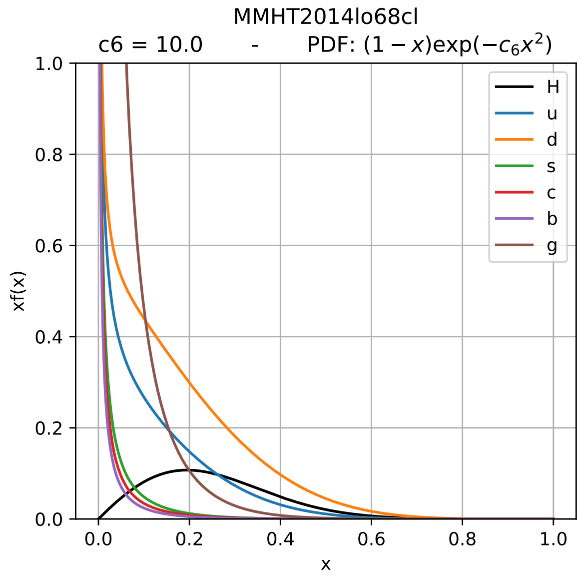

Fig. A.33.: Comparison to standard model cross section for $\eta_{t,\bar{t}}$ in $t\bar{t}Z$, higgs PDF C6 and $c = 10.0$

B. Code

B.1. main.sh

```
#! /bin/bash

##################################################
# USER INPUT:
##################################################

WDP=$PWD # sets the path to workdir (in this case main.sh is already in the
    workdir)
N_EVENTS=100 # number of events
N_CPU=8 # set number of cores to use
HMP=~/Programs/Herwig/bin/activate # path to Herwig activate script
RAN_array=("BBBAR" "TTBAR" "TTBARZ") # name of the rivet analysis
f_array=(0.015) # Higgs content scaling factor
HEPMC="n" # output HEPMC files?
PDFtype_array=("C1" "C2" "C34" "C5" "C6") # type of PDF-ansatz possible: C1,
    C2, C34, C5 C6 (defined in parameters.py)
range_array=("full" "limited") # determines what parameter range is used full
    : (0.01,0.1,1.0,10.0,100.0), limited: (1,3.25,5.5,7.75,10)
OUTPUT_PATH=$WDP/../OUTPUT # path to data output dir

mkdir $WDP/workdir 2> /dev/null
cross=$WDP/workdir/crosssections.txt # path to output-file for total cross-
    sections
printf "N\tPP\tGH\tHG\tHH\n" >> $cross
rm -rf $OUTPUT_PATH 2> /dev/null
mkdir $OUTPUT_PATH # output directory
mkdir $OUTPUT_PATH/PDFPlots
source $HMP # activates Herwig environment ( for lhapdf python module)
python parameters.py $OUTPUT_PATH/PDFPlots &> /dev/null # creates all the
    HiggsPDF plots

##################################################
# main loop
##################################################

i=0

for RAN in ${RAN_array[@]}
do

  mkdir $OUTPUT_PATH/$RAN
  RAP=$WDP/Process/without_HEPMC/$RAN/Rivet # path to Rivet Analysis
  HIFP=$WDP/Process/without_HEPMC/$RAN/Herwig_Infiles # path to Herwig
      Infiles for hard scattering only

  if [ $HEPMC == "y" ]
  then
```

```
    HIFP=$WDP/Process/with_HEPMC/$RAN/Herwig_Infiles # path to Herwig Infiles for showered results
    RAP=$WDP/Process/with_HEPMC/$RAN/Rivet # path to Rivet Analysis

  fi

  # creates the proper directory structure:
  cd $WDP/workdir
  export RIVET_ANALYSIS_PATH=$RAP
  rivet-buildplugin $RAP/Rivet$RAN.so $RAP/$RAN.cc &> /dev/null # compile library for Rivet Analysis

  cp $HIFP/*.in $WDP/Plugin/* . # copy Herwig-Infiles and HiggsPlugin files into the workdir

  Herwig read PP.in &> /dev/null
  Herwig run PP.run -N $N_EVENTS &> /dev/null

  zip $OUTPUT_PATH/$RAN/PP.zip PP.hepmc &> /dev/null
  rm -rf $WDP/workdir/Herwig-cache
  rm PP.in PP.hepmc 2> /dev/null
  cd ..

for range in ${range_array[@]}
do

  mkdir $OUTPUT_PATH/$RAN/$range

  if [ $range == "full" ]
  then

    parameters=(0.01 0.1 1.0 10.0 100.0)

  elif [ $range == "limited" ]
  then

    parameters=(1.0 3.25 5.5 7.75 10.0)

  fi

for f in ${f_array[@]}
do

  mkdir $OUTPUT_PATH/$RAN/$range/"f_${f%.*}d${f#*.}"

for PDFtype in ${PDFtype_array[@]}
do

  OUT=$OUTPUT_PATH/$RAN/$range/"f_${f%.*}d${f#*.}"/$PDFtype
  mkdir $OUT
  mkdir $OUT/HEPMC
  mkdir $OUT/LOG
  mkdir $OUT/YODA
  mkdir $OUT/PLOTS

  if [ $PDFtype == "C1" ]
  then

    PDFbase="exp(-C*pow(x,2))"
```

```
  elif [ $PDFtype == "C2" ]
  then

    PDFbase="x*exp(-C*pow(x,2))"

  elif [ $PDFtype == "C34" ]
  then

    PDFbase="x*exp(-C*pow(x-0.2,2))"

  elif [ $PDFtype == "C5" ]
  then

    PDFbase="(1-x)*exp(-C*pow(x,2))"

  elif [ $PDFtype == "C6" ]
  then

    PDFbase="x*(1-x)*exp(-C*pow(x,2))"

  fi

for c in ${parameters[@]}
do

  PDF=$(sed "s/C/$c/" <<< $PDFbase) # write parameter into PDF string
  cp -rf $WDP/workdir $WDP/temp_$RAN"_"$range"_"$PDFtype"_f_"${f%.*}"d"${f#*.}"_"${c%.*}"d"${c#*.} # make copy of workdir for subshell to jump into

  echo "Begin: f=$f, $PDFtype, f(x)=$PDF" | tee $OUT/LOG/"${c%.*}d${c#*.}_stdout.log" $OUT/LOG/"${c%.*}d${c#*.}_stderr.log" &> /dev/null
  bash run.sh $N_EVENTS $HMP $PDF $PDFtype $HIFP $RAN $RAP $f $OUT $HEPMC $c $range 1>> $OUT/LOG/"${c%.*}d${c#*.}_stdout.log" 2>> $OUT/LOG/"${c%.*}d${c#*.}_stderr.log" &

  if [ $i -lt $N_CPU ]
  then

    i=$((i+1))

  else

    i=0
    t_start=$(date +%s)
    echo "Batch started (Parent PID: $$)"
    wait
    t_end=$(date +%s)
    t_tot=$((t_tot+t_end-t_start))
    echo "Batch finished! Time taken: $((t_end-t_start))"

  fi

done
done
done
done
done
```

```
wait

if [ $HEPMC == "n" ]
then
  echo ${RAN_array[@]} > RAN_array.txt
  echo ${range_array[@]} > range_array.txt
  echo ${PDFtype_array[@]} > PDFtype_array.txt
  echo ${f_array[@]} > f_array.txt
  bash ComparisonPlots.sh $OUTPUT_PATH $OUTPUT_PATH $HMP
fi

rm -rf $WDP/workdir
echo "Finished! Total time: $t_tot"
```

B.2. parameters.py

```
from re import findall
from itertools import product
from numpy import linspace,logspace,exp,sin,cos,zeros
import matplotlib.pyplot as plt
import numpy as np
import lhapdf
import sys, os

OUTPUT_PATH = sys.argv[1]
# Higgs PDF function handle for evaluation in python script
function_handle = [lambda x,c1: 1/x*exp(-c1*x**2),lambda x,c2: exp(-c2*x**2)
      ,lambda x,c3,c4: exp(-c3*(x-c4)**2),lambda x,c5: (1-x)/x*exp(-c5*x**2)
      ,lambda x,c6: (1-x)*exp(-c6*x**2)]

# latex string for PDF
PDFstring = [r'$\frac{1}{x}\exp(-c_1x^2)$',r'$\exp(-c_2x^2)$'
      ,r'$\exp(-c_3(x-c_4)^2)$',r'$\frac{(1-x)}{x}\exp(-c_5x^2)$'
      ,r'$(1-x)\exp(-c_6x^2)$']

PDF_name = ["C1","C2","C34","C5","C6"]


def Plotting(x,y,c,c_name,savename,PDFstring):

    PDFSet = lhapdf.mkPDF("MMHT2014lo68cl") # making the PDF Set Object
    flavors = [1,2,3,4,5,21] # list of flavor indices
    labels = ["u","d","s","c","b","g"]
    scales = ["linear","log"]
    title = [c_name[i]+" = "+str(coeff) for i,coeff in enumerate(c)]
    #title[2] += "\n"
    title = " ; ".join(title)
    PDF = np.zeros([6,len(x)]) # empty array for the flavors and x dependence
    Q2 = 1.3*10**5 # Q^2 in GeV

    yscale = ["linear","log"]
    ylim = [[0,1],[10**-8,10**2]]

    for l in range(2):

        fig,ax = plt.subplots(figsize=[5,5])

        ax.plot(x,x*y,'-k',label="H")

        for i,f in enumerate(flavors):
            for j,X in enumerate(x):

                PDF[i,j] = PDFSet.xfxQ(f,X,Q2)

            ax.plot(x,PDF[i,:],label=labels[i])

        # calculating the scaling factors:
        c0 = np.trapz(np.sum(PDF,0),x)
        c1 = np.trapz(y*x,x)

        ax.set_yscale(yscale[l])
        ax.set_ylim(ylim[l])
        ax.set(xlabel='x',ylabel='xf(x)')
```

```
        ax.grid()
        ax.set_title("MMHT2014lo68cl\n"+title+"\t-\tPDF: "+PDFstring)
        ax.legend()
        ax.set_adjustable("box")
        ax.set_aspect(1/abs(ylim[l][1]-ylim[l][0]))

        fig.savefig(savename.strip()+"_"+yscale[l]+".pdf",dpi=200)

    return c0/(c0+c1),c1/(c0+c1)

for l in range(len(PDF_name)):

  pwd = os.getcwd()
  PATH = OUTPUT_PATH+"/"+PDF_name[l]
  print(PATH)
  os.mkdir(PATH)
  os.chdir(PATH)

  for m in range(2):

    if m == 0:

      params = [np.logspace(-2,2,5)]

      if PDF_name[l] == "C34":

        params = [np.logspace(-2,2,5),np.linspace(0.2,0.8,4)]

    elif m == 1:

      params = [np.linspace(1,10,5)]

      if PDF_name[l] == "C34":

        params = [np.linspace(1,10,5),np.linspace(0.2,0.8,4)]

    NPS = []
    x = linspace(10**-5,1,1000)

    for i,p in enumerate(product(*params)): # loops over pairings of param values

        name = ""

        for j,c in enumerate(p):

      name += "_"+str(float(c))

        if all(function_handle[l](x,*p) >= 0):

      NPS += [name[1:].replace(".","d").replace("-","m")+"\n"]
      Plotting(x,function_handle[l](x,*p),p,PDF_name[l],"HiggsPDF_"+PDF_name[l]+"_"+NPS[-1],PDFstring[l])

  os.chdir(pwd)
```

B.3. run.sh

```
#!/bin/bash

# WDP ... WorkDirectoryPath
# N_EVENTS ... Number of events
# HMP ... HerwigMainPath
# PDF ... HiggsPDF
# NPS ... NameParameterSet

WDP=$PWD
N_EVENTS=$1
HMP=$2
PDF=$3 # string containing Higgs-PDF
PDFtype=$4 # how to name this particular parameter set
HIFP=$5 # path to Herwig-Infiles
BPP=$HIFP/PP.in # baseline process path
RAN=$6 # rivet analysis name
RAP=$7 # path to Rivet Analysis
f=$8 # Higgs content parameter
OUT=$9 # Path where OUTPUT data is stored
HEPMC=${10} # flag wether or not HEPMC files are generated (no yoda files produced then)
c=${11} # particular Higgs parameter value
range=${12}
NPS="${c%.*}d${c#*.}"
NAME=$RAN"_"$range"_"$PDFtype"_f_"${f%.*}"d"${f#*.}"_"$NPS # complete specification of run

f_PP=$(bc -l <<< "(1-$f)*(1-$f)") # Proton-Proton weight
f_GH=$(bc -l <<< "(1-$f)*$f") # Gluon-Higgs weight
f_HH=$(bc -l <<< "$f*$f") # Higgs-Higgs weight

t_start=$(date +%s)
echo -e "\n\n---------------------------------------------"
echo -e "--- $RAN, $PDFtype, PID:$$, PPID:$PPID Started! "
echo -e "---------------------------------------------\n\n"

cd $WDP/temp_$NAME

source $HMP
sed -i 's:return x:return '"$PDF"':' HiggsPDF.cc # write the HiggsPDF into the plugin

make IntrinsicHiggs.so &> /dev/null # compile the plugin
export RIVET_ANALYSIS_PATH=$RAP
export LC_NUMERIC="en_US.UTF-8" # set the numerical convention used by printf

sigma=()
cross=$N_EVENTS

# array for total cross sections (PP,GH,HG,HH)
sigma[0]=$(grep "Total (from generated events):" PP.out | sed -e "s:[[:space:]]\+: :g;s:[(][0-9][)]::g;s:[e][+][0]:*10^:g;s:[e][-][0]:*10^-:g" | rev | cut -f 1 -d " " | rev | bc -l | xargs printf "%6f")

cross=$cross'\t'${sigma[0]}
k=1
```

```
for infile in *.in # loop over HerwigInfiles
do

  name=${infile%%.*}
  Herwig read $infile # create Herwig run-file

  # check if process is GH or HG cause they only have N=N_EVENTS/2 events
  if [ $name = "GH" ] || [ $name = "HG" ]
  then

    Herwig run $name.run -N $(expr $N_EVENTS / 2) # run Herwig run-file

  else

    Herwig run $name.run -N $N_EVENTS # run Herwig run-file

  fi

  zip $OUT/HEPMC/$NPS"_"$name.zip $name.hepmc

  # get total cross-section of process and add it to string-var cross:
  sigma[$k]=$(grep "Total (from generated events):" $name.out | sed -e "s:[[:space:]]\+: :g;s:[(][0-9][)]::g;s:[e][+][0]:*10^:g;s:[e][-][0]:*10^-:g" | rev | cut -f 1 -d " " | rev | bc -l | xargs printf "%6f")
  cross=$cross'\t'${sigma[$k]}

  mv $name.yoda $NPS'_'$name'-unscaled'.yoda &> /dev/null
  rm -rf Herwig-cache $name.hepmc
  k=$((k+1))

done


echo -e $cross'\n' | sed -e "s:[[:space:]]: :g" >> crosssections.txt # print string with N and cross sections to $NPS_crosssections.txt
cp crosssections.txt $OUT/HEPMC/$NPS"_crosssections".txt

if [ $HEPMC == "n" ]
then

  ##############################
  # Processing the YODA-files: #
  ##############################

  # calculating the normalization / weighting factors:
  sigma_c=$(bc -l <<< "$f_PP*${sigma[0]}+$f_GH*(${sigma[1]}+${sigma[2]})/2+$f_HH*${sigma[3]}") # total cross section as function of c
  c_PP_stdm=$(bc -l <<< "1/${sigma[0]}") # normalization factor for Standardmodel PP cross section
  c_PP=$(bc -l <<< "$f_PP/$sigma_c") # normalized weighting factor for PP histos
  c_GH=$(bc -l <<< "$f_GH/$sigma_c") # normalized weighting factor for GH histos
  c_HH=$(bc -l <<< "$f_HH/$sigma_c") # normalized weighting factor for HH histos

  mv PP.yoda $NPS'_PP-unscaled'.yoda

  # merge GH and HG to new GH yoda file
```

```
  yodamerge --add -o $NPS"_GH-unscaled".yoda $NPS'_GH-unscaled'.yoda $NPS'_HG-unscaled'.yoda
  rm $NPS'_HG-unscaled'.yoda

  yodamerge --add -o $NPS'_merge-unscaled'.yoda *.yoda

  yodascale -c '.* '$c_PP_stdm'x' $NPS'_PP-unscaled'.yoda # normalize PP histos
  mv $NPS'_PP-unscaled-scaled'.yoda $NPS'_PP-normalized'.yoda

  yodascale -c '.* '$c_PP'x' $NPS'_PP-unscaled'.yoda # scale PP histo with normalized weight factor
  mv $NPS'_PP-unscaled-scaled'.yoda $NPS'_PP-scaled'.yoda

  yodascale -c '.* '$c_GH'x' $NPS'_GH-unscaled'.yoda # scale GH histo with normalized weight factor
  mv $NPS'_GH-unscaled-scaled'.yoda $NPS'_GH-scaled'.yoda

  yodascale -c '.* '$c_HH'x' $NPS'_HH-unscaled'.yoda # scale HH histo with normalized weight factor
  mv $NPS'_HH-unscaled-scaled'.yoda $NPS'_HH-scaled'.yoda

  yodamerge --add -o $NPS'_merge-scaled'.yoda *-scaled.yoda

  cp *.yoda $OUT/YODA

  #rivet-mkhtml -o $OUT/PLOTS/$NPS'_scaled' $NPS"_PP-normalized".yoda:'$PP$' $NPS"_merge-scaled".yoda:'$P^{\prime}P^{\prime}$ - scaled' $NPS"_PP-scaled".yoda:'$PP$ - scaled' $NPS"_GH-scaled".yoda:'$gH$ - scaled' $NPS"_HH-scaled".yoda:'$HH$ - scaled'

  #rivet-mkhtml -o $OUT/PLOTS/$NPS'_unscaled' $NPS"_PP-normalized".yoda:'$PP$' $NPS"_merge-unscaled".yoda:'$P^{\prime}P^{\prime}$ - unscaled' $NPS"_PP-unscaled".yoda:'$PP$ - unscaled' $NPS"_GH-unscaled".yoda:'$gH$ - unscaled' $NPS"_HH-unscaled".yoda:'$HH$ - unscaled'

  #cd $OUT/PLOTS

  #for l in $NPS'_scaled'/$RAN/*.png
  #do
    #name=${l##*/} # name of observable
    #name=${name%.*}
    #mkdir $name
    #montage -tile 2x2 -geometry 500x500+4+4 $NPS'_scaled'/$RAN/$name.png $NPS'_unscaled'/$RAN/$name.png $WDP/HiggsPDF_$NPS'_linear'.png $WDP/HiggsPDF_$NPS'_log'.png $name/$NPS.png
  #done

fi

rm -rf $OUT/PLOTS/$NPS* 2> /dev/null
rm -rf $WDP/temp_$NAME 2> /dev/null
t_end=$(date +%s)

echo -e "\n\n-------------------------------------------------------------------------------"
echo -e "--- $RAN, $PDFtype, PID:$$, PPID:$PPID Finished! t=$((t_end-t_start))s"
```

```
echo -e "
    --------------------------------------------------------------------------------\
    n\n"
```

B.4. ComparisonPlotsCode

```bash
#! /bin/bash

shopt -s extglob # activate extglob for !() globbing
INPUT_PATH=$1
OUTPUT_PATH=$2
HMP=$3

readarray -d " " process_array < RAN_array.txt
readarray -d " " range_array < range_array.txt
readarray -d " " PDF_array < PDFtype_array.txt
readarray -d " " f_array < f_array.txt
rm RAN_array.txt range_array.txt PDFtype_array.txt f_array.txt

comparison_PDFs=()

for PDF in ${PDF_array[@]}
do

  if [ $PDF == "C1" ]
  then

    comparison_PDFs[1]=C1.yoda:'C1$=\frac{1}{x}\exp(-cx^2)$'

  elif [ $PDF == "C2" ]
  then

    comparison_PDFs[0]=C2.yoda:'C2$=\exp(-cx^2)$'


  elif [ $PDF == "C34" ]
  then

    comparison_PDFs[2]=C34.yoda:'C34$=\exp(-c(x-0.2)^2)$'

  elif [ $PDF == "C5" ]
  then

    comparison_PDFs[3]=C5.yoda:'C5$=\frac{(1-x)}{x}\exp(-cx^2)$'

  elif [ $PDF == "C6" ]
  then

    comparison_PDFs[4]=C6.yoda:'C6$=(1-x)\exp(-cx^2)$'

  fi

done

for process in ${process_array[@]}
do

for range in ${range_array[@]}
do

for f in ${f_array[@]}
do

```

```
WD=$(pwd)

source $HMP
export RIVET_ANALYSIS_PATH=$WD/Process/without_HEPMC/$process/Rivet

mkdir $process

if [ $range == "full" ]
then

  parameter_array=("0d01" "0d1" "1d0" "10d0" "100d0")

elif [ $range == "limited" ]
then

  parameter_array=("1d0" "3d25" "5d5" "7d75" "10d0")

else

  echo "Unknown parameter range specified!"
  exit 1

fi


for PDF in ${PDF_array[@]}
do

  mkdir $process/$PDF
  mkdir $OUTPUT_PATH/$process/$range/"f_"${f/\./d}/$PDF/PLOTS/ComparisonParameters 2> /dev/null
  mkdir $OUTPUT_PATH/$process/$range/"f_"${f/\./d}/ComparisonPDFs 2> /dev/null

  cp $INPUT_PATH/$process/$range/"f_"${f/\./d}/$PDF/YODA/*.yoda $process/$PDF
  cd $process/$PDF

  # comparison to standard model:

  for p in ${parameter_array[@]}
  do

    rivet-mkhtml -o scaled $p"_PP-normalized".yoda:'$PP$' $p"_merge-scaled".yoda:'$P^{\prime}P^{\prime}$ - scaled' $p"_PP-scaled".yoda:'$PP$ - scaled' $p"_GH-scaled".yoda:'$gH$ - scaled' $p"_HH-scaled".yoda:'$HH$ - scaled'

    rivet-mkhtml -o unscaled $p"_PP-normalized".yoda:'$PP$' $p"_merge-unscaled".yoda:'$P^{\prime}P^{\prime}$ - unscaled' $p"_PP-unscaled".yoda:'$PP$ - unscaled' $p"_GH-unscaled".yoda:'$gH$ - unscaled' $p"_HH-unscaled".yoda:'$HH$ - unscaled'

    for obs in scaled/$process/*.pdf
    do

      obs=${obs%.*}
      obs=${obs##*/}
```

```
      mkdir $OUTPUT_PATH/$process/$range/"f_"${f/\./d}/$PDF/PLOTS/$obs 2> /dev/null
      cp scaled/$process/$obs.pdf $OUTPUT_PATH/$process/$range/"f_"${f/\./d}/$PDF/PLOTS/$obs/$p"_scaled.pdf"
      cp unscaled/$process/$obs.pdf $OUTPUT_PATH/$process/$range/"f_"${f/\./d}/$PDF/PLOTS/$obs/$p"_unscaled.pdf"

    done

  done

  rm -rf scaled unscaled
  rm !(*merge-scaled*)

  # comparison among parameters:
  for file in *.yoda
  do

    mv $file "${file%%_*}.yoda"
    mkdir ../${file%%_*} 2> /dev/null
    mkdir $OUTPUT_PATH/$process/$range/"f_"${f/\./d}/ComparisonPDFs/${file%%_*} 2> /dev/null

  done

  rivet-mkhtml -o comp ${parameter_array[4]}.yoda:'$c=$'${parameter_array[4]/d/\.} ${parameter_array[3]}.yoda:'$c=$'${parameter_array[3]/d/\.} ${parameter_array[2]}.yoda:'$c=$'${parameter_array[2]/d/\.} ${parameter_array[1]}.yoda:'$c=$'${parameter_array[1]/d/\.} ${parameter_array[0]}.yoda:'$c=$'${parameter_array[0]/d/\.}

  cd comp/$process

  cp *.pdf $OUTPUT_PATH/$process/$range/"f_"${f/\./d}/$PDF/PLOTS/ComparisonParameters
  cd $WD

done

# comparison among PDFs:
echo "Comparison PDFs!"

for p in ${parameter_array[@]}
do

  for PDF in ${PDF_array[@]}
  do

    cp $process/$PDF/$p.yoda $process/$p/$PDF.yoda

  done

  cd $process/$p

  rivet-mkhtml -o comp ${comparison_PDFs[@]}

  cd comp/$process
  cp *.pdf $OUTPUT_PATH/$process/$range/"f_"${f/\./d}/ComparisonPDFs/$p
  cd $WD
```

```
done

rm -rf $WD/$process

done
done
done
```

B.5. ExclusionPlots.py

```
import numpy as np
from scipy import interpolate
import matplotlib

matplotlib.rcParams['text.usetex'] = True
matplotlib.rcParams['axes.titlepad'] = 10
matplotlib.rcParams['axes.titlesize'] = 10

f = [lambda x,a: 1/x*np.exp(-a*x**2),lambda x,a: np.exp(-a*x**2)
    ,lambda x,a: np.exp(-a*(x-0.2)**2),lambda x,a: (1-x)/x*np.exp(-a*x**2),
        lambda x,a: (1-x)*np.exp(-a*x**2)]
PDF_Label = ["C1","C2","C34","C5","C6"]

HiggsPDF_latex_string = [r"$\frac{1}{x}\exp\bigl(-cx^2\bigl)$",r"$\exp\bigl(-
    cx^2\bigl)$"
                    ,r"$\exp\bigl(-c(x-b)^2\bigl)$",r"$\frac{(1-x)}{x}\exp\bigl
                        (-cx^2\bigl)$",r"(1-x)\exp\bigl(-cx^2\bigl)"]

p = np.logspace(-2,2,5)
x = np.linspace(10**-3,1,100)

sigma_exp = [0.888,0.95*10**-3] # sigma_TTBAR,sigma_TTBARZ
err = [0.03,0.13] # error TTBAR,TTBARZ
process_str = [r"$t\bar{t}$",r"$t\bar{t}Z$"]
ylim_PDF = np.zeros((2,5))
ylim_PDF[1,[0,3]] = 4
ylim_PDF[0,[0,3]] = -4
ylim_PDF[1,[1,2,4]] = 0
ylim_PDF[0,[1,2,4]] = -8

sigma_gh = np.zeros((5,5,2))
sigma_hh = np.zeros((5,5,2))

# TTBAR / TTBARZ:
sigma_pp = [0.354,0.394*10**-3]

# TTBAR:
sigma_gh[0,:,0] = [3.93,3.82,2.99,1.142,0.272] # C1
sigma_gh[1,:,0] = [1.882,1.81,1.245,0.222,0.02076] # C2
sigma_gh[2,:,0] = [1.92,1.876,1.511,0.532,0.1639] # C34
sigma_gh[3,:,0] = [2.019,1.987,1.747,0.918,0.251] # C5
sigma_gh[4,:,0] = [0.676,0.660,0.524,0.16,0.0187] # C6


sigma_hh[0,:,0] = [1.105,1.089,0.947,0.514,0.1143]  # C1
sigma_hh[1,:,0] = [0.0385,0.0368,0.0,0.00547,0.00035] # C2
sigma_hh[2,:,0] = [0.0405,0.0397,0.0324,0.01279,0.00239] # C34 at b=0.2
sigma_hh[3,:,0] = [0.69,0.685,0.633,0.408,0.1006] # C5
sigma_hh[4,:,0] = [0.0135,0.0132,0.0107,0.00374,0.000353] # C6

# TTBARZ:
sigma_gh[0,:,1] = [0.0222,0.0212,0.015985,4.75*10**-3,7.56*10**-4] # C1
sigma_gh[1,:,1] = [0.0124,0.01134,0.00749,1.084*10**-3,6.6*10**-5] # C2
sigma_gh[2,:,1] = [0.012,0.01166,9.28*10**-3,2.9*10**-3,7.78*10**-4] # C34
sigma_gh[3,:,1] = [0.0101,9.9*10**-3,8.42*10**-3,3.66*10**-3,6.9*10**-4] # C5
sigma_gh[4,:,1] = [0.003915,0.0038,0.00293,7.54*10**-4,6*10**-5] # C6
```

```
sigma_hh[0,:,1] = [0.1624,0.1554,0.1081,0.0238,1.194*10**-3] # C1
sigma_hh[1,:,1] = [0.02388,0.022,0.0118,7.36*10**-4,9*10**-6] # C2
sigma_hh[2,:,1] = [0.02571,0.02482,0.01738,3.33*10**-3,4.44*10**-4] # C34
sigma_hh[3,:,1] = [0.0575,0.0564,0.0462,0.0159,9.88*10**-4] # C5
sigma_hh[4,:,1] = [0.00439,0.0042,0.0029,4.14*10**-4,7*10**-6] # C6

for l in range(5):

    c_bounds = np.zeros((5,2))
    alpha = np.zeros((5,2))
    beta = np.zeros((5,2))
    gamma = np.zeros(2)

    fig1 = matplotlib.pyplot.figure(dpi=100)

    # Subplot 1:
    ax = fig1.add_subplot(2,2,1)
    y = [f[l](x,p[k]) for k in range(5)]
    ax.plot(x,y[0],'-k',x,y[1],'-b',x,y[2],'-r',x,y[3],'-g',x,y[4],'-c')
    ax.set_xlabel('x')
    ax.set_ylabel('f(x)',rotation="horizontal",labelpad=15)
    ax.set_yscale("log")
    ax.set_ylim([10**ylim_PDF[0,l],10**ylim_PDF[1,l]])
    ax.set_yticks(np.logspace(ylim_PDF[0,l],ylim_PDF[1,l],5))
    ax.set_title("Higgs-PDF "+PDF_Label[l]+": "+r"f(x) = "+
        HiggsPDF_latex_string[l])
    ax.legend([r"$c = $"+str(c) for c in p])

    # Subplots 3,4:
    for j in range(2): # loops over ttbar,ttbarz

        alpha[:,j] = 1+(sigma_hh[l,:,j]-sigma_gh[l,:,j])/sigma_pp[j]
        beta[:,j] = sigma_gh[l,:,j]/sigma_pp[j]-2
        gamma[j] = err[j]

        for k in range(5):

            r = np.append(np.poly1d([alpha[k,j],beta[k,j],-gamma[j]]).r,np.
                poly1d([alpha[k,j],beta[k,j],gamma[j]]).r)
            L = np.isreal(r) & np.greater_equal(r,0)
            if np.any(L):

                if min(np.real(r[L])) > 1:

                    c_bounds[k,j] = 1

                else:

                    c_bounds[k,j] = min(np.real(r[L]))

            else:

                c_bounds[k,j] = 0

        c = np.atleast_2d(np.linspace(0,1,100))
        sigma = alpha[:,j].reshape((5,1))*c**2+beta[:,j].reshape((5,1))*c+1

        ax1 = fig1.add_subplot(2,2,j+3)
```

```
        ax1.plot(c[0,:],sigma[0,:],"-k",c[0,:],sigma[1,:],"-b",c[0,:],sigma
            [2,:],"-r",c[0,:],sigma[3,:],"-g",c[0,:],sigma[4,:],"-c")
        ax1.set_xlabel(r"$\alpha$")
        ax1.set_ylabel(r"$\frac{\sigma(f)}{\sigma_{exp}}$",rotation="
            horizontal",labelpad=15)
        ax1.set_title("Deviation of measured total XS for "+process_str[j])
        ax1.legend([r"$c = $"+str(c) for c in p])
        ax1.set_xscale("linear")
        ax1.set_ylim([1-err[j],1+err[j]])
        ax1.set_xticks([0,0.25,0.5,0.75,1])
        ax1.set_yticks([1-err[j],1,1+err[j]])

    # Subplot 2:
    P = np.logspace(-2,2,1000)
    ax1 = fig1.add_subplot(2,2,2)
    ax1.plot(p,c_bounds[:,0],'-b',p,c_bounds[:,1],'-r')
    ax1.set_xlabel("c")
    ax1.set_ylabel(r"$\alpha$",rotation="horizontal",labelpad=15)
    ax1.set_title("maximally allowed Higgs fraction "+r"\alpha")
    ax1.legend([r"$t\bar{t}$",r"$t\bar{t}Z$"])
    ax1.set_xscale("log")
    ax1.set_ylim([0,1])
    ax1.set_xticks(p)

    matplotlib.pyplot.tight_layout(pad=1,w_pad=1,h_pad=1)

    # Exclusion Plot Zoom:
    fig2 = matplotlib.pyplot.figure(dpi=100)
    ax2 = fig2.add_subplot(1,1,1)
    ax2.plot(p,c_bounds[:,0],'xb',p,c_bounds[:,1],'xr',p,np.amin(c_bounds,
        axis=1),'-k')
    ax2.set_xlabel("c")
    ax2.set_ylabel(r"$\alpha$",rotation="horizontal",labelpad=15)
    ax2.set_title("maximally allowed Higgs fraction "+r"\alpha")
    ax2.legend([r"$t\bar{t}$"+" - data",r"$t\bar{t}Z$"+" - data","max.
        allowed"])
    ax2.set_xscale("log")
    ax2.set_ylim([0,max(np.amin(c_bounds,axis=1))*1.1])
    ax2.set_xticks(p)
    ax2.grid("on")

    with open("bounds.txt","a") as file:

        file.write("C"+str(l+1)+": "+str(np.amin(c_bounds,axis=1))[1:-1]+"\n"
            )

    matplotlib.pyplot.tight_layout(pad=1,w_pad=1,h_pad=1)
    matplotlib.pyplot.show()
    fig1.savefig("ExclusionPlot_C"+str(l+1)+".png",dpi=200)
    fig2.savefig("ExclusionPlot_zoom_C"+str(l+1)+".png",dpi=200)
    matplotlib.pyplot.close()
```

B.6. Rivet-Analyses

B.6.1. TTBAR

```
// -*- C++ -*-
#include "Rivet/Analysis.hh"
#include "Rivet/Projections/FinalState.hh"
#include "Rivet/Projections/IdentifiedFinalState.hh"

namespace Rivet {


  /// @brief Add a short analysis description here
  class TTBAR : public Analysis {
  public:

    /// Constructor
    DEFAULT_RIVET_ANALYSIS_CTOR(TTBAR);


    /// @name Analysis methods
    //@{

    /// Book histograms and initialize projections before the run
    void init() {

  // Initialize and register projections
        const FinalState fs;
        declare(fs, "FS");
        declare(IdentifiedFinalState(fs,6),"T");
        declare(IdentifiedFinalState(fs,-6),"TBAR");

      // Book histograms

        // pT
        _Hist_pT_T = bookHisto1D("pT_T",nbins,0,1000);
        _Hist_pT_TBAR = bookHisto1D("pT_TBAR",nbins,0,1000);
        _Hist_pT_TTBAR = bookHisto1D("pT_TTBAR",nbins,0,1000);
        _Hist_pT_TTBAR_sum = bookHisto1D("pT_TTBAR_sum",nbins,0,1000);

        // eta
        _Hist_eta_T = bookHisto1D("eta_T",nbins,-max_eta,max_eta);
        _Hist_eta_TBAR = bookHisto1D("eta_TBAR",nbins,-max_eta,max_eta);
        _Hist_eta_T_TBAR = bookHisto1D("eta_T_TBAR",nbins,-max_eta,max_eta);

        // phi
        _Hist_phi_T = bookHisto1D("phi_T",nbins,0,2*M_PI);
        _Hist_phi_TBAR = bookHisto1D("phi_TBAR",nbins,0,2*M_PI);
        _Hist_phi_T_TBAR = bookHisto1D("phi_T_TBAR",nbins,0,2*M_PI);

        // invariant mass
        _Hist_inv_T = bookHisto1D("inv_T",nbins,0,200);
        _Hist_inv_TBAR = bookHisto1D("inv_TBAR",nbins,0,200);
        _Hist_inv_TTBAR = bookHisto1D("inv_TTBAR",nbins,0,2000);
    }


    /// Perform the per-event analysis
```

```
    void analyze(const Event& event)
    {
  const double weight = event.weight();
        const IdentifiedFinalState& tfs = apply<IdentifiedFinalState>(event,
           "T");
        const IdentifiedFinalState& tbfs = apply<IdentifiedFinalState>(event,
           "TBAR");

        // T final state particle projection:

        Particle T = tfs.particles()[0];
        double pT_T = T.pT();
        double eta_T = T.eta();
        double phi_T = T.phi();
        FourMomentum P_T = T.mom();

        _Hist_pT_T -> fill(pT_T,weight);
        _Hist_eta_T -> fill(eta_T,weight);
        _Hist_phi_T -> fill(phi_T,weight);
        _Hist_inv_T -> fill(sqrt(P_T*P_T),weight);

        // TBAR final state particle projection:

        Particle TBAR = tbfs.particles()[0];
        double pT_TBAR = TBAR.pT();
        double eta_TBAR = TBAR.eta();
        double phi_TBAR = TBAR.phi();
        FourMomentum P_TBAR = TBAR.mom();

        _Hist_pT_TBAR -> fill(pT_TBAR,weight);
        _Hist_eta_TBAR -> fill(eta_TBAR,weight);
        _Hist_phi_TBAR -> fill(phi_TBAR,weight);
        _Hist_inv_TBAR -> fill(sqrt(P_TBAR*P_TBAR),weight);

        // difference and sums of observable quantities:

        FourMomentum P_TTBAR = P_T+P_TBAR;
        double phi_TTBAR = (P_TTBAR).phi();
        double eta_TTBAR = (P_TTBAR).eta();

        _Hist_phi_T_TBAR -> fill(phi_T-phi_TBAR,weight);
        _Hist_eta_T_TBAR -> fill(eta_T-eta_TBAR,weight);
        _Hist_inv_TTBAR -> fill(sqrt(P_TTBAR*P_TTBAR),weight);
        _Hist_pT_TTBAR_sum -> fill((pT_T+pT_TBAR),weight); // sum of the two
           transverse momenta
        _Hist_pT_TTBAR -> fill(P_TTBAR.pT(),weight); // actual pT_TTBAR
    }


    /// Normalize histograms etc., after the run
    void finalize()
    {
  // normalize histograms to cross section
        // pT - Histograms for T,TBAR,TTBAR
        normalize(_Hist_pT_T,crossSection());
        normalize(_Hist_pT_TBAR,crossSection());
        normalize(_Hist_pT_TTBAR,crossSection());
        normalize(_Hist_pT_TTBAR_sum,crossSection());

```

```
      // eta - Histograms for T,TBAR,T_TBAR
      normalize(_Hist_eta_T,crossSection());
      normalize(_Hist_eta_TBAR,crossSection());
      normalize(_Hist_eta_T_TBAR,crossSection());

      // phi - Histograms for T,TBAR,T_TBAR
      normalize(_Hist_phi_T,crossSection());
      normalize(_Hist_phi_TBAR,crossSection());
      normalize(_Hist_phi_T_TBAR,crossSection());

      // invariant mass - Histograms for T,TBAR,T_TBAR
      normalize(_Hist_inv_T,crossSection());
      normalize(_Hist_inv_TBAR,crossSection());
      normalize(_Hist_inv_TTBAR,crossSection());

  // scale histograms to nb from pb
      // pT - Histograms for T,TBAR,TTBAR
      scale(_Hist_pT_T,0.001);
      scale(_Hist_pT_TBAR,0.001);
      scale(_Hist_pT_TTBAR,0.001);
      scale(_Hist_pT_TTBAR_sum,0.001);

      // eta - Histograms for T,TBAR,T_TBAR
      scale(_Hist_eta_T,0.001);
      scale(_Hist_eta_TBAR,0.001);
      scale(_Hist_eta_T_TBAR,0.001);

      // phi - Histograms for T,TBAR,T_TBAR
      scale(_Hist_phi_T,0.001);
      scale(_Hist_phi_TBAR,0.001);
      scale(_Hist_phi_T_TBAR,0.001);

      // invariant mass - Histograms for T,TBAR,T_TBAR
      scale(_Hist_inv_T,0.001);
      scale(_Hist_inv_TBAR,0.001);
      scale(_Hist_inv_TTBAR,0.001);
    }

    private:

      double max_eta = 5.; // accelerator max eta
  int nbins = 50; // number of bins

      // Histogram pointers

      // pT
      Histo1DPtr _Hist_pT_T;
      Histo1DPtr _Hist_pT_TBAR;
      Histo1DPtr _Hist_pT_TTBAR;
      Histo1DPtr _Hist_pT_TTBAR_sum;

      // eta
      Histo1DPtr _Hist_eta_T;
      Histo1DPtr _Hist_eta_TBAR;
      Histo1DPtr _Hist_eta_T_TBAR;

      // phi
      Histo1DPtr _Hist_phi_T;
      Histo1DPtr _Hist_phi_TBAR;
```

```
        Histo1DPtr _Hist_phi_T_TBAR;

        // invariant mass
        Histo1DPtr _Hist_inv_T;
        Histo1DPtr _Hist_inv_TBAR;
        Histo1DPtr _Hist_inv_TTBAR;
  };


  // The hook for the plugin system
  DECLARE_RIVET_PLUGIN(TTBAR);


}
```

B.6.2. TTBARZ

```
// -*- C++ -*-
#include "Rivet/Analysis.hh"
#include "Rivet/Projections/FinalState.hh"
#include "Rivet/Projections/IdentifiedFinalState.hh"

namespace Rivet {

  /// @brief Add a short analysis description here
  class TTBARZ : public Analysis {
  public:

    /// Constructor
    DEFAULT_RIVET_ANALYSIS_CTOR(TTBARZ);

    /// @name Analysis methods
    //@{

    /// Book histograms and initialize projections before the run
    void init() {

  // Initialize and register projections
        const FinalState fs;
        declare(fs, "FS");
        declare(IdentifiedFinalState(fs,PID::Z0),"Z0");
        declare(IdentifiedFinalState(fs,6),"T");
        declare(IdentifiedFinalState(fs,-6),"TBAR");

      // Book histograms

        // pT
        _Hist_pT_Z = bookHisto1D("pT_Z",nbins,0,1000);
        _Hist_pT_T = bookHisto1D("pT_T",nbins,0,1000);
        _Hist_pT_TBAR = bookHisto1D("pT_TBAR",nbins,0,1000);
        _Hist_pT_TTBAR = bookHisto1D("pT_TTBAR",nbins,0,1000);
        _Hist_pT_TTBARZ = bookHisto1D("pT_TTBARZ",nbins,0,1000);
        _Hist_pT_TTBAR_sum = bookHisto1D("pT_TTBAR_sum",nbins,0,1000);
        _Hist_pT_TTBARZ_sum = bookHisto1D("pT_TTBARZ_sum",nbins,0,1000);

        // eta
        _Hist_eta_Z = bookHisto1D("eta_Z",nbins,-max_eta,max_eta);
        _Hist_eta_T = bookHisto1D("eta_T",nbins,-max_eta,max_eta);
```

```
        _Hist_eta_TBAR = bookHisto1D("eta_TBAR",nbins,-max_eta,max_eta);
        _Hist_eta_T_TBAR = bookHisto1D("eta_T_TBAR",nbins,-max_eta,max_eta);
        _Hist_eta_TTBAR_Z = bookHisto1D("eta_TTBAR_Z",nbins,-max_eta,max_eta)
            ;

        // phi
        _Hist_phi_Z = bookHisto1D("phi_Z",nbins,0,2*M_PI);
        _Hist_phi_T = bookHisto1D("phi_T",nbins,0,2*M_PI);
        _Hist_phi_TBAR = bookHisto1D("phi_TBAR",nbins,0,2*M_PI);
        _Hist_phi_T_TBAR = bookHisto1D("phi_T_TBAR",nbins,0,2*M_PI);
        _Hist_phi_TTBAR_Z = bookHisto1D("phi_TTBAR_Z",nbins,0,2*M_PI);

        // invariant mass
        _Hist_inv_Z = bookHisto1D("inv_Z",nbins,0,200);
        _Hist_inv_T = bookHisto1D("inv_T",nbins,0,200);
        _Hist_inv_TBAR = bookHisto1D("inv_TBAR",nbins,0,200);
        _Hist_inv_TTBAR = bookHisto1D("inv_TTBAR",nbins,0,2000);
        _Hist_inv_TTBARZ = bookHisto1D("inv_TTBARZ",nbins,0,2000);
    }

    /// Perform the per-event analysis
    void analyze(const Event& event)
    {
  const double weight = event.weight();
        const IdentifiedFinalState& zfs = apply<IdentifiedFinalState>(event,
            "Z0");
        const IdentifiedFinalState& tfs = apply<IdentifiedFinalState>(event,
            "T");
        const IdentifiedFinalState& tbfs = apply<IdentifiedFinalState>(event,
             "TBAR");

        // Z final state particle projections:
        Particle Z = zfs.particles()[0];
        double pT_Z = Z.pT();
        double eta_Z = Z.eta();
        double phi_Z = Z.phi();
        FourMomentum P_Z = Z.mom();

        _Hist_pT_Z -> fill(pT_Z,weight);
        _Hist_eta_Z -> fill(eta_Z,weight);
        _Hist_phi_Z -> fill(phi_Z,weight);
        _Hist_inv_Z -> fill(sqrt(P_Z*P_Z),weight);

        // T final state particle projection:

        Particle T = tfs.particles()[0];
        double pT_T = T.pT();
        double eta_T = T.eta();
        double phi_T = T.phi();
        FourMomentum P_T = T.mom();

        _Hist_pT_T -> fill(pT_T,weight);
        _Hist_eta_T -> fill(eta_T,weight);
        _Hist_phi_T -> fill(phi_T,weight);
        _Hist_inv_T -> fill(sqrt(P_T*P_T),weight);

        // TBAR final state particle projection:

        Particle TBAR = tbfs.particles()[0];
```

```
        double pT_TBAR = TBAR.pT();
        double eta_TBAR = TBAR.eta();
        double phi_TBAR = TBAR.phi();
        FourMomentum P_TBAR = TBAR.mom();

        _Hist_pT_TBAR -> fill(pT_TBAR,weight);
        _Hist_eta_TBAR -> fill(eta_TBAR,weight);
        _Hist_phi_TBAR -> fill(phi_TBAR,weight);
        _Hist_inv_TBAR -> fill(sqrt(P_TBAR*P_TBAR),weight);

        // difference and sums of observable quantities:

        FourMomentum P_TTBAR = P_T+P_TBAR;
        FourMomentum P_TTBARZ = P_TTBAR+P_Z;
        double phi_TTBAR = (P_TTBAR).phi();
        double eta_TTBAR = (P_TTBAR).eta();

        _Hist_phi_T_TBAR -> fill(phi_T-phi_TBAR,weight);
        _Hist_phi_TTBAR_Z -> fill(phi_TTBAR-phi_Z,weight);
        _Hist_eta_T_TBAR -> fill(eta_T-eta_TBAR,weight);
        _Hist_eta_TTBAR_Z -> fill(eta_TTBAR-eta_Z,weight);
        _Hist_inv_TTBAR -> fill(sqrt(P_TTBAR*P_TTBAR),weight);
        _Hist_inv_TTBARZ -> fill(sqrt(P_TTBARZ*P_TTBARZ),weight);
        _Hist_pT_TTBAR -> fill(P_TTBAR.pT(),weight); // actual pT_TTBAR
        _Hist_pT_TTBARZ -> fill(P_TTBARZ.pT(),weight); // actual pT_TTBARZ
        _Hist_pT_TTBAR_sum -> fill((pT_T+pT_TBAR),weight); // not actual
           pT_TTBAR
        _Hist_pT_TTBARZ_sum -> fill((pT_T+pT_TBAR+pT_Z),weight); // not
           actual pT_TTBARZ

    }

    /// normalize histograms etc., after the run
    void finalize()
    {
  // normalize histograms to cross section
        // pT - Histograms for Z,T,TBAR,TTBAR,TTBARZ
        normalize(_Hist_pT_Z,crossSection());
        normalize(_Hist_pT_T,crossSection());
        normalize(_Hist_pT_TBAR,crossSection());
        normalize(_Hist_pT_TTBAR,crossSection());
        normalize(_Hist_pT_TTBARZ,crossSection());
        normalize(_Hist_pT_TTBAR_sum,crossSection());
        normalize(_Hist_pT_TTBARZ_sum,crossSection());

        // eta - Histograms for Z,T,TBAR,T_TBAR,TTBAR_Z
        normalize(_Hist_eta_Z,crossSection());
        normalize(_Hist_eta_T,crossSection());
        normalize(_Hist_eta_TBAR,crossSection());
        normalize(_Hist_eta_T_TBAR,crossSection());
        normalize(_Hist_eta_TTBAR_Z,crossSection());

        // phi - Histograms for Z,T,TBAR,T_TBAR,TTBAR_Z
        normalize(_Hist_phi_Z,crossSection());
        normalize(_Hist_phi_T,crossSection());
        normalize(_Hist_phi_TBAR,crossSection());
        normalize(_Hist_phi_T_TBAR,crossSection());
        normalize(_Hist_phi_TTBAR_Z,crossSection());
```

```
        // invariant mass - Histograms for Z,T,TBAR,T_TBAR,TTBAR_Z
        normalize(_Hist_inv_Z,crossSection());
        normalize(_Hist_inv_T,crossSection());
        normalize(_Hist_inv_TBAR,crossSection());
        normalize(_Hist_inv_TTBAR,crossSection());
        normalize(_Hist_inv_TTBARZ,crossSection());

  // scale histograms to nb from pb
        // pT - Histograms for Z,T,TBAR,TTBAR,TTBARZ
        scale(_Hist_pT_Z,0.001);
        scale(_Hist_pT_T,0.001);
        scale(_Hist_pT_TBAR,0.001);
        scale(_Hist_pT_TTBAR,0.001);
        scale(_Hist_pT_TTBARZ,0.001);
        scale(_Hist_pT_TTBAR_sum,0.001);
        scale(_Hist_pT_TTBARZ_sum,0.001);

        // eta - Histograms for Z,T,TBAR,T_TBAR,TTBAR_Z
        scale(_Hist_eta_Z,0.001);
        scale(_Hist_eta_T,0.001);
        scale(_Hist_eta_TBAR,0.001);
        scale(_Hist_eta_T_TBAR,0.001);
        scale(_Hist_eta_TTBAR_Z,0.001);

        // phi - Histograms for Z,T,TBAR,T_TBAR,TTBAR_Z
        scale(_Hist_phi_Z,0.001);
        scale(_Hist_phi_T,0.001);
        scale(_Hist_phi_TBAR,0.001);
        scale(_Hist_phi_T_TBAR,0.001);
        scale(_Hist_phi_TTBAR_Z,0.001);

        // invariant mass - Histograms for Z,T,TBAR,T_TBAR,TTBAR_Z
        scale(_Hist_inv_Z,0.001);
        scale(_Hist_inv_T,0.001);
        scale(_Hist_inv_TBAR,0.001);
        scale(_Hist_inv_TTBAR,0.001);
        scale(_Hist_inv_TTBARZ,0.001);

    }

    private:

        double max_eta = 5.; // accelerator max eta
  int nbins = 50; // number of bins

        // Histogram pointers

        // pT
        Histo1DPtr _Hist_pT_Z;
        Histo1DPtr _Hist_pT_T;
        Histo1DPtr _Hist_pT_TBAR;
        Histo1DPtr _Hist_pT_TTBAR;
        Histo1DPtr _Hist_pT_TTBARZ;
        Histo1DPtr _Hist_pT_TTBAR_sum;
        Histo1DPtr _Hist_pT_TTBARZ_sum;

        // eta
        Histo1DPtr _Hist_eta_Z;
        Histo1DPtr _Hist_eta_T;
```

```
        Histo1DPtr _Hist_eta_TBAR;
        Histo1DPtr _Hist_eta_T_TBAR;
        Histo1DPtr _Hist_eta_TTBAR_Z;

        // phi
        Histo1DPtr _Hist_phi_Z;
        Histo1DPtr _Hist_phi_T;
        Histo1DPtr _Hist_phi_TBAR;
        Histo1DPtr _Hist_phi_T_TBAR;
        Histo1DPtr _Hist_phi_TTBAR_Z;

        // invariant mass
        Histo1DPtr _Hist_inv_Z;
        Histo1DPtr _Hist_inv_T;
        Histo1DPtr _Hist_inv_TBAR;
        Histo1DPtr _Hist_inv_TTBAR;
        Histo1DPtr _Hist_inv_TTBARZ;
  };

  // The hook for the plugin system
  DECLARE_RIVET_PLUGIN(TTBARZ);

}
```

B.6.3. BBBAR

```
// -*- C++ -*-
#include "Rivet/Analysis.hh"
#include "Rivet/Projections/FinalState.hh"
#include "Rivet/Projections/IdentifiedFinalState.hh"
#include "Rivet/Projections/PromptFinalState.hh"
#include "Rivet/Projections/PartonicTops.hh"

namespace Rivet {


  /// CMS 13 TeV dilepton channel ttbar spin correlations and polarisation
     analysis
  class BBBAR : public Analysis {
  public:

    /// Constructor
    DEFAULT_RIVET_ANALYSIS_CTOR(BBBAR);


    /// Book histograms and initialise projections
    void init() {


      // Parton-level top quarks
      declare(PartonicTops(PartonicTops::E_MU, false), "LeptonicPartonTops");

      // Booking of histograms

      // The remaining histos use parton-level information
      _h_dphi = bookHisto1D("dphi_l_lbar",50,0.,M_PI);

    }
```

```
    /// Perform the per-event analysis
    void analyze(const Event& event) {

      const double weight = event.weight();

      // The remaining variables use parton-level information.

      // Get the leptonically decaying tops
      const Particles& leptonicpartontops = apply<ParticleFinder>(event, "
         LeptonicPartonTops").particlesByPt();
      Particles chargedleptons;
      unsigned int ntrueleptonictops = 0;
      bool oppositesign = false;

      if ( leptonicpartontops.size() == 2 ) {
        for (size_t k = 0; k < leptonicpartontops.size(); ++k) {

          // Get the lepton
          const Particle lepTop = leptonicpartontops[k];
          const auto isPromptChargedLepton = [](const Particle& p){return (
             isChargedLepton(p) && isPrompt(p, false, false));};
          Particles lepton_candidates = lepTop.allDescendants(
             firstParticleWith(isPromptChargedLepton), false);
          if ( lepton_candidates.size() < 1 ) MSG_WARNING("error,
             PartonicTops::E_MU top quark had no daughter lepton candidate,
             skipping event.");

          // In some cases there is no lepton from the W decay but only
             leptons from the decay of a radiated gamma.
          // These hadronic PartonicTops are currently being mistakenly
             selected by PartonicTops::E_MU (as of April 2017), and need to
             be rejected.
          // PartonicTops::E_MU is being fixed in Rivet, and when it is the
             veto below should do nothing.
          /// @todo Should no longer be necessary -- remove
          bool istrueleptonictop = false;
          for (size_t i = 0; i < lepton_candidates.size(); ++i) {
            const Particle& lepton_candidate = lepton_candidates[i];
            if ( lepton_candidate.hasParent(PID::PHOTON) ) {
              MSG_DEBUG("Found gamma parent, top: " << k+1 << " of " <<
                 leptonicpartontops.size() << " , lepton: " << i+1 << " of "
                 << lepton_candidates.size());
              continue;
            }
            if ( !istrueleptonictop && sameSign(lepTop,lepton_candidate) ) {
              chargedleptons.push_back(lepton_candidate);
              istrueleptonictop = true;
            }
            else MSG_WARNING("Found extra prompt charged lepton from top
               decay (and without gamma parent), ignoring it.");
          }
          if ( istrueleptonictop ) ++ntrueleptonictops;
        }
      }

      if ( ntrueleptonictops == 2 ) {
        oppositesign = !( sameSign(chargedleptons[0],chargedleptons[1]) );
```

```
        if ( !oppositesign ) MSG_WARNING("error, same charge tops, skipping
           event.");
      }

      if ( ntrueleptonictops == 2 && oppositesign ) {

        // Get the four-momenta of the positively- and negatively-charged
           leptons
        FourMomentum lepPlus = chargedleptons[0].charge() > 0 ?
           chargedleptons[0] : chargedleptons[1];
        FourMomentum lepMinus = chargedleptons[0].charge() > 0 ?
           chargedleptons[1] : chargedleptons[0];

        const double dphi_temp = deltaPhi(lepPlus,lepMinus);

        // Fill parton-level histos
        _h_dphi -> fill(dphi_temp,weight);

      }

    }


    /// Normalise histograms to unit area
    void finalize() {

  normalize(_h_dphi,crossSection());
  scale(_h_dphi,0.001);

    }


  private:

    Histo1DPtr _h_dphi;

  };


  // The hook for the plugin system
  DECLARE_RIVET_PLUGIN(BBBAR);


}
```

Bibliography

[1] Johannes Bellm et al. "Herwig 7.0/Herwig++ 3.0 release note". In: *Eur. Phys. J.* C76.4 (2016), p. 196. DOI: 10.1140/epjc/s10052-016-4018-8. arXiv: 1512.01178 [hep-ph].

[2] Johannes Bellm et al. "Herwig 7.1 Release Note". In: (2017). arXiv: 1705.06919 [hep-ph].

[3] M. Bahr et al. "Herwig++ Physics and Manual". In: *Eur. Phys. J.* C58 (2008), pp. 639–707. DOI: 10.1140/epjc/s10052-008-0798-9. arXiv: 0803.0883 [hep-ph].

[4] J. de Favereau et al. "DELPHES 3, A modular framework for fast simulation of a generic collider experiment". In: *JHEP* 02 (2014), p. 057. DOI: 10.1007/JHEP02(2014)057. arXiv: 1307.6346 [hep-ex].

[5] CMS Collaboration. "Anomalous couplings in the tt+Z final state at the HL-LHC". In: (2018).

[6] *Anomalous couplings in the tt+Z final state at the HL-LHC.* Tech. rep. CMS-PAS-FTR-18-036. Geneva: CERN, 2018. URL: http://cds.cern.ch/record/2652018.

[7] Simon Fernbach et al. "Constraining the Higgs valence contribution in the proton". In: (2019). (in preparation).

[8] Andy Buckley et al. "Rivet user manual". In: *Comput. Phys. Commun.* 184 (2013), pp. 2803–2819. DOI: 10.1016/j.cpc.2013.05.021. arXiv: 1003.0694 [hep-ph].

[9] Katherine Brading and Harvey R. Brown. "Noether's theorems and gauge symmetries". In: (2000). arXiv: hep-th/0009058 [hep-th].

[10] Michael E. Peskin; Daniel V. Schroeder. *An Introduction to Quantum Field Theory.* Ed. by David Pines. Westview Press, 1995.

[11] Hans Joos Manfred Böhm Ansgar Denner. *Gauge Theories of the Strong and Electroweak Interaction.* 3rd ed. Vieweg+Teubner Verlag, 2001. ISBN: 978-3-322-80160-9. DOI: 10.1007/978-3-322-80160-9.

[12] Anthony J.G. Hey Ian J.R. Aitchison. *Gauge Theories in Particle Physics A.* 4th ed. Vol. 2. CRC Press, 2013. ISBN: 978-1-4665-1307-5.

[13] G. von Gehlen S. Pakuliak. *Integrable Structures of Exactly Solvable Two-Dimensional Models of Quantum Field Theory.* Springer, Dordrecht. ISBN: 978-94-010-0670-5. DOI: https://doi.org/10.1007/978-94-010-0670-5.

[14] Alexander B Zamolodchikov and Alexey B Zamolodchikov. "Factorized S-matrices in two dimensions as the exact solutions of certain relativistic quantum field theory models". In: *Annals of Physics* 120.2 (1979), pp. 253 –291. ISSN: 0003-4916. DOI: https://doi.org/10.1016/0003-4916(79)90391-9. URL: http://www.sciencedirect.com/science/article/pii/0003491679903919.

[15] L. D. Faddeev and V. N. Popov. "Feynman Diagrams for the Yang-Mills Field". In: *Phys. Lett.* B25 (1967). [,325(1967)], pp. 29–30. DOI: 10.1016/0370-2693(67)90067-6.

[16] L. O'Raifeartaigh. *Group Structure of Gauge Theories.* First Edition. Cambridge Monographs on Mathematical Physics. Cambridge University Press, 1988. ISBN: ISBN-13: 978-0521347853.

[17] Noboru Nakanishi. "Indefinite-Metric Quantum Theory of Genuine and Higgs-Type Massive Vector Fields". In: *Progress of Theoretical Physics* 49.2 (Feb. 1973), pp. 640–651. ISSN: 0033-068X. DOI: 10.1143/PTP.49.640. eprint: http://oup.prod.sis.lan/ptp/article-pdf/49/2/640/5257476/49-2-640.pdf. URL: https://doi.org/10.1143/PTP.49.640.

[18] C Becchi, A Rouet, and R Stora. "Renormalization of gauge theories". In: *Annals of Physics* 98.2 (1976), pp. 287 –321. ISSN: 0003-4916. DOI: https://doi.org/10.1016/0003-4916(76)90156-1. URL: http://www.sciencedirect.com/science/article/pii/0003491676901561.

[19] Taichiro Kugo and Izumi Ojima. "Manifestly Covariant Canonical Formulation of the Yang-Mills Field Theories. I: — General Formalism —". In: *Progress of Theoretical Physics* 60.6 (Dec. 1978), pp. 1869–1889. ISSN: 0033-068X. DOI: 10.1143/PTP.60.1869. eprint: http://oup.prod.sis.lan/ptp/article-pdf/60/6/1869/5224080/60-6-1869.pdf. URL: https://doi.org/10.1143/PTP.60.1869.

[20] Axel Maas. "Gauge bosons at zero and finite temperature". In: *Physics Reports* 524.4 (2013). Gauge bosons at zero and finite temperature, pp. 203 –300. ISSN: 0370-1573. DOI: https://doi.org/10.1016/j.physrep.2012.11.002. URL: http://www.sciencedirect.com/science/article/pii/S0370157312004097.

[21] V.N. Gribov. "Quantization of non-Abelian gauge theories". In: *Nuclear Physics B* 139.1 (1978), pp. 1 –19. ISSN: 0550-3213. DOI: https://doi.org/10.1016/0550-3213(78)90175-X. URL: http://www.sciencedirect.com/science/article/pii/055032137890175X.

[22] Claudio Teitelboim Marc Henneaux. *Quantization of Gauge Systems*. Princeton University Press, 1994. ISBN: 978-0691037691.

[23] Herbert Neuberger. "Nonperturbative BRS invariance and the Gribov problem". In: *Physics Letters B* 183.3 (1987), pp. 337 –340. ISSN: 0370-2693. DOI: https://doi.org/10.1016/0370-2693(87)90974-9. URL: http://www.sciencedirect.com/science/article/pii/0370269387909749.

[24] I. M. Singer. "Some remarks on the Gribov ambiguity". In: *Communications in Mathematical Physics* 60.1 (1978), pp. 7–12. ISSN: 1432-0916. DOI: 10.1007/BF01609471. URL: https://doi.org/10.1007/BF01609471.

[25] Daniel Zwanziger. "Renormalizability of the critical limit of lattice gauge theory by BRS invariance". In: *Nuclear Physics B* 399.2 (1993), pp. 477 –513. ISSN: 0550-3213. DOI: https://doi.org/10.1016/0550-3213(93)90506-K. URL: http://www.sciencedirect.com/science/article/pii/055032139390506K.

[26] Gianfausto Dell'Antonio and Daniel Zwanziger. "Every gauge orbit passes inside the Gribov horizon". In: *Communications in Mathematical Physics* 138.2 (1991), pp. 291–299. ISSN: 1432-0916. DOI: 10.1007/BF02099494. URL: https://doi.org/10.1007/BF02099494.

[27] Attilio Cucchieri and Tereza Mendes. "Critical slowing down in SU(2) Landau gauge fixing algorithms". In: *Nucl. Phys.* B471 (1996), pp. 263–292. DOI: 10.1016/0550-3213(96)00177-0. arXiv: hep-lat/9511020 [hep-lat].

[28] Axel Maas. "On the structure of the residual gauge orbit". In: *PoS* QCD-TNT-II (2011), p. 028. DOI: 10.22323/1.136.0028. arXiv: 1111.5457 [hep-th].

[29] L. von Smekal, M. Ghiotti, and A. G. Williams. "Decontracted double BRST symmetry on the lattice". In: *Phys. Rev. D* 78 (8 2008), p. 085016. DOI: 10.1103/PhysRevD.78.085016. URL: https://link.aps.org/doi/10.1103/PhysRevD.78.085016.

[30] Lorenz von Smekal et al. "Modified Lattice Landau Gauge". In: *PoS* LATTICE2007 (2007), p. 382. DOI: 10.22323/1.042.0382. arXiv: 0710.2410 [hep-lat].

[31] Lorenz von Smekal. "Landau Gauge QCD: Functional Methods versus Lattice Simulations". In: *13th International Conference on Selected Problems of Modern Theoretical Physics (SPMTP 08): Dedicated to the 100th Anniversary of the Birth of D.I. Blokhintsev (1908-1979) Dubna, Russia, June 23-27, 2008*. 2008. arXiv: 0812.0654 [hep-th].

[32] Peter Hirschfeld. "Strong evidence that Gribov copying does not affect the gauge theory functional integral". In: *Nuclear Physics B* 157.1 (1979), pp. 37 –44. ISSN: 0550-3213. DOI: https://doi.org/10.1016/0550-3213(79)90052-X. URL: http://www.sciencedirect.com/science/article/pii/055032137990052X.

[33] Kazuo Fujikawa. "Comment on the Covariant Path Integral Formalism in the Presence of Gribov Ambiguities*)". In: *Progress of Theoretical Physics* 61.2 (Feb. 1979), pp. 627–632. ISSN: 0033-068X. DOI: 10.1143/PTP.61.627. eprint: http://oup.prod.sis.lan/ptp/article-pdf/61/2/627/5235284/61-2-627.pdf. URL: https://doi.org/10.1143/PTP.61.627.

[34] Martin Lavelle and David McMullan. "On the physical propagators of QED". In: *Physics Letters B* 312.1 (1993), pp. 211 –214. ISSN: 0370-2693. DOI: https://doi.org/10.1016/0370-2693(93)90512-G. URL: http://www.sciencedirect.com/science/article/pii/037026939390512G.

[35] Paul A. M. Dirac. "Gauge invariant formulation of quantum electrodynamics". In: *Can. J. Phys.* 33 (1955), p. 650. DOI: 10.1139/p55-081.

[36] Rudolf Haag. *Local Quantum Physics*. 2nd ed. Springer-Verlag Berlin Heidelberg, 1996. ISBN: 978-3-540-61049-6. DOI: 10.1007/978-3-642-61458-3.

[37] Kenneth G. Wilson. "Confinement of Quarks". In: *Phys. Rev.* D10 (1974). [,319(1974)], pp. 2445–2459. DOI: 10.1103/PhysRevD.10.2445.

[38] J. Fröhlich, G. Morchio, and F. Strocchi. "Higgs phenomenon without a symmetry breaking order parameter". In: *Physics Letters B* 97 (Dec. 1980), pp. 249–252. DOI: 10.1016/0370-2693(80)90594-8.

[39] J. Fröhlich, G. Morchio, and F. Strocchi. "Higgs phenomenon without symmetry breaking order parameter". In: *Nuclear Physics B* 190.3 (1981), pp. 553 –582. ISSN: 0550-3213. DOI: https://doi.org/10.1016/0550-3213(81)90448-X. URL: http://www.sciencedirect.com/science/article/pii/055032138190448X.

[40] Pascal Törek and Axel Maas. "Testing gauge-invariant perturbation theory". In: *PoS* LATTICE2016 (2016), p. 203. DOI: 10.22323/1.256.0203. arXiv: 1610.04188 [hep-lat].

[41] AXEL MAAS. "BOUND-STATE/ELEMENTARY-PARTICLE DUALITY IN THE HIGGS SECTOR AND THE CASE FOR AN EXCITED "HIGGS" WITHIN THE STANDARD MODEL". In: *Modern Physics Letters A* 28.28 (2013), p. 1350103. DOI: 10.1142/S0217732313501034. eprint: https://doi.org/10.1142/S0217732313501034. URL: https://doi.org/10.1142/S0217732313501034.

[42] A. Maas, R. Sondenheimer, and P. Törek. "On the observable spectrum of theories with a Brout–Englert effect". In: *Annals of Physics* 402 (2019), pp. 18 –44. ISSN: 0003-4916. DOI: https://doi.org/10.1016/j.aop.2019.01.010. URL: http://www.sciencedirect.com/science/article/pii/S0003491619300107.

[43] Larissa Egger, Axel Maas, and René Sondenheimer. "Pair production processes and flavor in gauge-invariant perturbation theory". In: *Modern Physics Letters A* 32.38 (2017), p. 1750212. DOI: 10.1142/S0217732317502121. eprint: https://doi.org/10.1142/S0217732317502121. URL: https://doi.org/10.1142/S0217732317502121.

[44] Axel Maas. "Brout–Englert–Higgs physics: From foundations to phenomenology". In: *Progress in Particle and Nuclear Physics* 106 (2019), pp. 132 –209. ISSN: 0146-6410. DOI: https://doi.org/10.1016/j.ppnp.2019.02.003. URL: http://www.sciencedirect.com/science/article/pii/S0146641019300055.

[45] Axel Maas. "Observables in Higgsed Theories". In: *Nuclear and Particle Physics Proceedings* 273-275 (2016). 37th International Conference on High Energy Physics (ICHEP), pp. 1604 –1610. ISSN: 2405-6014. DOI: https://doi.org/10.1016/j.nuclphysbps.2015.09.260. URL: http://www.sciencedirect.com/science/article/pii/S240560141500749X.

[46] Axel Maas and Tajdar Mufti. "Two- and three-point functions in Landau gauge Yang-Mills-Higgs theory". In: *JHEP* 04 (2014), p. 006. DOI: 10.1007/JHEP04(2014)006. arXiv: 1312.4873 [hep-lat].

[47] Axel Maas and Tajdar Mufti. "Spectroscopic analysis of the phase diagram of Yang-Mills-Higgs theory". In: *Phys. Rev.* D91.11 (2015), p. 113011. DOI: 10.1103/PhysRevD.91.113011. arXiv: 1412.6440 [hep-lat].

[48] K.A. Olive. "Review of Particle Physics". In: *Chinese Physics C* 38.9 (2014), p. 090001. DOI: 10.1088/1674-1137/38/9/090001. URL: https://doi.org/10.1088%2F1674-1137%2F38%2F9%2F090001.

[49] Christian B. Lang Christof Gattringer. *Quantum Chromodynamics on the Lattice*. 1st ed. Lecture Notes in Physics. Springer-Verlag Berlin Heidelberg, 2010. ISBN: 978-3-642-01849-7. DOI: 10.1007/978-3-642-01850-3.

[50] Albert M. Sirunyan et al. "Measurement of the $t\bar{t}$ production cross section using events with one lepton and at least one jet in pp collisions at $\sqrt{s} = 13$ TeV". In: *JHEP* 09 (2017), p. 051. DOI: 10.1007/JHEP09(2017)051. arXiv: 1701.06228 [hep-ex].

[51] Morad Aaboud et al. "Measurement of the $t\bar{t}Z$ and $t\bar{t}W$ cross sections in proton-proton collisions at $\sqrt{s} = 13$ TeV with the ATLAS detector". In: (2019). arXiv: 1901.03584 [hep-ex].

[52] Buckley, Andy et al. "LHAPDF6: parton density access in the LHC precision era". In: *Eur. Phys. J. C* 75.3 (2015), p. 132. DOI: 10.1140/epjc/s10052-015-3318-8. URL: https://doi.org/10.1140/epjc/s10052-015-3318-8.